ENHANCING THE PHOTOINITIATOR IRGACURE 2959 AND THE DRUG IBUPROFEN: MONOMERS, SALTS, AND POLYMERS

By
Simay Denizkuşu
B.S., Chemistry, Boğaziçi University, 2021

Submitted to the Institute for Graduate Studies in
Science and Engineering in partial fulfillment of
the requirements for the degree of
Master of Science

Graduate Program in Chemistry
Boğaziçi University
2024

Dedicated to my lovely family…

ACKNOWLEDGEMENTS

First, my deepest gratitude goes out to Prof. Duygu Avcı Semiz for all of her assistance, kind demeanor, and insightful advice during my graduate studies. It was a great pleasure to do academic research under her guidance.

I would like to thank my committee members Assoc. Prof. Ali Ersin Acar and Assist. Prof. Bekir Dizman for graciously giving their important time to examine the final version of my thesis and for their insightful feedback.

I would like to thank Prof. Dr. Hande Sipahi and Ece Sabuncu. I am very grateful for their valuable work and support on the in vitro cytotoxicity and in vitro evaluation of the anti-inflammatory experiments.

I would like to extend my great thanks to Melek and Türkan due to their assistance and advice in the laboratory. Further, I would like to express my gratitude to my good friends from the group, Burcu, Neslihan, Merve, Aleyna, Yusuf and Tolga for their assistance, friendship, support, and encouragement.

I would like to thank my family, who have been there for me unconditionally in every decision I have made throughout my life, for their love, encouragement, and support.

First part of this research was financed supported by The Scientific and Technological Research Council of Turkey (TÜBİTAK) [120Z729] and second part was financed supported by Bogazici University Research Fund (50003). I also would like to acknowledge the financial support of TÜBİTAK 2211 National MSc/MA Scholarship Program (2210/A National MSc/MA Scholarship Program).

ABSTRACT

ENHANCING THE PHOTOINITIATOR IRGACURE 2959 AND THE DRUG IBUPROFEN: MONOMERS, SALTS, AND POLYMERS

The enhancements referred to in the title are in the reactivity of the photoinitiators (PIs), the migration stability of the resulting polymers, also possibly other properties thereof, the water solubility of the drugs, hence their bioavailability, or mitigation of their potential side effects. Therefore, they aim to make photopolymerization more environmentally friendly and ibuprofen safer and more effective. For these purposes: 1) Two novel monomeric PIs (I2959-NTBDA and I2959-NDAA) with 1,6-heptadiene structure and based on Irgacure 2959 (I2959) and the photoinitiating cyclocopolymer of the first (has six-membered rings in the backbone) were synthesized. 2) Two novel mono- and dimethacrylate-based PIs (I2959-NH-AHM, I2959-N-2xAHM) were synthesized based on I2959 and 3-(acryloyloxy)-2-hydroxypropyl methacrylate (AHM). 3) Two novel ibuprofen cystamine salts (IBU-CYS 1 and IBU-CYS 2) were synthesized by coupling the anion of ibuprofen with cystamine in 1:1 and 2:1 ratio. 4) An ibuprofen functionalized alkyl α-hydroxymethacrylate-based crosslinker/prodrug (CYS-2xIBU) was synthesized and used to fabricate poly(ethylene glycol) diacrylate (PEGDA) hydrogels. PIs/drugs were characterized by NMR, FTIR, UV-Vis spectrometry, DSC and TGA/ DTA. The chemical mechanism of PIs investigated by electron spin resonance (ESR) and steady state photolysis confirms generation of isopropyl ketyl radicals. Photoinitiating abilities of the photoinitiators were studied during polymerizations of 2-hydroxyethyl methacrylate (HEMA), PEGDA, and trimethylol propane triacrylate (TMPTA). The migration stability of the residual PIs in the cured film is much higher than that of I2959 due to incorporation into the network structure. In comparison with ibuprofen, the salts show higher solubility (152 and 195 times) in water and (3.82 and 4.71 times) in PBS. In vitro studies indicate that the salts are effective in relieving inflammatory responses induced by lipopolysaccharide in RAW264.7 macrophage cells while indicating no cytotoxicity.

ÖZET

FOTO BAŞLATICI IRGACURE 2959 VE İLAÇ İBUPROFENİN GELİŞTİRİLMESİ: MONOMERLER, TUZLAR VE POLİMERLER

Başlıkta bahsedilen geliştirmeler, foto başlatıcıların (PI'ler) reaktivitesinde, elde edilen polimerlerin migrasyon kararlılığında ve ayrıca bunların muhtemelen diğer özelliklerinde olmasıyla beraber, ilaçların suda çözünürlüğünde, dolayısıyla biyoyararlanımlarında veya potansiyel yan etkilerinin azaltılmasındadır. Bu nedenle fotopolimerizasyonun daha çevre dostu, ibuprofenin ise daha güvenli ve etkili hale getirilmesi hedeflenmektedir. Bu amaçlar doğrultusunda: 1) 1,6-heptadien yapısına sahip ve Irgacure 2959 (I2959) bazlı iki yeni monomerik PI (I2959-NTBDA ve I2959-NDAA) ve ilkinin (ana zincirinde altı üyeli halkalara sahip) fotobaşlatıcı siklokopolimeri sentezlendi. 2) I2959 ve 3-(akriloiloksi)-2-hidroksipropil metakrilat (AHM) temelli iki yeni mono- ve dimetakrilat (I2959-NH-AHM, I2959-N-2xAHM) sentezlendi. 3) İki yeni ibuprofen sistamin tuzu (IBU-CYS 1 ve IBU-CYS 2), ibuprofen anyonunun sistamin ile 1:1 ve 2:1 oranında reaksiyonundan sentezlendi. 4) Bir ibuprofen işlevselleştirilmiş alkil a-hidroksimetakrilat bazlı çapraz bağlayıcı/ön ilaç (CYS-2xIBU) sentezlendi ve poli(etilen glikol) diakrilat (PEGDA) hidrojellerini üretmek için kullanıldı. PI'ler/ilaçlar NMR, FTIR, UV-Vis spektrometresi, DSC ve TGA/DTA ile karakterize edildi. Elektron spin rezonansı (ESR) ve kararlı durum fotolizi ile araştırılan PI'lerin kimyasal mekanizması, izopropil ketil radikallerinin oluşumunu doğruladı. Fotobaşlatıcıların fotobaşlatma yetenekleri, 2-hidroksietil metakrilat (HEMA), PEGDA ve trimetilol propan triakrilatın (TMPTA) polimerizasyonları sırasında incelenmiştir. Kürlenmiş filmdeki artık PI'lerin migrasyon kararlılığı, ağ yapısına dahil edilmesinden dolayı I2959'unkinden çok daha yüksektir. İbuprofen ile karşılaştırıldığında tuzlar suda (152 ve 195 kat) ve PBS'de (3,82 ve 4,71 kat) daha yüksek çözünürlük gösterir. In vitro çalışmalar, tuzların, RAW264.7 makrofaj hücrelerinde lipopolisakkarid tarafından indüklenen inflamatuar yanıtların hafifletilmesinde etkili olduğunu ancak sitotoksik olmadıklarını göstermektedir.

TABLE OF CONTENTS

ACKNOWLEDGEMENTS iv
ABSTRACT….. v
ÖZET……. vi
LIST OF FIGURES xi
LIST OF TABLES xix
LIST OF SYMBOLS xx
LIST OF ACRONYMS/ABBREVIATIONS xxi
1. INTRODUCTION 1
1.1. Photopolymerization. 1
1.1.1. Free Radical Photopolymerization 2
1.1.2. Free Radical Photoinitiators 4
1.1.2.1. Type I Photoinitiators 6
1.1.2.2. Type II Photoinitiators 7
1.1.3. Functionalized Photoinitiators 9
1.1.3.1. Monomeric and Polymeric Photoinitiators 10
1.1.3.2. Cyclopolymerizable and Cyclopolymeric Photoinitiators 13
1.2. Non-Steroidal Anti-Inflammatory Drugs 17
1.2.1. Classification of NSAIDs 18
1.2.2. Side Effects of NSAIDs 20
1.2.3. Arylpropionic Acid Derived NSAIDs 22
1.2.4. Ibuprofen 23
1.2.4.1. Derivatives of Ibuprofen 23
2. OBJECTIVES 25
3. STRUCTURE-REACTIVITY RELATIONSHIPS OF NOVEL α-HYDROXY-KETONE-FUNCTIONALIZED CYCLOPOLYMERIZABLE AND CYCLO-POLYMERIC PHOTOINITIATORS 26

3.1. Introduction..... 26
3.2. Experimental..... 27
3.2.1. Materials and Characterization Methods..... 27
3.2.2. Synthesis of Photoinitiators..... 28
3.2.2.1. Synthesis of I2959-NTBDA..... 28
3.2.2.2. Synthesis of I2959-NDAA..... 28
3.2.2.3. Synthesis p-BA-NTBDA-*co*-I2959-NTBDA..... 29
3.2.3. UV-Visible Absorption Measurements..... 29
3.2.4. ESR Spin Trapping (ESR-ST) Experiments..... 30
3.2.5. Photoinitiating Activity Measurements..... 30
3.2.6. Migration Studies..... 30
3.2.7. Color analysis..... 31
3.3. Results and Discussion..... 31
3.3.1. Synthesis and Characterization of Monomeric Photoinitiators..... 31
3.3.2. Synthesis and Characterization of Polymeric Photoinitiator..... 37
3.3.3. Light Absorption Properties..... 40
3.3.4. Electron Spin Resonance (ESR) Experiments..... 42
3.3.5. Photopolymerization..... 43
3.3.6. Migration Stability..... 45
3.3.7. Color Analysis..... 46
3.4. Conclusions..... 47
4. MONOMERIC PHOTOINITIATORS FROM 3-(ACRYLOYLOXY)- 2-HYDROXYPROPYL METHACRYLATE..... 48
4.1. Introduction..... 48
4.2. Experimental..... 49
4.2.1. Materials and Characterization..... 49
4.2.2. Synthesis of Photoinitiators..... 49

4.2.2.1. Synthesis of I2959-NH-AHM 49
4.2.2.2. Synthesis of I2959-N-2xAHM 50
4.2.3. Photopolymerization Experiments 50
4.2.4. Migration Study 51
4.3. Results and Discussion. 51
4.3.1. Synthesis and Characterization of Monomeric Photoinitiators 51
4.3.2. Light Absorption Properties 55
4.3.3. Photopolymerization Results 56
4.3.4. Migration Stability 58
4.4. Conclusions 59
5. NEW IBUPROFEN CYSTAMINE SALTS WITH IMPROVED SOLUBILITY 60
5.1. Introduction 60
5.2. Experimental. 61
5.2.1. Materials and Characterization 61
5.2.2. Synthesis of Ibuprofen Salts 61
5.2.2.1. Synthesis of IBU-CYS 1 61
5.2.2.2. Synthesis of IBU-CYS 2 62
5.2.3. Synthesis of Hydrogels 62
5.2.4. Solubility Study 62
5.2.5. In Vitro Drug Release Studies 63
5.2.6. Cell Viability Assay 63
5.2.7. Anti-inflammatory Activity 64
5.2.8. Statistical Analysis 64
5.3. Results and Discussion. 65
5.3.1. Synthesis and Characterization of Ibuprofen Salts 65
5.3.2. Solubility Study 69
5.3.3. Thermal Studies 70

5.3.4. Release Studies 71
5.3.5. In Vitro Cytotoxicity of The Ibuprofen Salts..... 72
5.3.6. In Vitro Evaluation of The Anti-Inflammatory Effect of The Ibuprofen Salts..... 73
5.4. Conclusions..... 75
6. SYNTHESIS OF AN IBUPROFEN FUNCTIONALIZED ALKYL α-HYDROXY-METHACRYLATE-BASED CROSSLINKER 76
6.1. Introduction..... 76
6.2. Experimental..... 76
6.2.1. Materials and Characterization 76
6.2.2. Synthesis of Monomeric Prodrug 77
6.2.2.1. Synthesis of CYS-2xIBU 77
6.2.3. Synthesis of Hydrogels 78
6.2.4. In Vitro Drug Release Studies 78
6.3. Results and Discussion. 78
6.3.1. Synthesis and Characterization of Monomeric Prodrug 78
6.3.2. Release Studies 82
6.4. Conclusions..... 83
7. CONCLUDING REMARKS..... 84
REFERENCES. 86
APPENDIX A: COPYRIGHT LICENCES..... 104

LIST OF FIGURES

Figure 1.1. General process for photopolymerization. Permission from [14] American Chemical Society, Copyright (2010) (Figure A.1)..... 2

Figure 1.2. Illustration of photopolymerization reaction process resulting cross-linked polymer network where photoinitiators, monomers and oligomers are shown in blue, orange, and purple colors respectively [15]. Published under an open access..... 3

Figure 1.3. General reaction steps of photopolymerization. Permission from [33] American Chemical Society, Copyright (2015) (Figure A.2)…….. 4

Figure 1.4. Jablonski diagram illustrating possible transitions between singlet (S) and triplet (T) valence excited states [36]. Published under an open access..... 5

Figure 1.5. Criteria for photoinitiators [38]. Published under an open access……... 6

Figure 1.6. Photocleavage reaction of Type I PIs [43]. Published under an open access.. 6

Figure 1.7. Type I PIs that are commonly used [43]. Published under an open access. 7

Figure 1.8. Photocleavage reaction of Type II PIs [43]. Published under an open access. 8

Figure 1.9. Type II PIs that are commonly used [43]. Published under an open access. 8

Figure 1.10. Examples of secondary reactions of photoinitiators. Permission from [51] Elsevier, Copyright (2019) (Figure A.3).. 9

Figure 1.11. Thiol-functionalized photoinitiators. Permission from [55] Elsevier, Copyright (2010)(Figure A.4).. 10

Figure 1.12. Monomeric photoinitiator and its cleavage. Permission from [44] Royal Society of Chemistry (2022) (Figure A.5).. 10

Figure 1.13. Examples of polimeric photoinitiators. Permission from [51] Elsevier,Copyright (2019) (Figure A.3).. 11

Figure 1.14. Synthesis pathways for polymerizable photoinitiators that contain. Permission from [58] John Wiley and Sons, Copyright (2006) (Figure A.6). 12

Figure 1.15. Synthesis pathways for polymerizable photoinitiators that contain. Permission from [62] Elsevier, Copyright (2020) (Figure A.7)……..... 12

Figure 1.16. The photocyclization of substituted dienes with seven atom centers. Permission from [74] Royal Society of Chemistry (2004) (Figure A.8).... 14

Figure 1.17. The volumetric shrinkage during photopolymerization. Permission from [65] John Wiley and Sons, Copyright (2021) (Figure A.9)……..... 15

Figure 1.18. Structure of the novel monomeric photoinitiator synthesized by Eren et al [52]. Permission from [52] Elsevier, Copyright (2019) (Figure A.10).. 16

Figure 1.19. Synthesis of cyclopolyemeric photoinitiator. Permission from [44] Elsevier, Copyright (2019) (Figure A.5). 16

Figure 1.20. The development of NSAIDs in chronological order. Permission from [82] Springer Nature, Copyright (2022) (Figure A.11).. 18

Figure 1.21. Structural based classification of non-steroidal anti-inflammatory drugs (NSAIDs). Permission from [87] Elsevier, Copyright (2020) (Figure A.12).. 19

Figure 1.22. Organs affected by overdose usage of NSAIDs. Permission from [100] Elsevier, Copyright (2023) (Figure A.13).. 20

Figure 1.23. The synthesis HEMA derivative of naproxen (NP-HEMA) [107]. Published under an open access... 21

Figure 1.24. Chemical structure of profens. Permission from [108] Elsevier, Copyright (2019) (Figure A.14).... 22

Figure 1.25. Figure 1.6. Representation of ibuprofen release from a polymeric nanoparticle system. Permission from [122] Elsevier, Copyright (2020) (Figure A.15)..... 24

Figure 3.1. Structures of synthesized PIs (I2959-NTBDA, I2959-NDAA and p-BA-NTBDA-*co*-I2959-NTBDA).. 27

Figure 3.2. Synthesis of I2959-NTBDA and I2959-NDAA..... 32

Figure 3.3. ^{1}H NMR spectra of I2959-Ts, I2959-N_3 and I2959-NH_2. 33

Figure 3.4. FTIR spectra of I2959-Ts, I2959-N_3 and I2959-NH_2. 34

Figure 3.5. ^{1}H-NMR spectra of I2959-NTBDA and I2959-NDAA.. 35

Figure 3.6. FTIR spectra of I2959-NTBDA and I2959-NDAA. 36

Figure 3.7. ^{1}H-NMR spectrum of BA-NTBDA……..... 38

Figure 3.8. ^{1}H-NMR spectrum of p-BA-NTBDA-*co*-I2959-NTBDA. 38

Figure 3.9. FTIR spectrum of p-BA-NTBDA-*co*-I2959-NTBDA.. 39

Figure 3.10. TGA plot of p-BA-NTBDA-*co*-I2959-NTBDA.. 39

Figure 3.11. UV–vis absorption spectra of (A) I2959-NTBDA and I2959-NDAA ($2x10^{-5}$ M) in $CHCl_3$ and MeOH, (B) p-BA-NTBDA-*co*-I2959-NTBDA ($0.2x10^{-6}$, $0.5x10^{-6}$, $1x10^{-6}$ and 2x10-6 M) in $CHCl_3$. 40

Figure 3.12. The photolysis of I2959-NTBDA ($3.2x10^{-5}$ M in $CHCl_3$) in chloroform using a 320-500 nm light source.. ……..... 41

Figure 3.13. The photolysis of (A) I2959-NDAA (4 x 10^{-5} M) in methanol and (B) p-BA- NTBDA-*co*-I2959-NTBDA (1.1 x 10^{-5} M) in chloroform using a 320-500 nm light source 42

Figure 3.14. Electron spin resonance spectra of free radicals captured by PBN in a toluene solution of (A) I2959 and (B) I2959-NTBDA by a 320-500 nm light source. 42

Figure 3.15. Rate-time and conversion-time graphs of I2959-NTBDA during homo-polymerization at 25 ºC under nitrogen and 320-500 nm irradiation. 43

Figure 3.16. Rate-time and conversion-time plots for HEMA containing I2959-NTBDA (1 wt%, 0.41 wt % I2959-eq), I2959-NDAA (1 wt%, 0.53 wt% I2959-eq) and I2959 (1 wt%) at 25 ºC under nitrogen and 320-500 nm irradiation. . 44

Figure 3.17. Rate-time and conversion-time plots for PEGDA and/or TMPTA containing I2959-NTBDA (1 wt%, 0.41 wt% I2959-eq), I2959-NDAA (1 wt %, 0.53 wt% I2959-eq), p-BA-NTBDA-*co*- I2959-NTBDA (1 wt%, 6.4 wt% I2959-eq) and I2959 (1 wt%) at 25 ºC under nitrogen and 320- 500 nm irradiation..... 45

Figure 3.18. Heat Flow-time graph of HEMA formulations containing TX:EDB (0.25 :0.75 wt%), TX:I2959-NTBDA (0.25:0.75 wt%) and TX:I2959 (0.25:0.75 wt%) (inset) at 25 ºC under nitrogen and 400-500 nm irradiation 45

Figure 3.19. UV-VIS absorption spectra of I2959-NTBDA and I2959 extracted with chloroform from the PEGDA gels. 46

Figure 4.1. Structure of the novel photoinitiators I2959-NH-AHM and I2959-N-2x AHM 48

Figure 4.2. Synthesis of the PIs, I2959-NH-AHM and I2959-N-2xAHM 52

Figure 4.3. ^{1}H-NMR spectrum of I2959-NH-AHM. 53

Figure 4.4. ^{1}H-NMR spectrum of I2959-N-2xAHM. 53

Figure 4.5. FTIR spectrum of I2959-NH-AHM. 54

Figure 4.6. FTIR spectrum of I2959-N-2xAHM 54

Figure 4.7. Rate-time and conversion-time graphs of I2959-NH-AHM and I2959-N-2xAHM during homopolymerization at 25°C under nitrogen and 320-500 nm irradiation..... 56

Figure 4.8. Rate-time and conversion-time plots for HEMA, PEGDA and TMPTA containing I2959-NH-AHM (1 wt. %) and I2959 (1 wt.%) at 25 ºC under nitrogen and 320-500 nm irradiation.. 57

Figure 4.9. Rate-time and conversion-time plots for HEMA, PEGDA and TMPTA containing I2959-N-2xAHM (1 wt. %) and I2959 (1 wt.%) at 25 ºC under nitrogen and 320-500 nm irradiation.. 58

Figure 4.10. Rate-time and conversion-time plots for HEMA, PEGDA and TMPTA containing I2959-N-2xAHM (1 wt. %) and I2959-NH-AHM (1 wt.%) at 25 ºC under nitrogen and 320-500 nm irradiation... 58

Figure 4.11. UV-Visible absorption spectra of I2959 I2959-N-2xAHM and I2959-NA-AHM extracted with chloroform from the HEMA/PEGDA (50/50 mmol%) polymer samples 59

Figure 5.1. Synthesized salts IBU-CYS 1 and IBU-CYS2..... 60

Figure 5.2. Synthesis of ibuprofen salts.. 66

Figure 5.3. ^{1}H NMR spectrum of IBU-Na, cystamine dihydrochloride and IBU-CYS 1..... 66

Figure 5.4. ^{1}H NMR spectrum of IBU-Na, cystamine dihydrochloride and IBU-CYS 2..... 67

Figure 5.5. ^{13}C NMR spectrum of IBU-CYS 2. 67

Figure 5.6. FTIR spectra of ibuprofen sodium salt, cystamine dihydrochloride, IBU-CYS 1 and IBU-CYS 2. 68

Figure 5.7. UV-Vis spectra of IBU, IBU-CYS 1 and IBU-CYS 2 (3.4 x10^{-5} M) in water 68

Figure 5.8. Calibration curve of ibuprofen in water and PBS 69

Figure 5.9. Calibration curve of IBU-CYS 1 in water and PBS..... 70

Figure 5.10. Calibration curve of IBU-CYS 2 in water and PBS..... 70

Figure 5.11. (A) DSC spectra of IBU, IBU sodium salt, IBU-CYS 1 and CYS 2, (B) TGA and DTA spectra of IBU-CYS 1 and IBU-CYS 2 71

Figure 5.12. The release profiles of ibuprofen, IBU-CYS 1, IBU-CYS 2 and IBU-CYS 2 from HEMA/PEGDA gel 72

Figure 5.13. The effects of IBU-CYS 1 and IBU-CYS 2 at different doses (12.5, 25, 50 and 100 μM) on cell viability (A), on nitrite production (B) on LPS stimulated RAW 264.7 cell 74

Figure 6.1. Synthesized cross-linker CYS-2xIBU 76

Figure 6.2. Synthesis of CYS-2xIBU.. 79

Figure 6.3. ^{1}H-NMR spectrum of CYS-2xIBU. 80

Figure 6.4. ^{13}C-NMR spectrum of CYS-2xIBU 80

Figure 6.5. FTIR spectrum of CYS-2xIBU 81

Figure 6.6. Synthesis of hydrogel 81

Figure 6.7. SEM images of hydrogel 82

Figure 6.8. The release profiles of ibuprofen: pure drug and from CYS-2xIBU cross-linked PEGDA hydrogels in PBS 83

Figure A.1. Permission from [14] American Chemical Society, Copyright (2010) ... 104

Figure A.2. Permission from [33] American Chemical Society, Copyright (2015).... 105

Figure A.3. Permission from [51] Elsevier, Copyright (2019) 105

Figure A.4. Permission from [55] Elsevier, Copyright (2010)..... 106

Figure A.5. Permission from [44] Royal Society of Chemistry (2022). 106

Figure A.6. Permission from [58] John Wiley and Sons, Copyright (2006).. 107

Figure A.7. Permission from [62] Elsevier, Copyright (2020)..... 107

Figure A.8. Permission from [74] Royal Society of Chemistry (2004).. 108

Figure A.9. Permission from [65] John Wiley and Sons, Copyright (2021).. 109

Figure A.10. Permission from [52] Elsevier, Copyright (2019)..... 109

Figure A.11. Permission from [82] Springer Nature, Copyright (2022).. 110

Figure A.12. Permission from [87] Elsevier, Copyright (2020)..... 110

Figure A.13. Permission from [100] Elsevier, Copyright (2023)..... 111

Figure A.14. Permission from [108] Elsevier, Copyright (2019)..... 111

Figure A.15. Permission from [122] Elsevier, Copyright (2020)..... 112

LIST OF TABLES

Table 3.1. Solubilities of the synthesized PIs and I2959.. 36

Table 3.2. Absorption characteristics of I2959, I2959-NTBDA and I2959-NDAA... 40

Table 3.3. Colorimetry results of the cured films... 46

Table 4.1. Solubilities of the synthesized and commercial PIs.. 55

Table 4.2. Absorption characteristics of I2959-N-2xAHM in ethanol 55

Table 5.1. Solubility of IBU, IBU-CYS 1 and IBU-CYS 2.. 68

Table 5.2. Solubility table of IBU-CYS salts and ibuprofen in both water and PBS expressed in mg/mL.. 69

Table 5.3. Effects of different salt forms of ibuprofen on the viability of RAW264.7 macrophage cells and the effects of the different salt forms of Ibuprofen on nitrite levels and % nitrite inhibition in RAW 264.7 cells stimulated with 1 μg/mL LPS..... 73

Table 6.1. Solubilities of the synthesized monomer and IBU..... 81

LIST OF SYMBOLS

A	The Van-der-Waals distance
m	The mass of monomer in the sample
M	The molar mass of the monomer
M_n	Number average molecular weight
n	The number of double bonds per monomer molecule
PI	Photoinitiator
Q/s	The heat flow per second
R_{pmax}	The maximum rate of polymerization
S_0	Ground state
S_n	Excited singlet state
T_1	First excited triplet state
t½	Plasma half-life
TA	Thermal Analyzer
T_g	Glass transition temperature
t_{max}	Time to reach the maximum heat of polymerization
ΔH_p	The heat of reaction
ε	Extinction coefficient
λ_{max}	The wavelengths for maximum absorption

LIST OF ACRONYMS / ABBREVIATIONS

AHM	3-(acryloyloxy)-2-hydroxypropyl methacrylate
BP	Benzophenone
COX	Cyclooxygenase
DCC	1,3-dicyclohexylcarbodiimide
DCM	Dichloromethane
DMF	N,N-Dimethylformamide
DMAP.	Dimethylaminopyridine
DSC	Differential Scanning Calorimetry
EDB	Ethyl 4- (dimethylamino) benzoate
ESR-ST	Electron Spin Resonance Spin Trapping
FT-IR	Fourier Transform Infrared Spectroscopy
HEMA	2-Hydroxyethyl methacrylate
I2959	2-Hydroxy-4'-(2-hydroxyethoxy)-2-methylpropiophenone
Iod	Bis-(4-tert-butylphenyl)-iodonium hexafluorophosphate
IBU	Ibuprofen
MeOH	Methanol
MTT	(4,5-dimethylthiazol-2-yl)-2,5-diphenyltetrazolium bromide
Na_2SO_4	Sodium sulfate
NMR	Nuclear Magnetic Resonance spectroscopy
NO	Nitrite oxide
NSAID	Non-steroidal anti-inflammatory drug
PBS	Phosphate-buffered saline
PEGDA	Poly(ethylene glycol) diacrylate
TBBr	*Tert*-butyl α-bromomethacrylate
TFA	Trifluoroacetic acid
TGA	Thermal Gravimetric Analysis
THF	Tetrahydrofuran
TMPTA	Trimethylolpropane triacrylate
TX	Thioxanthone

1. INTRODUCTION

This thesis consists of two main parts, the first in the field of photopolymerization, and the second on novel delivery methods of non-steroidal anti-inflammatory drugs. Below we give brief introductions to the two fields, separately.

1.1. Photopolymerization

Light is one of the most important resources for the mother Earth. More than just creating day and night, it determines the world climate through solar radiation and the greenhouse effect, whose increase causes global warming, which has been on the agenda lately [1,2]. Apart from that, light has an important place in both natural life and the industrial world [1]. Primary industrial applications using light include free-radical chlorination, sulfochlorination, sulfoxidation, and nitrosation, but light is also increasingly used for vitamin, drug, and fragrance synthesis. [3-5] More importantly, photosynthesis, which generates oxygen via converting light energy into chemical energy by plants, algae, and certain bacteria [6,7], hence in a sense creates life, can be given as an example of biological activity that depends on light.

Photochemistry is a branch of chemistry that focuses on investigating chemical reactions initiated by light absorption [1]. Photochemical processes play an important role in environmental remediation, assisting in the purification of water and the degradation of air pollutants [8-10]. As a result, photochemistry should be better researched and understood not only to understand the planet and maintain climate and life balance, but also for more environmentally friendly technological developments. [11,12].

One of the most significant types of photochemical reactions is photopolymerization, which is made extensive use of by a wide variety of industrial processes [13]. The production of coatings, adhesives, and materials for 3D printing can be given as an example of such application areas [14-16]. When thermal polymerization is compared with

photopolymerization, the latter one has some clear benefits, such as fast polymerization rates, no need for high temperature, and the capability for selective curing in specific areas [15], [17,18].

Photopolymerization is a polymerization process which is initiated by light [19]. After the light source supplies energy to create active species, the typical polymerization process takes place [19]. There are three basic components: a photoinitiator (PI), a polymerizable monomer/oligomer, and a light source, typically ultraviolet (UV) or visible light [20]. First, PI absorbs light and then undergoes photolysis to produce reactive species like free radicals or cations [21]. After radicals are generated, they initiate the linkage of small monomers to form a polymer with a chainlike structure (Figure 1.1) [22].

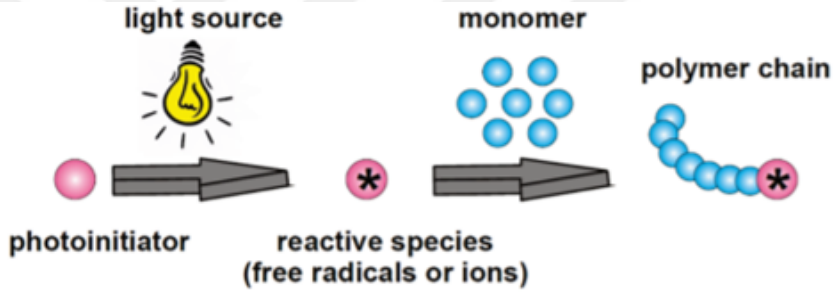


Figure 1.1. General process for photopolymerization. Permission from [14] American Chemical Society, Copyright (2010) (Figure A.1).

1.1.1. Free Radical Photopolymerization

A method that is frequently used for the manufacture of polymeric materials is called free radical photopolymerization. This approach is particularly useful in situations where its distinctive characteristics, such as spatial resolution and exact control of the process, are of high significance [23]. Upon exposure to light, the PI produces free radicals that start the process of polymerization. The multifunctional monomers like the ones with carbon–carbon double bonds undergo a chemical reaction where these double bonds are converted into single covalent bonds. This reaction leads to the formation of a three-dimensional polymer network that is cross-linked. Consequently, resulting structure gives the polymer advantageous characteristics such as enhanced mechanical strength, thermal stability, and resistance to solvents (Figure 1.2) [24-28].

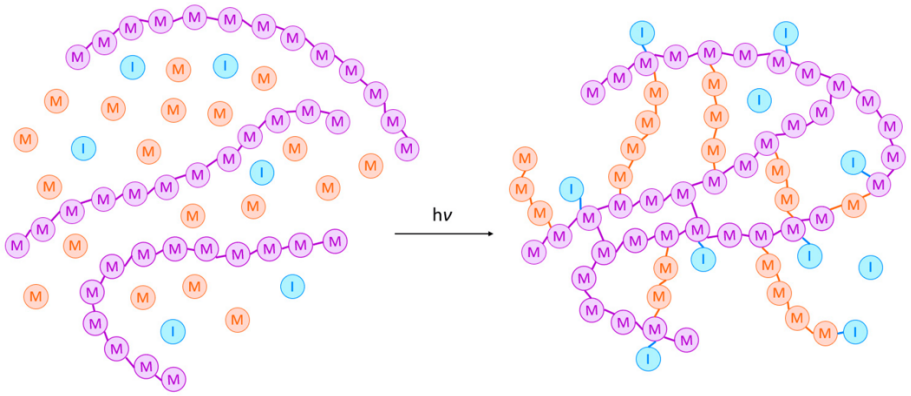


Figure 1.2. Illustration of photopolymerization reaction process resulting cross-linked polymer network where photoinitiators, monomers and oligomers are shown in blue, orange, and purple colors respectively [15]. Published under an open access.

The steps that are involved in free radical photopolymerization are initiation, propagation, and termination (Figure 1.3) [15].

During the first stage, known as photoinitiation, the PI system undergoes excitation upon light absorption, transitioning to a higher electronic state and generating radicals, either by cleavage or in the presence of an electron/hydrogen donor. [24,15]. In the second step, initiated free radicals react with monomer molecules containing double bonds and add them to the growing polymer. This process forms a new radical on the monomer molecule. The recently created radical can also interact with other monomer molecules, extending the polymerization chain which leads to the creation of cross-links between oligomers. The propagation process persists until termination occurs. [15], [28-30]. The last step where polymerization ends is called termination. This can happen in two different ways. These are combination termination and disproportionation reaction. In the former one, two radicals come together to form a stable new final polymer [31]. In the latter one, one of the radicals absorbs a hydrogen atom from the other radical and a stable new product and new radical species are formed [31]. These termination steps stop the propagation of polymer chains, leading to the formation of the final polymer product [29], [31,32].

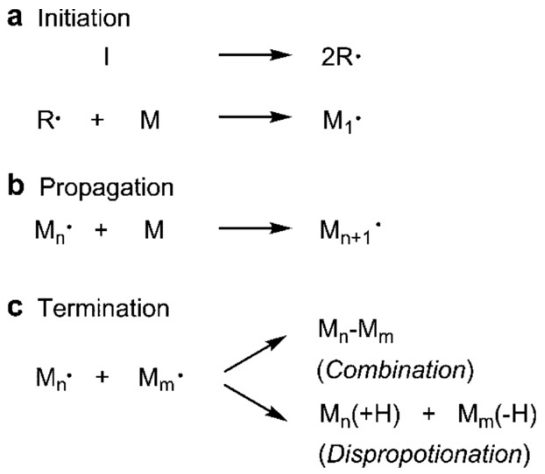


Figure 1.3. General reaction steps of photopolymerization. Permission from [33] American Chemical Society, Copyright (2015) (Figure A.2).

1.1.2. Free Radical Photoinitiators

Not all atoms can take part in photochemistry. Atoms and molecules are capable of absorbing a photon only if the energy difference between levels of their structure has exactly the same amount as the photon's energy [34]. Such molecules are called PIs. After absorption takes place, molecule's internal energy increases. Conversely, a molecule which was excited can release its energy in the form of a photon. Depending on the energy of the photon, these can result in a change in vibrational, electronic, or rotational energy levels [34,35]. The Jablonski diagram is a way to illustrate the changes between energy levels called as transitions (Figure 1.4) [36]. Firstly, a photon is absorbed by the PI and an electron goes from a ground state (S_0) to an excited state (S_n) which has higher energy [35]. At this point, there are different ways that can be followed. The singlet excited state can emit light while going back to ground state (fluorescence, $S_1 \rightarrow S_0$) [35]. It may also lose energy by heat (internal conversion (S→S) or intersystem crossing (S→T)). The triplet excited state may lose energy by light (phosphorescence ($T_1 \rightarrow S_0$) and it may lose energy by heat (internal conversion (T→T)) [35], [37]. Photochemical processes mostly take place from the excited triplet state T_1, involving isomerization, coupling, and bond cleavage reactions [35].

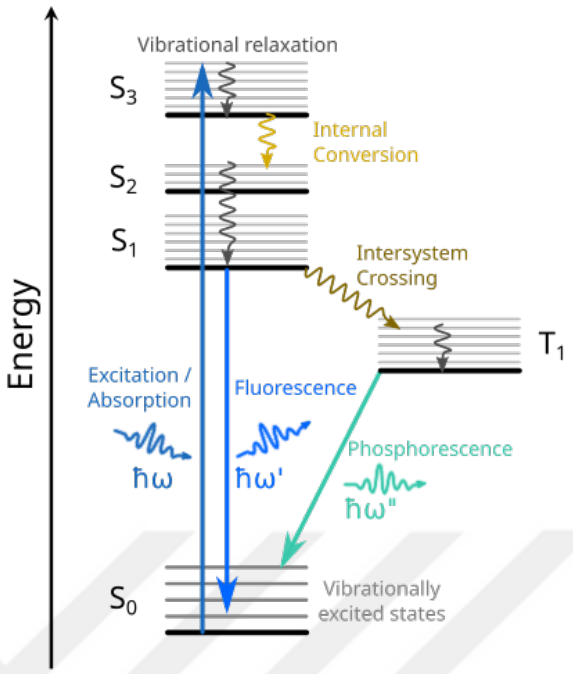


Figure 1.4. Jablonski diagram illustrating possible transitions between singlet (S) and triplet (T) valence excited states [36]. Published under an open access.

Considering that the photopolymerization reaction begins with light absorption, PIs appear to be the most important elements of this process. The choice of PI is crucial to achieve the required photopolymerization reaction rate and produce desired polymer properties such as non-yellowing properties, as it affects everything from the efficiency of the photopolymerization reaction to the final properties of the product [38]. Since the absorption range and quantum efficiency of the photochemical and photophysical processes occurring in excited states depend on the photoinitiator's structure, it can be said that there are two key parameters to consider when choosing a PI: maximum absorption wavelength (λ_{max}) and molar extinction coefficient (ε) [38,39]. Apart from these, there are some basic features that PIs should have no matter of the type of it (Figure 1.7): (i) nonyellowing property, (ii) non-cytotoxicity, (iii) good solubility in the polymerized composition, (iv) high quantum efficiency, (v) absorptivity in the emission range of the irradiation source, (vi) low odor and low migration property (thermal and temporal stability) [38,39].

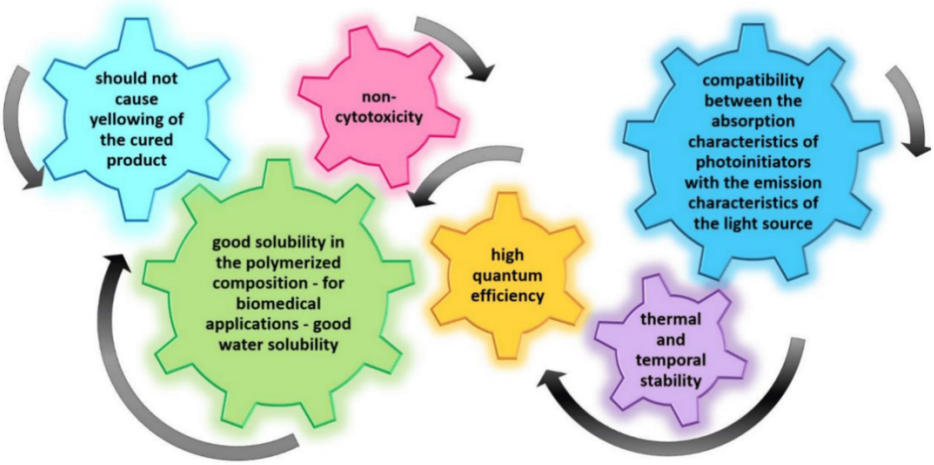


Figure 1.5 Criteria for photoinitiators [38]. Published under an open access.

There are two different pathways for radical formation, depending on the structure of the PI. If free radicals are formed in the process of homolytic photodissociation of the PI molecule, that initiator is called Type I PI [40]. On the other hand, if the excited initiator molecule reacts with the appropriate co-initiator such as an electron or a hydrogen donor in order to produce the radicals, this initiator is called Type II PI [41].

1.1.2.1. Type I Photoinitiators. In Type I photoreaction, which is also called Norrish I, two radicals which both can react with double bonds, are formed upon homolytic cleavage of PI molecule via absorption of light (Figure 1.6) [38]. This cleavage can occur at any week bond, but it typically happens at the α position of the carbonyl group (α-cleavage), and less frequently at the β position (β-cleavage) [42]. Hydroxyacetophenones (HAP's), benzylketals, benzoin derivatives, α- aminoalkylacetophenones (AAAP's) and phosphine oxides can be given as an example of the main chemical groups of Type I PI (Figure 1.7) [42,43].

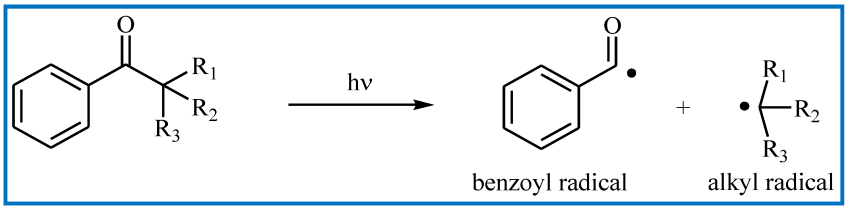


Figure 1.6. Photocleavage reaction of Type I PIs [43]. Published under an open access.

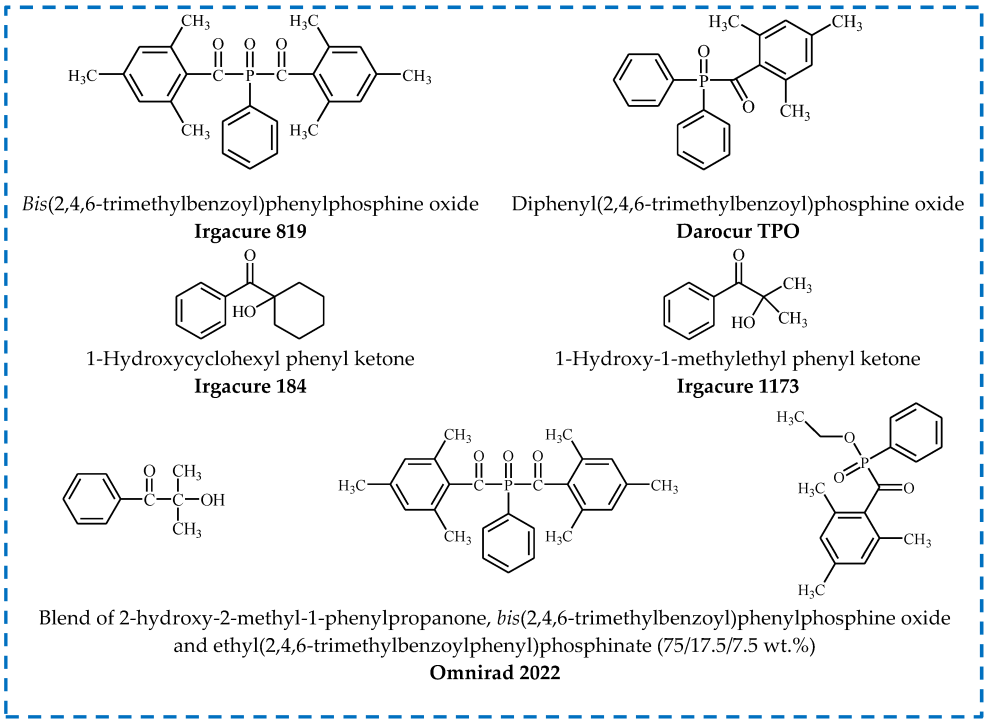


Figure 1.7. Type I PIs that are commonly used [43]. Published under an open access.

In this thesis, Irgacure 2959 (I2959), which is commercial PI, is used. It is an example of α-hydroxy ketones that have $1\pi\pi^* \rightarrow 1n\pi^* \rightarrow 3\pi\pi^* \rightarrow 3n\pi^*$ transitions in their photodissociation mechanism. The final transition is essential for the cleavage to the benzoyl and ketyl radicals [44-46].

1.1.2.2. Type II Photoinitiators. The photoinitiators that can absorb light and be excited but cannot spontaneously generate radicals because of high bond energies that carbonyl compounds have known as Type II PIs (Norrish II). That is why, there should be a coinitiator. In these systems, the initiation of polymerization can take place via hydrogen abstraction from an H donor as well as electron transfer from an electron donor (Figure 1.8) [42], [47]. After abstraction of light, one potential reaction pathway is based on hydrogen abstraction by the long-lived n-π* excited triplet state from the donor molecule. Consequently, the formation of a highly active donor radical occurs [43]. The other possibility is an electron transfer from the amine to the PI. Then the H is transferred from the coinitiator to PI. Since the ketyl radicals have low reactivity caused by delocalization of unpaired electron and sterical hindrance, the radical coupling takes place for the radical formed from PI. And the radical formed on the coinitiator initiate the polymerization [48]. Among Type II initiators,

the most popular are benzophenone, thioxanthone, camphorquinone and benzyl derivatives (Figure 1.9) [49].

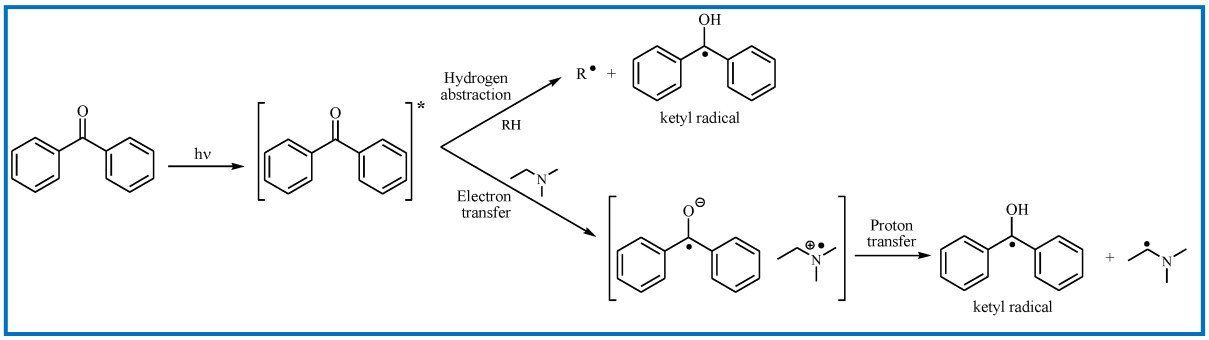


Figure 1.8. Photocleavage reaction of Type II PIs [43]. Published under an open access.

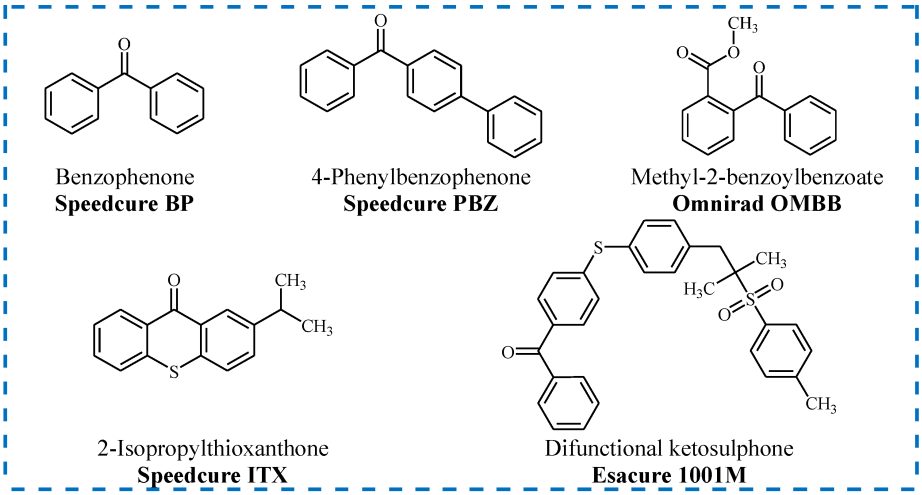


Figure 1.9. Type II PIs that are commonly used [43]. Published under an open access.

Unlike Type I photoinitiators, the effectiveness of Type II initiators is influenced by both their physico-chemical characteristics and the type of co-initiator used [43]. Tertiary amines are the most often used co-initiators, and they also function as oxygen scavengers. Other options, such as alcohols, ethers, and thiols, are available but are less effective [42], [48], [50].

1.1.3. Functionalized Photoinitiators

Despite its many advantages, photopolymerization also has some disadvantages. The main problem is that the photoproducts of both Type-I and Type-II PIs may undergo further reactions due to the instability of the radicals. On the other hand, the residues of PIs, the byproducts of their photodissociation, and/or co-initiators may leak out. These situations can affect both the efficiency of photoinitiation and the performance of the cured product. For example, some of these remaining small molecules may be colored or odorous and may migrate in the polymer networks and can cause serious problems in some application areas such as food packaging and biomedical applications (Figure 1.10) [51,52].

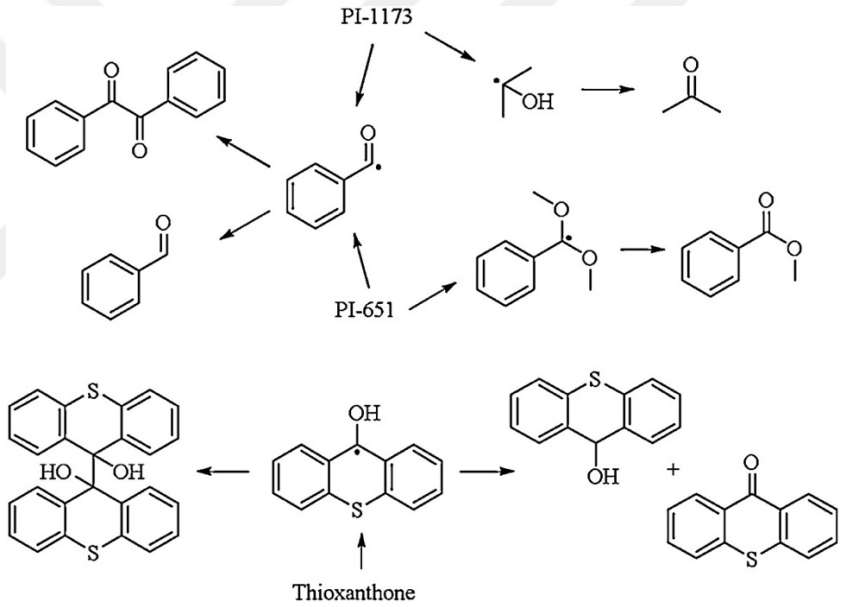


Figure 1.10. Examples of secondary reactions of photoinitiators. Permission from [51] Elsevier, Copyright (2019) (Figure A.3).

In recent years, there has been significant interest in the functionalization of photoinitiators to create materials with desirable features, such as greater biocompatibility, water solubility, improved absorption, and enhanced performance [21]. So, there have been many new improvements in the synthesis of novel PI molecules [53]. For instance, introduction of triethoxysilyl and epoxy functionalities to I2959 allows covalent coupling of photoinitiators to surfaces of different materials and trigger photopolymerization [54]. As another example, sulfide linkages on the phenyl rings enhance benzophenone and thioxanthone photoinitiators' extinction coefficient. They are evaluated as one-component

PI systems. Thus, the new derivatives are much more efficient compared to their unmodified analogs (Figure 1.11) [55]. Development of reactively functionalized monomeric and polymeric photoinitiators is two important fields in this regard [53]. These PIs have gained popularity lately as part of initiatives to make photopolymerization a more environmentally friendly process [54]. Cyclopolymerizable PIs with a 1,6-heptadiene structure can be said as another option. [51], [56,57].

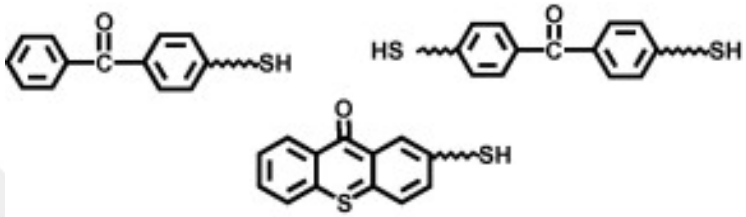


Figure 1.11. Thiol-functionalized photoinitiators. Permission from [55] Elsevier, Copyright (2010) (Figure A.4).

1.1.3.1. Monomeric and Polymeric Photoinitiators**.** One of the things that can be done to solve the above-mentioned problems is to use monomeric or polymeric PIs that are developed basically with the aim to reduce unwanted migration in the photocured matrix when small-molecule non-monomeric PIs are used [51]. In general, monomeric PIs can join to the final network via covalent bond, since they contain active polymerizable groups in their structures (Figure 1.12) [44].

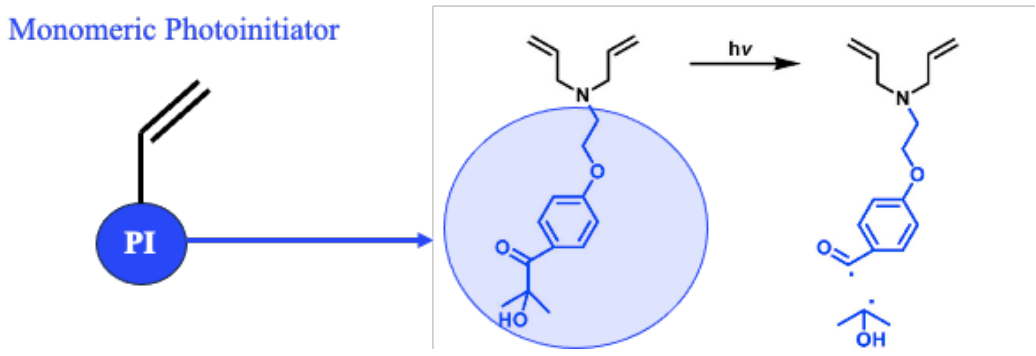


Figure 1.12. Monomeric photoinitiator and its cleavage. Permission from [44] Royal Society of Chemistry (2022) (Figure A.5).

Meanwhile polymeric PIs are less likely to migrate in the network because they are too large molecules containing pendant or in chain photoinitiating groups [52], [44,51]. In Figure 1.13. polymeric PIs are divided into three categories based on their molecular structure: multifunctional PIs, hyperbranched and cross-linked polymeric PIs (HCPPI), and linear polymeric PIs (LPPI). Several examples of polymerizable PIs [44],[47],[56], [57,58], and polymeric PIs [59-63] can be found in the literature.

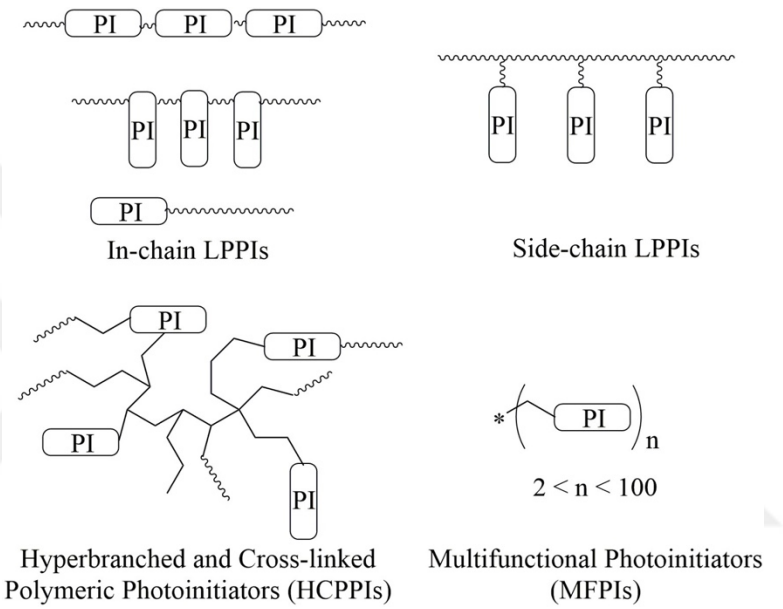


Figure 1.13. Examples of polymeric photoinitiators. Permission from [51] Elsevier, Copyright (2019) (Figure A.3).

For example, sulfur-containing polymerizable benzophenone PIs were synthesized. These initiators have the dual function of acting as both a PI and a polymerizable monomer. This means that they may generate radical species and also be used up during the free radical propagation process (Figure 1.14) [58].

Another literature example is the synthesis of a novel water-soluble polymerizable PI that can initiate both only photopolymerization and also take part in both stages of a one-pot dual curing process. It was named as PAATX. In the first part, it is used as the nucleophile and base for an aza-Michael reaction and later it is used as PI in conjunction with Iod (Figure 1.15) [62]. As a result, unlike other dual curing techniques documented in the literature to date, this processs does not need the inclusion of an amine during the first stage and/or a PI during the second [62].

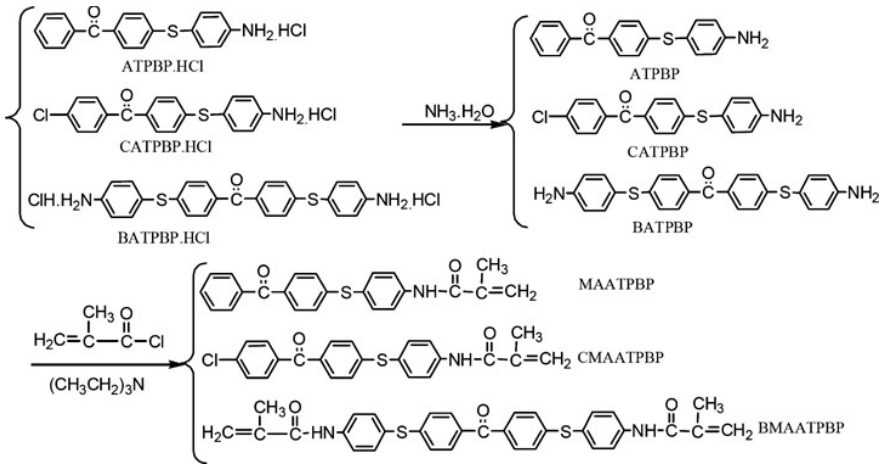


Figure 1.14. Synthesis pathways for polymerizable photoinitiators that contain. Permission from [58] John Wiley and Sons, Copyright (2006). (Figure A.6).

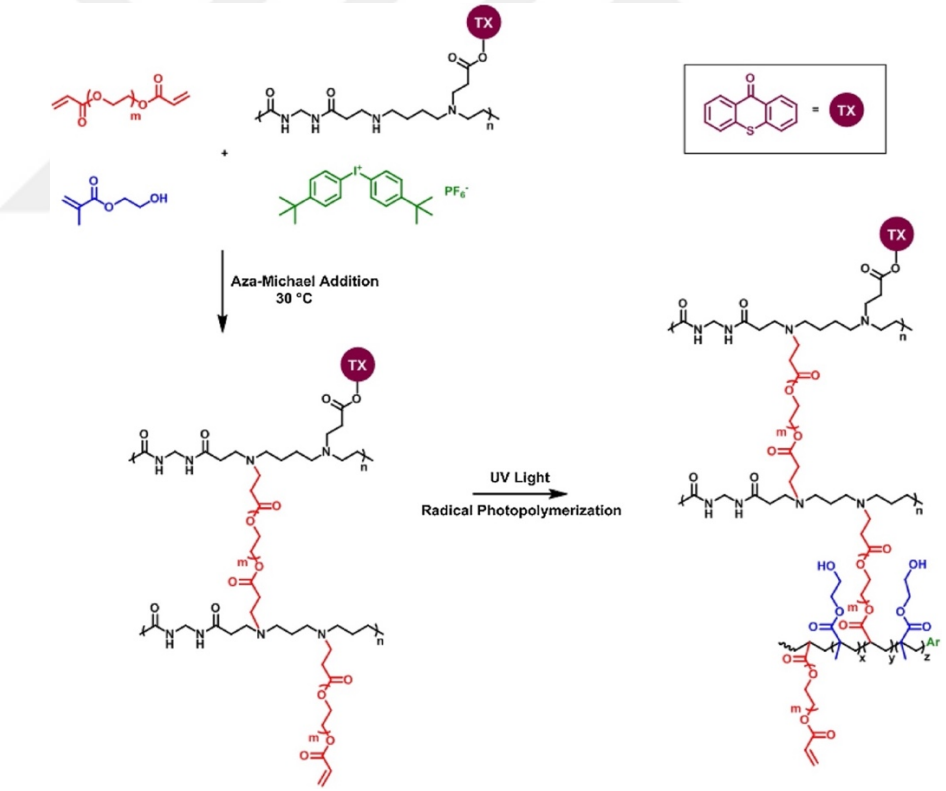


Figure 1.15. Synthesis pathways for polymerizable photoinitiators that contain. Permission from [62] Elsevier, Copyright (2020). (Figure A.7).

1.1.3.2. Cyclopolymerizable and Cyclopolymeric Photoinitiators. Another possibility for monomeric and polymeric PIs are cyclopolymerizable and cyclopolymeric ones. They are really important in comparison to their noncyclic counterparts, the cyclopolymers exhibit a number of favorable characteristics, including decreased polymerization shrinkage, excellent mechanical qualities, and comparatively high glass transition temperatures [64-67].

A noval mechanism for the polymerization of several polymers were discovered by Butler and his colleagues in the 1950s, while they were polymerizing diallyldimethylammonium bromide using peroxide initiators to form a cross-linked network. Although it was thought that unconjugated dienes form nonlinear, crosslinked polymers, their product was found to consist of linear chains of intramolecularly cyclized monomer. which was non-crosslinked and water soluble. Through further research on kinetic, fragmentation, and degradation, this has been confirmed that the polymerization process occurs by means of a series of alternating intra- and intermolecular chain propagations. This unique polymerization, which is for range divinyl, allyl-vinyl and diallyl monomers, is called cyclopolymerization. [68-73].

Chemical steps that are involved in cyclopolymerization can be summarized as intra-inter-molecular polymerization. First, an intramolecular radical cyclization takes place, and it continues with intermolecular propagation which is often resulting in polymer backbones with rings of varying sizes [65], [74]. Figure 1.16 shows initiated cyclopolymerization of seven atom center systems for an unidentified substituted diene. Five-membered rings are most common and easy to build [74]. Since the synthesis of a primary radical intermediate is needed to build the linear polymer, five-membered rings predominate. On the other hand, the creation of the six-membered ring structure requires the production of the secondary radical, which is more thermodynamically stable. Comparing the formation processes of five- and six-membered ring structures under conditions where the polymerization process is kinetically controlled, the latter would be less favorable due to the conformational structure of the intermediate obtained before polymerization occurs [74]. Additionally, there is possibility to form seven-membered ring structures, even though they are much less likely. Such ring structures need the development of a primary radical and then secondary radicals from seven-membered ring systems. As a result, directly connected rings form along

polymer backbones. This appears implausible due to the polymer's rigid backbone during formation [74].

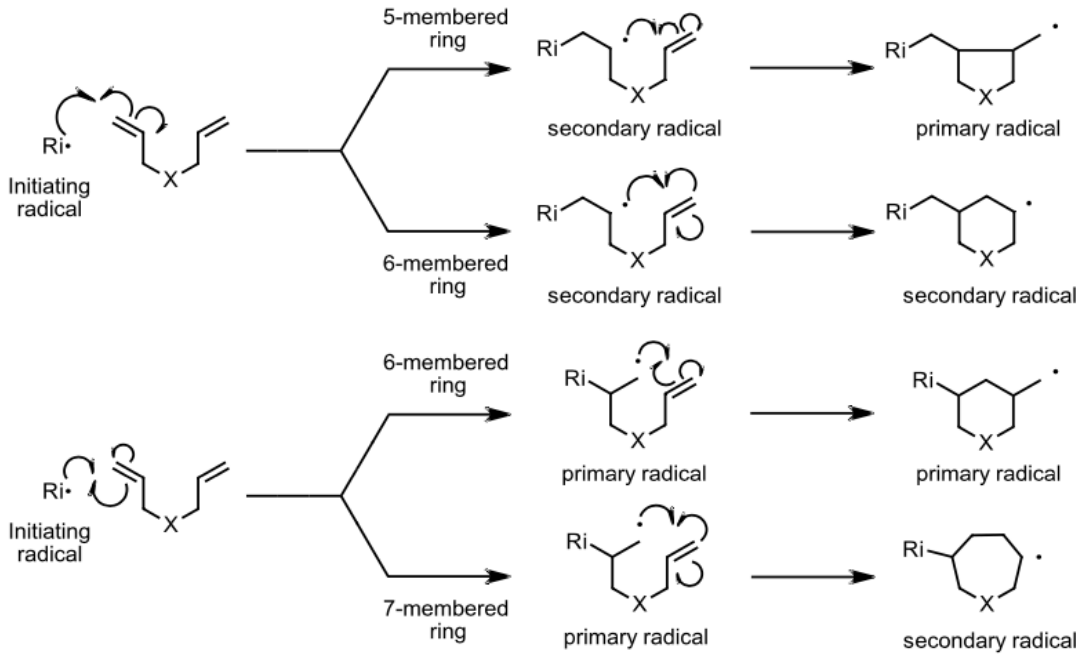


Figure 1.16. The photocyclization of substituted dienes with seven atom centers. Permission from [74] Royal Society of Chemistry (2004). (Figure A.8).

Many factors impact cyclopolymerization efficiency. Dilute solutions improve polymerization efficiency. Generally, bulky side groups are beneficial for cyclopolymerization, and they inhibit crystallization. Additionally, electron withdrawing groups next to the radically reactive double bond can boost vinyl or allyl molecular reactivity [75,76].

Compared to noncyclic linear analogs, cyclopolymers offer a number of beneficial features, including high glass transition temperatures, superior thermal stabilities, and minimal shrinkage during the polymerization process [52]. Among these advantages that cyclopolymerizable monomers provide, low shrinkage stress can be said as one of the most important benefits. Volumetric shrinkage which is the significant disadvantages of free radical polymerization can be explained as the changes in distance between the monomers during the polymerization process. In bulk, the monomers are separated by a distance of approximately 3.4 A (the Van-der-Waals distance). After polymerization, a covalent bond is formed resulting in a decrease in distance to around 1.5 A (Figure 1.17) [65]. Nevertheless,

the presence of cyclic units in the polymer backbone is able to reduce the volumetric shrinkage [65].

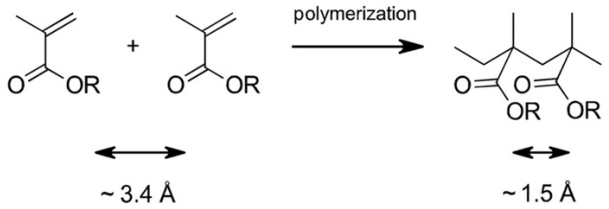


Figure 1.17. The volumetric shrinkage during photopolymerization. Permission from [65] John Wiley and Sons, Copyright (2021). (Figure A.9).

Like other polymerizable and polymeric photoinitiators, cyclopolymerizable and cyclopolymeric PIs initiate polymerization by generating radicals upon light exposure and participate in the polymer network formation. But as mentioned above, compared to noncyclic linear analogs, cyclopolymers offer a number of beneficial features, including high glass transition temperatures, superior thermal stabilities, and minimal shrinkage during the polymerization process [52]. As a result of its ability to impart favorable mechanical qualities to materials, the cyclopolymerization method has the potential to be utilized in a variety of fields, including the dentistry industry and 3D printing [65].

There are few examples of cyclopolymerizable and cyclopolymeric PIs in the literature. One of them, which is also the first TX-based PI that has 1,6-heptadiene structure with two active acrylic acid groups was reported by Eren et al [52]. While acid components that make monomer polymerizable and crosslinkable bring surface attachment ability, 1,6-heptadienes structure allows cylcopolymerization depending on concentration and/or temperature. Additionaly since it has not only TX chromophore but also hydrogen donating tertiary amine functionality on its structure, it does no need co-initiator during photopolymerization process (Figure 1.18) [52].

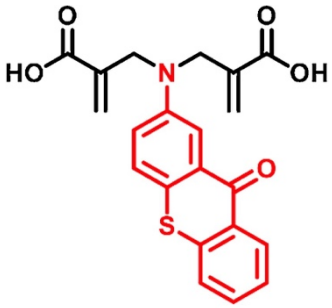


Figure 1.18. Structure of the novel monomeric photoinitiator synthesized by Eren et al [52]. Permission from [52] Elsevier, Copyright (2019). (Figure A.10).

Another example is I2959 and diallyl amine based novel cyclopolymerizable and cyclopolymeric PIs that were synthesized by Balaban et al [44]. First of all, attaching diallyl amine groups to the commercial PI I2959 creates cyclopolymerizable PI DAA-I2959, which prevents the photoinitiating groups from migrating out of the polymer network. Then the copolymerization of DAA-I2959 with diallyldimethylammonium chloride (DADMAC) is resulted in novel water soluble polymeric PI which is the first PI with a cyclic backbone in the literature (Figure 1.19) [44].

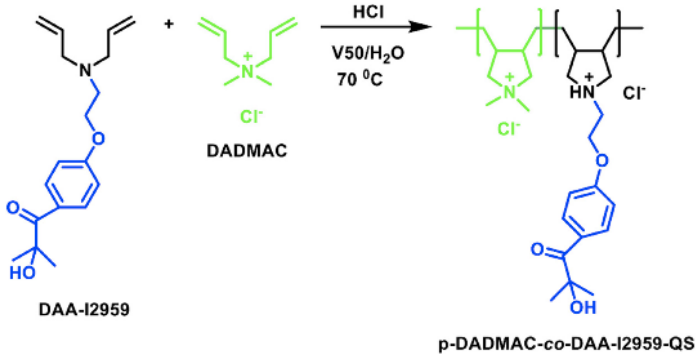


Figure 1.19. Synthesis of cyclopolyemeric photoinitiator. Permission from [44] Elsevier, Copyright (2019) (Figure A.5).

1.2. Non-Steroidal Anti-Inflammatory Drugs

Drug discovery may be defined as the process of finding chemical entities with the potential to be therapeutic agents [77]. Use of herbs as therapeutics “Medical herbs”, dates back to ancient cultures as well as to the emergence of human civilization [83]. “Drug”, derived from French “Drogue”, meaning “dry herb”, clearly implies that the first medications were mostly plant-based [79], although animal products, minerals were occasionally used. Starting from plants, today's advanced pharmacology has come a very long way to create [78].

Drugs may be classified based on their structural characteristics, pharmacological action, chemical nature, or chemical similarity. They are divided into various categories, such as antibiotics, antacids, antigas medicines, wormicides, steroid medicines, and more [80]. One of these classes of medications is non-steroidal anti-inflammatory drugs (NSAIDs). These drugs are among the most frequently prescribed drugs in modern medicine [81]. The evolution of NSAID's begins with the usage of salicylate-containing willow leaves which were used for treating inflammatory rheumatic diseases dating back to the Sumerians and continues with highly selective cyclooxygenase-2 (COX-2) inhibitors [82]. The importance of the willow leaf and bark extracts of the Salix plants against inflammatory symptoms have been transmitted from generation to generation (Figure 1.20) [82, 83]. One of the most important points on this timeline is the synthesis of acetylsalicylic acid by Dr FeIix Hoffman that was resulted in the birth of Aspirin in 1897. Aspirin is the progenitor of NSAIDs and has been the most widely used pharmaceutical since then [82], [84].

The success of aspirin in the pharmaceutical industry led the development of more NSAIDs. Eventually, phenylbutazone, indomethacin, and ibuprofen were introduced to the market [82]. These non-steroidal anti-inflammatory drugs, which have significant antipyretic and anti-inflammatory effects, are used to relieve acute pain and as antipyretics. They are frequently used in the treatment of conditions such as musculoskeletal system traumas, rheumatoid arthritis, osteoarthritis and ankylosing spondylitis [85]. The main effect of these drugs is to inhibit cyclooxygenase (COX) enzymes, namely COX-1 and COX-2. In

this way, they affect the synthesis of prostaglandins, which have an important role in inflammation signaling [86].

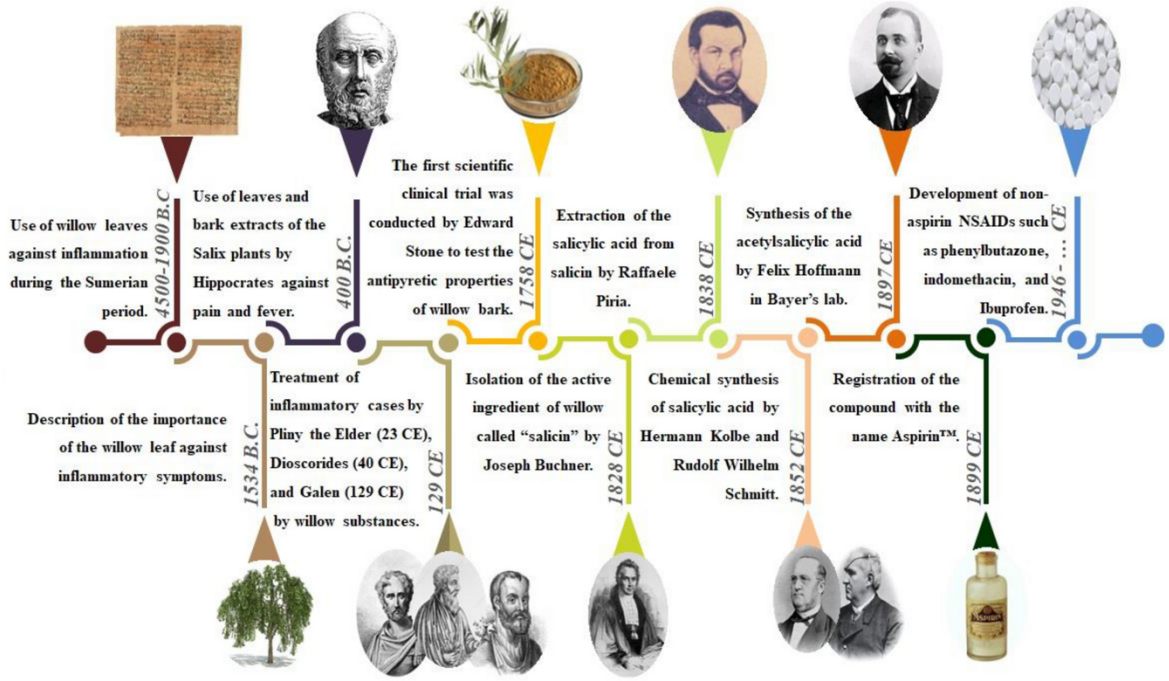


Figure 1.20. The development of NSAIDs in chronological order. Permission from [82] Springer Nature, Copyright (2022) (Figure A.11).

1.2.1. Classification of NSAIDs

There are many NSAIDs that have a wide range of structural and functional variations. These drugs are mostly weak organic acids with aromatic functional groups [87]. Functional diversity is determined by the selectivity of isoform-specific inhibition of COX. Another categorization considers the bioavailability of NSAIDs in the serum, which takes into consideration the pharmacokinetic characteristics of NSAID activity in the systemic setting [87].

According to chemical structure, NSAIDs can be classified into five groups as salicylic acid derivatives, aryl and heteroarylacetic acid derivatives, indole/indene acetic acid derivatives, anthranilic acid derivatives, and enolic acid derivatives (Figure 1.21) [87,88].

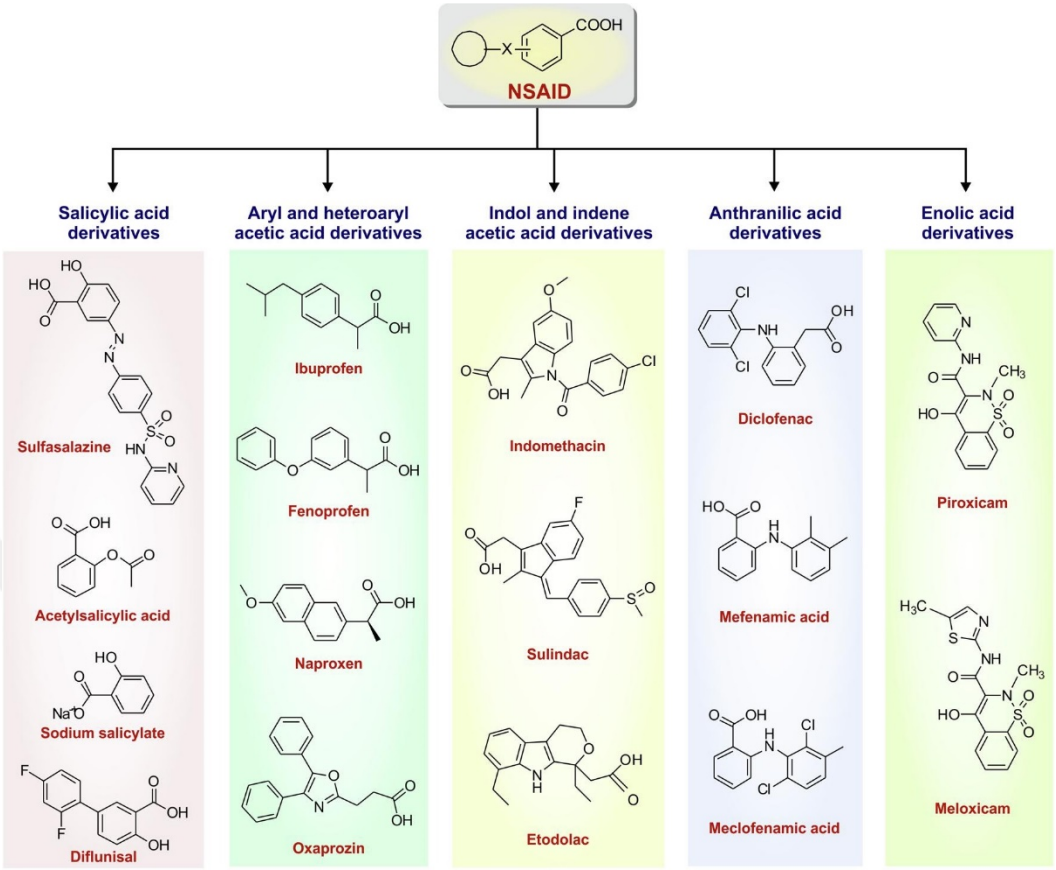


Figure 1.21. Structural based classification of non-steroidal anti-inflammatory drugs (NSAIDs). Permission from [87] Elsevier, Copyright (2020) (Figure A.12).

NSAIDs can also classified the basis of plasma half-life (t½). There are short-acting drugs like aspirin, diclofenac and ibuprofen which have plasma half-life less than 6 h. These NSAIDs are good for acute pain. And there are long-acting drugs such as naproxen, celecoxib which are suitable for treating chronic conditions [89].

Furthermore, they may also be categorized based on their selectivity. They can be non-selective NSAIDs which inhibit both COX-1 and COX-2 enzymes to a significant degree [90]. Non-selective NSAIDs are the most popular drugs used to treat a wide range of diseases that cause pain, swelling, and fever [91]. Selective NSAIDs, on the other hand, block COX-2 more than COX-1, an enzyme that is usually found in the stomach, blood platelets, and blood vessels. COX-2 is found in places where there is inflammation While there are many examples of non-selective NSAIDs (diflunisal, etodolac, fenoprofen, ibuprofen etc.), selective ones are few (celecoxib, rofecoxib, valdecoxib etc.) [87], [92-96].

1.2.2. Side effects of NSAIDs

NSAIDs have a lot of healing benefits as discussed above. Furthermore, they have the potential to be used in the prevention and treatment of some types of cancer due to the relationship between inflammation and cancer development [99]. Nevertheless, several studies in the past have demonstrated the detrimental consequences of overdose on NSAIDs on different systems of the body, including the cardiovascular, gastrointestinal, hepatic, renal, and neurological systems (Figure 1.22) [92], [100]. These side effects result from suppression by NSAIDs of the synthesis of prostaglandins, which do not only cause painful inflammation but also have important physiological functions [101]. Still, the short-term use of NSAIDs is generally well tolerated. But due to their short half-life, frequent doses to maintain treatment efficacy are needed over long time periods [89], in which case, the above-said side effects can appear.

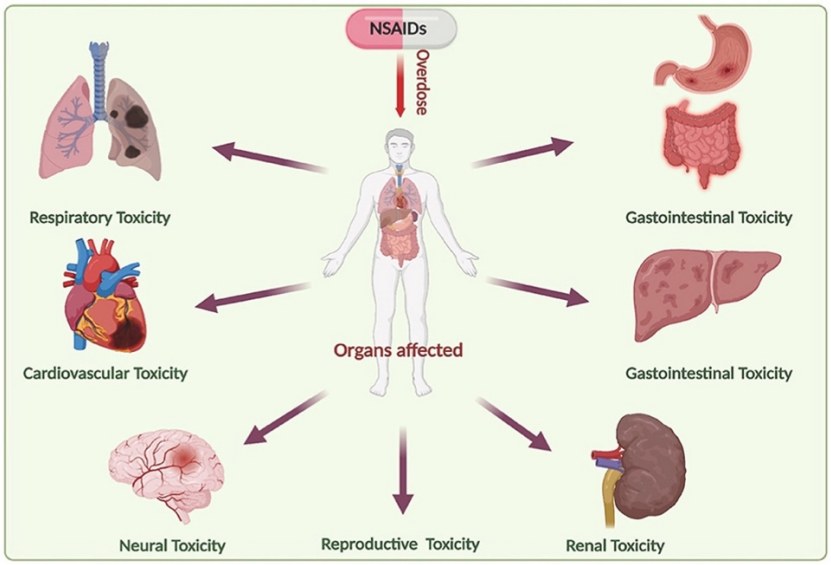


Figure 1.22. Organs affected by overdose usage of NSAIDs. Permission from [100] Elsevier, Copyright (2023) (Figure A.13).

Various solutions have been produced to get rid of these side effects. One approach to them is tissue targeting, that is, blocking the activity of the drug until it reaches the target tissue, which preserves its potential, and ensuring its release once it reaches the target [102]. As a result, localized drug delivery vehicles offer significant benefits as they completely remove off-target effects and lead to lower doses to attain the desired concentration in the specific area of treatment [102]. Hydrogels, microparticles, microspheres, films/membranes,

and fibers can be used to deliver drugs [102]. In the literature there are many examples of localized and targeted delivery of NSAIDs, in fact many other drugs as well. For example, electrospun nanofibers made of temperature-responsive poly(N-isopropylacrylamide) (pNIPAM) and biodegradable poly(ε-caprolactone) (PCL) were used to release ibuprofen slowly without a burst effect. Using electrospinning methods, three types of nanofibers were made: PCL, pNIPAM, and pNIPAM/PCL hybrid NFs with ibuprofen [103].

Another method which addresses the short half-life issue of NSAIDs can be the synthesis of polymeric prodrugs. This can be achieved via adding the drug molecule to a polymer with a covalent or similar strong bond. In this way, releasing the drugs involves breaking down chemical bonds by biological methods [101], [104]. Furthermore, conjugating bioactive compounds to synthetic or natural polymers is thought to be a way to decrease the toxicity of the bioactive molecules while also improving treatment efficiency [105,106]. As a literature example, the synthesis of polymeric naproxen prodrug can be given. Naproxen which is one of the most widely used NSAIDs is linked to 2-hydroxyethyl methacrylate (HEMA) by hydrolysable ester linkages (Figure 1.23) [107]. After polymerizing the produced NP-HEMA, a polymeric prodrug can be obtained. This prodrug can hydrolyze ester bonds to sustainably cleave the parent drug, maintaining plasma levels within the therapeutic range. The release profile was seen to depend on the pH value of the hydrolysis solution. So, this can be called a useful controlled release system where the controlling factor is the pH [107].

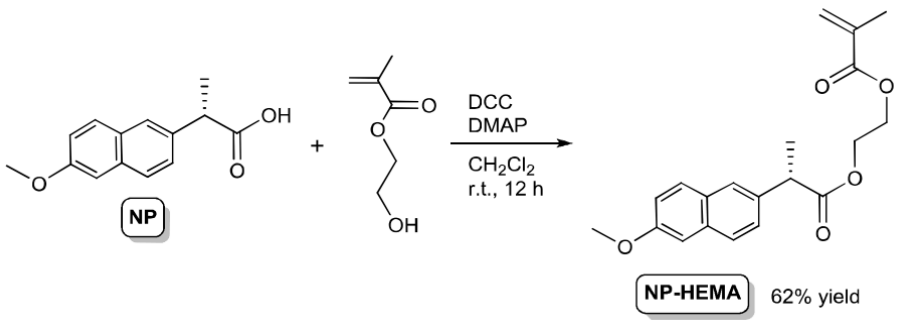


Figure 1.23. The synthesis HEMA derivative of naproxen (NP-HEMA). [107]. Published under an open access.

1.2.3. Arylpropionic Acid Derived NSAIDs

An important subclass of NSAIDs are arylpropionic acid derivatives. They are 2-arylpropionic acid (2APA) derivatives called profens. Profens consist of a wide range of drugs, including ibuprofen, ketoprofen, naproxen, fenoprofen, flurbiprofen, carprofen, suprofen, benoxaprofen, pranoprofen, and tiaprofenic acid. Except for tiaprofenic acid, all profens have a phenyl ring directly attached to the α-carbon of propionic acid (Figure 1.24) [108].

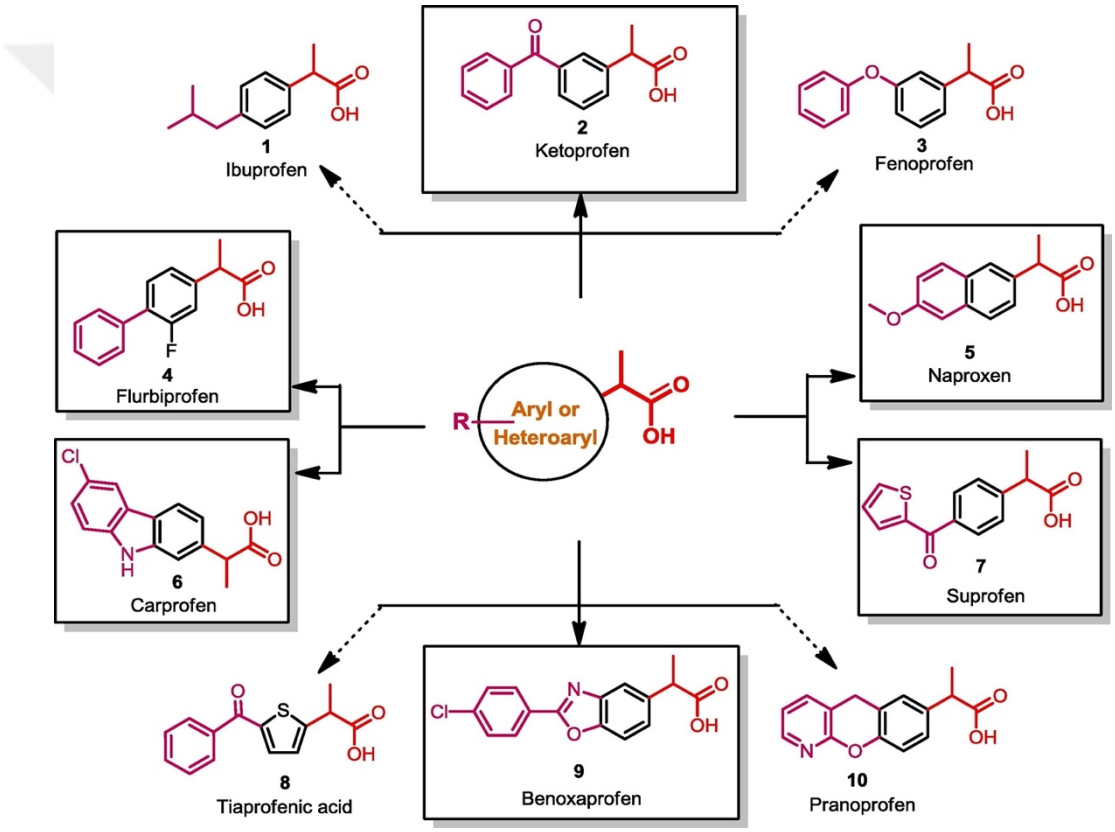


Figure 1.24. Chemical structure of profens. Permission from [108] Elsevier, Copyright (2019). (Figure A.14).

These derivatives contain a chiral carbon atom in the propionic acid side chain and exist as two enantiomers, namely S- and R-enantiomers. So, their biological activities are stereospecific [109,110]. The R-enantiomer is considered to be less active or not work at all as an anti-inflammatory. On the other hand, the S-enantiomer is the isomer that has more biological activity as an anti-inflammatory drug. Despite being so functionally different from each other, these enantiomers are sold as a racemic mixture [108]. But there is an ezyme

called isomerase that can convert R-enantiomer to the S-enantiomer and brings beneficial results [111]. Some 2APAs' R-enantiomer showed cancerous action. Because of this, 2APAs are mixed as a racemic mixture to treat inflammation or prevent the formation of cancer [108], [111].

Profens are a notable NSAID subclass used for analgesia, antipyrexia, and anti-inflammatory effects. Additionally, they have shown different biological actions unrelated to inflammation or COX inhibition. For example, it was discovered that ibuprofen and carprofen could inhibit the growth of the Mycobacterium tuberculosis complex [112].

1.2.4. Ibuprofen

In this thesis, ibuprofen was used as the parent drug. In the 1960s, Boots Group developed ibuprofen while searching for a safer NSAID than aspirin [113]. It is used in the treatment of many diseases such as rheumatoid arthritis, traumatic soft-tissue inflammation dysmenorrhea, and for headaches thanks to its analgesic, antipyretic, and anti-inflammatory effects. But stomach ulcer sufferers should avoid it. [114].

1.2.4.1. Derivatives of Ibuprofen. To achieve intended concentration in the target area, a high dosage or too frequent dosing is required, which may lead to adverse effects, due to potential side effects discussed above. [115]. Ibuprofen is characterized by a relatively poor solubility (21 mg dm^{-3} in water at 25 degrees Celsius), especially in the acidic environment of the stomach (0.024 mg cm^{-3} at pH 2.2 and 14.8 mg dm^{-3} at pH 9.2) [116,137].

In the literature, many examples of new derivatives with similar pharmaceutical activity but increased solubility and bioavailability and therefore rapid pain relief can be found to solve such problems [116-121]. In one example, a study has been conducted on the release of ibuprofen from a polymeric nanoparticle system that was created via ring-opening metathesis polymerization. The release was regulated by the architecture of the system and triggered by changes in pH. Polymers with block and random sequence topologies were generated using the co-polymerization of norbornene-derived ibuprofen (NB-Ibu) and poly(ethylene glycol) (NB-PEG) monomers. The management of self-assembly into

nanoparticle systems and the release of ibuprofen only under basic conditions was shown to be controlled by the polymer sequence (Figure 1.25) [122].

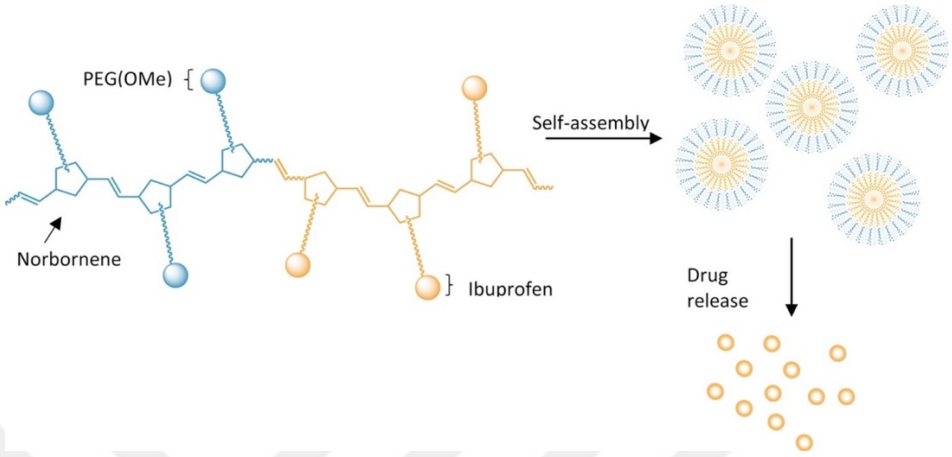


Figure 1.25. Representation of ibuprofen release from a polymeric nanoparticle system. Permission from [122] Elsevier, Copyright (2020) (Figure A.15).

2. OBJECTIVES

First part of this work aims to synthesize and evaluate new photoinitiators with the following desirable properties: multifunctionality, migration stability, high photoinitiation efficiency and high thermal stability. Using I2959 as the parent PI: (i) two novel *tert*-butyl α-hydroxymethacrylate-based cyclopolymerizable PIs with 1,6-heptadiene structure and one photoinitiating cyclocopolymer with six-membered rings in the backbone and (ii) two novel AHM-based (di)methacrylate PIs were synthesized and characterized. The polymerizable or polymeric nature of PIs is expected to provide high migration stabilities compared to I2959. The structure-photoinitiation reactivity relationships of the PIs and their photophysical and photochemical properties were investigated.

The aim of the second part is to synthesize novel ibuprofen pro-drugs with enhanced bioavalibility and controlled drug release rate to target inflamed or cancerous tissues so that side effects of ibuprofen can be alleviated. Using ibuprofen as a parent drug: (i) two novel ibuprofen cystamine salts and (ii) an alkyl α-hydroxymethacrylate-based ibuprofen and disulfide-functional crosslinking monomer/prodrug and its PEGDA hydrogel were synthesized and characterized. The solubility and the cytotoxicity of the synthesized salts and hydrolytic release of ibuprofen in phosphate buffer saline were investigated.

3. STRUCTURE-REACTIVITY RELATIONSHIPS OF NOVEL α-HYDROXYKETONE-FUNCTIONALIZED CYCLOPOLYMERIZABLE AND CYCLOPOLYMERIC PHOTOINITIATORS

The work described in this section has been published as: Denizkusu S., Dolgun M., Ozen S., Morlet-Savary F., Lalevee J., Avci D., "Structure-Reactivity Relationships of Novel α-Hydroxyketone-Functionalized Cyclopolymerizable and Cyclopolymeric Photoinitiators", *Journal of Photochemistry and Photobiology A: Chemistry*, Vol.451, 2024, 115520.

3.1.Introduction

This chapter focuses on the synthesis of two cyclopolymerizable photoinitiators (I2959-NTBDA, I2959-NDAA) based on 2-hydroxy-4'-(2-hydroxyethoxy)-2-methylpropiophenone (I2959) and a cyclopolymeric PI (p-BA-NTBDA-*co*-I2959-NTBDA) (Figure 3.1). Monomeric and cyclopolymeric PIs enhance the mechanical properties of the products by contributing to crosslinked network formation and by their backbones containing 6-membered rings respectively. These PIs overcome the low migration stability of commercial I2959. An investigation was carried out to examine the solubility, UV absorbance, photoinitiation efficiency, photolysis, migration and thermal stabilities of the synthesized PIs.

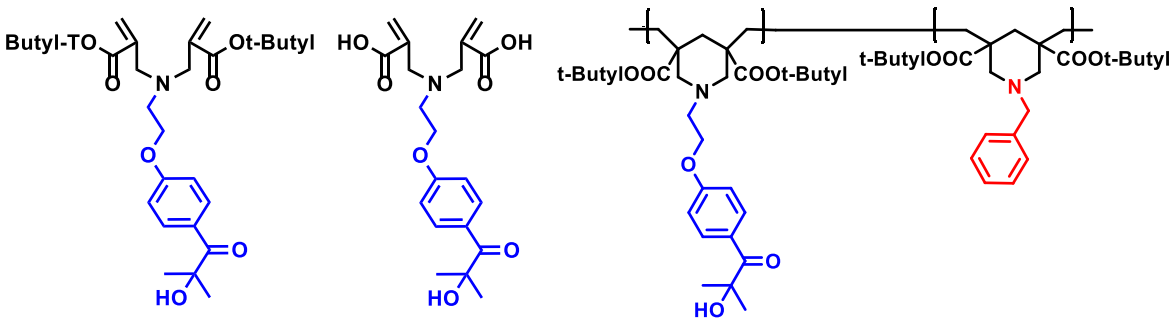


Figure 3.1. Structures of synthesized PIs (I2959-NTBDA, I2959-NDAA and p-BA-NTBDA-*co*-I2959-NTBDA).

3.2. Experimental

3.2.1 Materials and Characterization Methods

I2959, p-toluenesulfonyl chloride (TsCl), triethylamine, trimethylol propane triacrylate (TMPTA), 2-hydroxyethyl methacrylate (HEMA), poly(ethylene glycol) diacrylate (PEGDA, M_n = 575 D), thioxanthone (TX), ethyl 4- (dimethylamino) benzoate (EDB), benzylamine and the other reagents and solvents were purchased from Sigma-Aldrich and used as received. 2-(4-(2-hydroxy-2- methylpropanoyl)phenoxy)ethyl 4-methylbenzenesulfonate (I2959-Ts) and *tert*-butyl α- bromomethacrylate (TBBr) were synthesized according to literature procedures [123,124].

NMR spectra were recorded in $CDCl_3$ at ambient temperature with a Varian Gemini (400 MHz) spectrometer. The chemical shifts are represented in ppm downfield from TMS signal, using residual chloroform (7.26 ppm in ^{1}H NMR) as an internal standard. A Nicolet 6700 FT-IR spectrophotometer fitted with an attenuated total reflectance (ATR) accessory was used to obtain IR spectra. UV-vis spectra were recorded on a Varian®Cary 3 spectrometer. Malvern VISCOTEK gel permeation chromatograph (GPC) was used to determine the molecular weight of the synthesized polymeric PI with a refractive index detector. Molecular weights were calculated using polystyrene standards. Thermal gravimetric analysis (TGA) of the copolymer was carried out using Mettler Toledo TGA in the temperature range between 25-700 °C under nitrogen.

3.2.2. Synthesis of Photoinitiators

3.2.2.1. Synthesis of I2959-NTBDA. The starting materials of this PI, 1-(4-(2-azidoethoxy)phenyl)-2-hydroxy-2- methylpropan-1-one (I2959-N_3) and 1-[4-(2-aminoethoxy)phenyl]-2-hydroxy-2- methylpropan-1-one (I2959-NH_2), were synthesized according to procedures described in the literature [125,126]. I2959-NH_2 (0.069 g, 0.31 mmol) and K_2CO_3 (0.152 g, 1.1 mmol) were dissolved in a mixture of dimethylformamide (DMF) (0.174 mL) and tetrahydrofuran (THF) (0.48 mL) in an ice bath. To this solution TBBr (0.252 g, 1.14 mmol) was added dropwise. After stirring at 65 °C for 2 days, the solvent was removed under reduced pressure. Distilled water (5 mL) was added to the residue and extracted with dichloromethane (DCM) (3 x 5 mL). The organic phases were combined, dried over anhydrous Na_2SO_4, filtered and solvents were removed under reduced pressure. Column chromotography (silica gel, hexane-ethyl acetate: 90/10) was used for further purification to obtain the product as a colorless viscous liquid in 52% yield.

^{1}H-NMR ($CDCl_3$, 400 MHz, δ): 1.45 (s, 9H, $(CH_3)_3C$), 1.64 (s, 6H, $(CH_3)_2$-C-OH), 2.9 (t, 2H, CH_2-N), 3.35 (s, 4H, CH_2-N), 4.10 (2H, t, CH_2-O), 5.75 (s, 2H, CH_2=C), 6.10 (s, 2H, CH_2=C), 6.90 (d, 2H, Ar-H), 8.13 (d, 2H, Ar-H) ppm.

^{13}C-NMR ($CDCl_3$, 400 MHz, δ): 28.30 (*C*H_3-C), 28.53 (*C*H_3-C-OH), 52.83 (*C*H_2-N), 55.07 (*C*H_2-N), 62.54 (*C*H_2-O), 76.91 (*C*-$(CH_3)_2$), 80.63 (*C*-$(CH_3)_3$), 114.01 (Ar-*C*H), 124.67 (*C*H_2=C), 133.59 (Ar-*C*), 138 (Ar-*C*H), 140.66 (*C*=CH_2), 162.64 (Ar-*C*-O), 166.09 (O-*C*=O), 202.43 (Ar-*C*=O).

FTIR (ATR): 3426 (O-H), 2962 (C-H), 1707 (C=O, ester), 1667 (C=O, ketone), 1634 (C=C), 1599 (Ar, C=C), 1150 (C-O) cm^{-1}.

3.2.2.2. Synthesis of I2959-NDAA. To I2959-NTBDA (0.039 g, 0.077 mmol) excess TFA (2.6 mL) was added dropwise at 0 °C and stirred at room temperature for 4 h. Thereafter, TFA was evaporated, and the crude product was purified by washing with diethyl ether and dichloromethane to yield the pure product as a white solid in 76% yield.

^{1}H-NMR ($CDCl_3$, 400 MHz, δ): 1.50 (s, 6H, $(CH_3)_2$-C-OH), 3.68 (t, 2H, CH_2-N), 4.18 (s, 4H, CH_2-N), 4.47 (t, 2H, CH_2-O), 6.25 (s, 2H, CH_2=C), 6.64 (s, 2H, CH_2=C), 7.03 (d, 2H, Ar-H), 8.22 (d, 2H, Ar-H) ppm.

FTIR (ATR): 3436 (O-H), 1669 (C=O, carboxylic acid, ketone), 1598 (Ar, C=C) cm^{-1}.

3.2.2.3. Synthesis p-BA-NTBDA-*co*-I2959-NTBDA. I2959-NTBDA was copolymerized with BA-NTBDA (benzyl amine derivative of TBBr) in 10:90 mol% ratio using thermal polymerization in bulk. BA-NTBDA was synthesized using a procedure similar to that for I2959-NTBDA as follows: Benzylamine (0.10 g, 0.93 mmol) and K_2CO_3 (0.22 g, 1.59 mmol) were dissolved in a mixture of DMF (0.26 mL) and THF (0.70 mL) in an ice bath. To this solution TBBr (0.364 g, 1.65 mmol) was added dropwise. After stirring at 65 °C for 2 days, solvent was removed under reduced pressure. Distilled water (5 mL) was added to the residue and extracted with DCM (3x 5 mL). The organic phases were combined, dried over anhydrous sodium sulfate, filtered and solvent was evaporated under reduced pressure to give the pure product as a white solid in 20% yield.

^{1}H-NMR ($CDCl_3$, 400 MHz, δ): 1.45 (s, 9H, $(CH_3)_3$C), 3.24 (s, 4H, CH_2-N), 3.59 (s, 2H, CH_2- N), 5.86 (s, 2H, CH_2=C), 6.14 (s, 2H, CH_2=C), 7.24 (m, 5H, Ar-H).

I2959-NTBDA (23.6 mg, 0.047 mmol), BA-NTBDA (163.43 mg, 0.42 mmol) and AIBN (4.08 mg, 0.025 mmol) were placed in a test tube, which was then immersed in an oil bath at 75 °C. The solution was purged with nitrogen for 15 min. After 2-4 hours, dichloromethane was added to dissolve the polymer. Then the polymer was precipitated by adding the solution to a large excess of methanol and dried under vacuum.

3.2.3. UV-visible absorption measurements

The UV-visible absorption measurements were performed in a Cary 3 UV/vis spectrophotometer in the wavelength range of 200–500 nm using 10 mm quartz cuvettes. For photolysis experiments, chloroform solution of I2959-NTBDA and p-BA-NTBDA-*co*-I2959- NTBDA; methanol solution of I2959-NDAA were irradiated with a 320-500 nm light

source (Omnicure 1000, 150 W, 50% intensity). The UV–visible absorption spectra were recorded at different irradiation times.

3.2.4. ESR Spin Trapping (ESR-ST) Experiments

Electron spin resonance (ESR-ST) experiments were performed using a Bruker EMX-plus spectrometer. Toluene solutions of PIs were deoxygenated with nitrogen 15 min prior to measurements and irradiated with UV-vis light (Omnicure 1000, 150 W, 50% intensity) at 320- 500 nm. The radicals generated were captured by phenyl-N-*tert*-butylnitrone (PBN). The ESR spectra simulations were carried out with the WINSIM program.

3.2.5. Photoinitiating Activity Measurements

For photopolymerization experiments, a TA Instruments DSC 250 differential scanning photocalorimeter with an Omnicure 2000 light source equipped with a 320-500 nm filter was used. HEMA, PEGDA (Mn = 575 D) or TMPTA (3-4 mg) containing 1 wt% of PIs or the references were exposed to irradiation at 25 °C under nitrogen. The heat flow was monitored as a function of time, and the polymerization rate was calculated as

$$\text{Rate} = \frac{(Q/s)M}{n(\Delta H_p)m} \tag{3.1}$$

where Q/s is the heat flow per second, M the molar mass of the monomer, n the number of double bonds per monomer molecule, ΔH_p the heat of reaction evolved and m the mass of monomer in the sample [127]. The theoretical heat for the total conversion of a methacrylate and acrylate double bonds are 55 and 86.5 6 kJ mol^{-1}.

3.2.6. Migration Studies

PEGDA (M_n = 575 D) was photopolymerized in the presence of I2959 (1 wt%) and I2959- NTBDA (1 wt%) via UV irradiation, using a photoreactor (Kerman UV/18) containing 12 Philips TL 8 W BLB lamps with light emission at 365 nm, for 1 h in glass vials under air. The crosslinked polymers were soaked in 25 mL chloroform for 3 days. The percentages of the extracted PIs were determined by UV–vis spectroscopy [128].

3.2.7. Color Analysis

The color parameters L*, a* and b* of PEGDA samples photopolymerized using 1 wt% of I2959, I2959-NTBDA and I2959-NDAA (UV irradiation, using a photoreactor (Kerman UV/18) containing 12 Philips TL 8 W BLB lamps with light emission at 365 nm) were measured after curing with a chromometer (Model CR-400, Konica Minolta Sensing Inc., Tokyo, Japan). The instrument was calibrated using a standard white calibration plate (CRA43, Konica Minolta Sensing Inc., Tokyo, Japan) [129].

3.3. Results and Discussion

3.3.1. Synthesis and Characterization of Monomeric Photoinitiators

Two novel monomeric PIs with 1,6-heptadiene structures were prepared starting from I2959. The first PI (I2959-NTBDA) was synthesized by nucleophilic substitution reaction of I2959-NH_2 to TBBr using 1:4 mol ratio in the presence of K_2CO_3 (Figure 3.2). I2959-NH_2 was prepared according to literature procedures in three steps [125,126]. First I2959 was converted to its tosylate derivative in good yield, which was then reacted with sodium azide to provide azide derivative of I2959, then reduced to amine by treatment with triphenylphosphine and water. The structures of these intermediates were confirmed by ^1H NMR and FTIR spectroscopies (Figure 3.3 and Figure 3.4). The reason for the use of high TBBr to amine ratio (4:1 mol) during monomeric PI synthesis is to prevent formation of monoadduct (secondary amine) which is known as inhibitor of free radical polymerization under neutral conditions [130]. Also, column chromatography was used to remove any residual monoadduct and pure I2959-NTBDA was obtained as a colorless oil in 52% yield. The second PI (I2959-NDAA) was synthesized by cleavage of the ester groups of I2959-NTBDA using TFA. This PI was obtained as a white solid in 76 % yield (Figure 3.2).

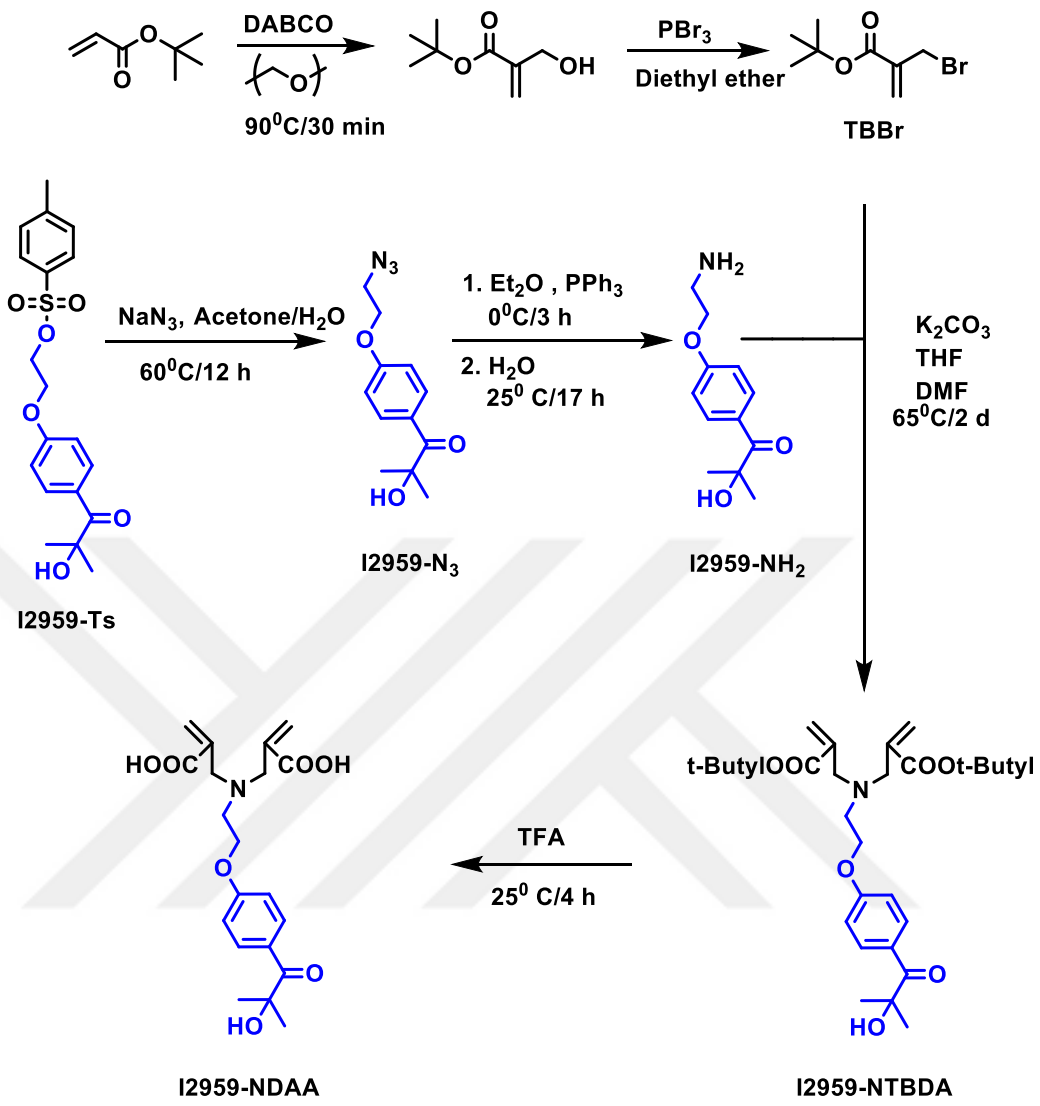


Figure 3.2. Synthesis of I2959-NTBDA and I2959-NDAA.

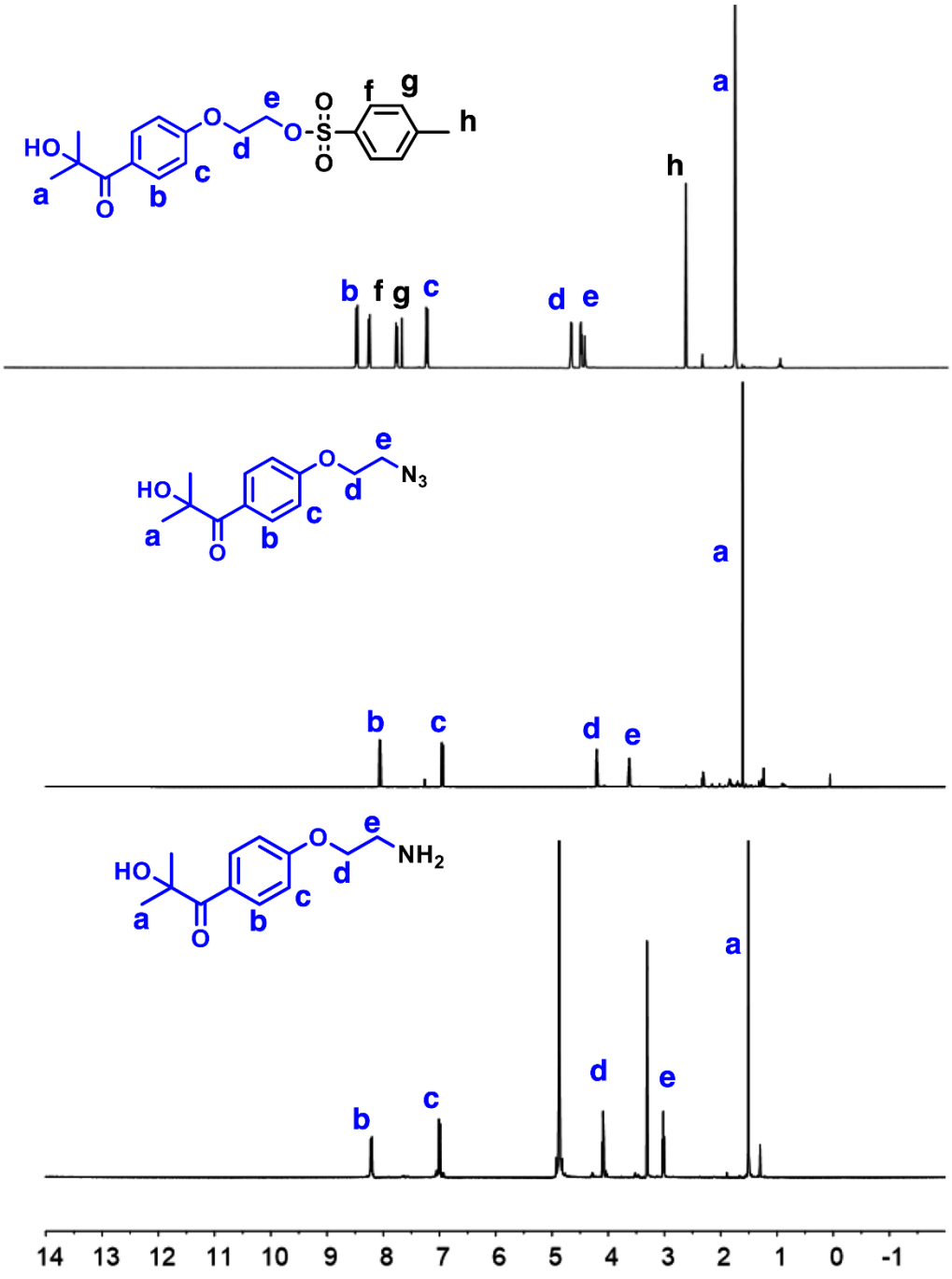


Figure 3.3. ^{1}H NMR spectra of I2959-Ts, I2959-N_3 and I2959-NH_2.

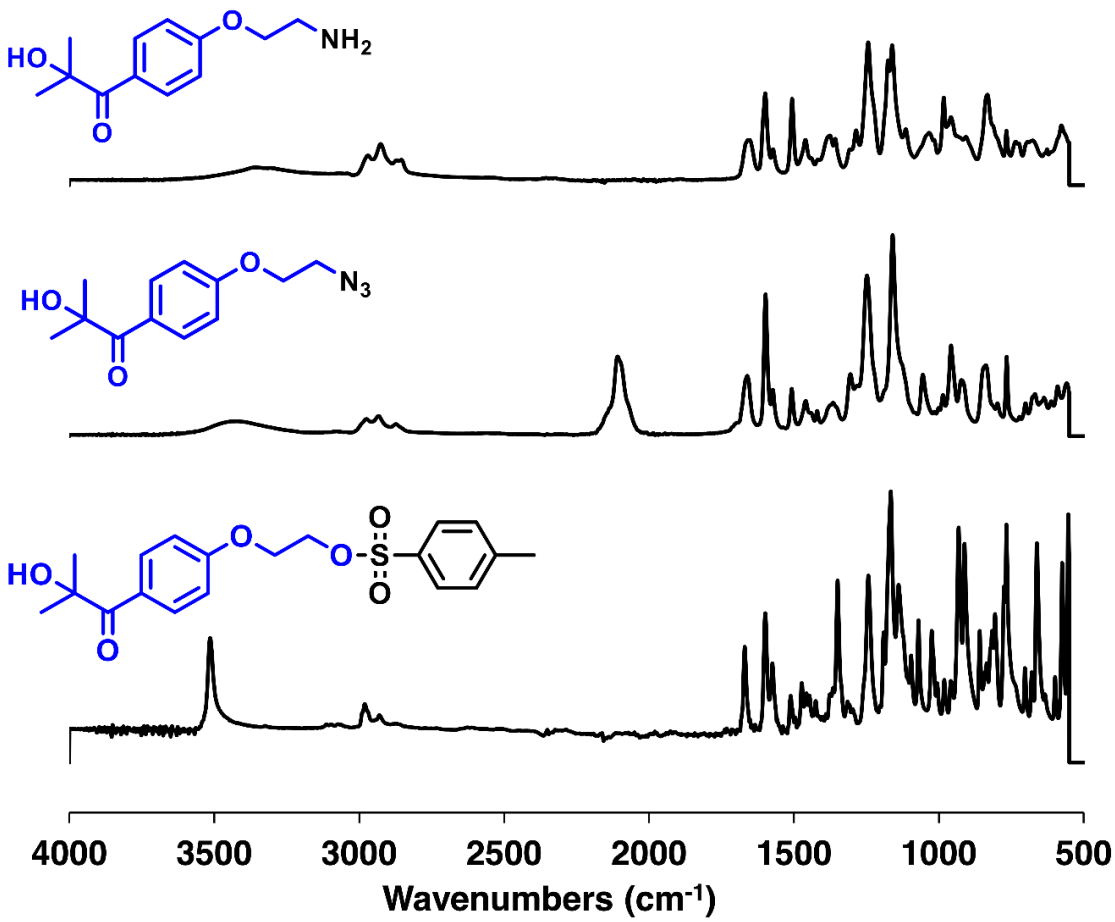


Figure 3.4. FTIR spectra of I2959-Ts, I2959-N_3 and I2959-NH_2.

The structural features of the PIs were confirmed by the NMR and FTIR spectra. The ^{1}H NMR spectrum of I2959-NTBDA revealed two doublets of doublets at 6.90 and 8.13 ppm for the aromatic protons and two singlets at 6.10 and 5.75 ppm were assigned to methacrylate protons, showing successful TBBr substitution reaction on I2959-NH_2 (Figure 3.5). Two methyl protons of I2959 and TBBr resonated as a singlet at 1.45 and 1.64 ppm. The disappearance of *tert*-butyl peak in the ^{1}H NMR spectrum of I2959-NDAA confirmed the complete clevage of ester groups. Apart from that, methylene protons are observed at 3.68, 4.18 and 4.47 ppm. (Figure 3.5). The FTIR spectrum of I2959-NTBDA revealed intense ester and ketone carbonyl absorptions at 1707 and 1667 cm^{-1}, double bond peaks at 1634 cm^{-1} and a broad peak was found in the range from 3400 to 3600 cm^{-1} due to the presence of a OH group (Figure 3.6). The FTIR spectrum of I2959-NDAA did not show any absorption due to the presence of ester group, showing overlapping ketone and carboxylic acid absorptions at 1669 cm^{-1} (Figure 3.6).

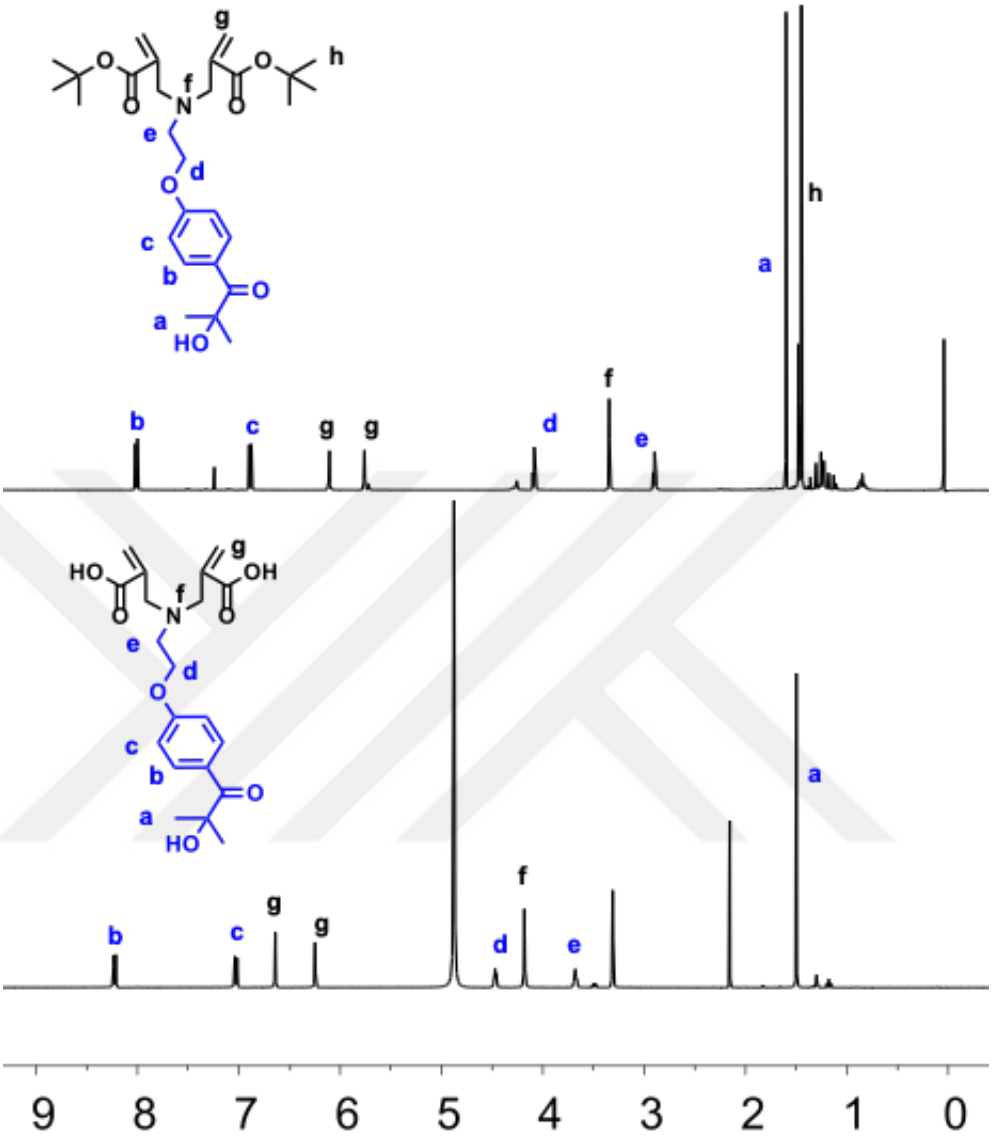


Figure 3.5. [1]H-NMR spectra of I2959-NTBDA and I2959-NDAA.

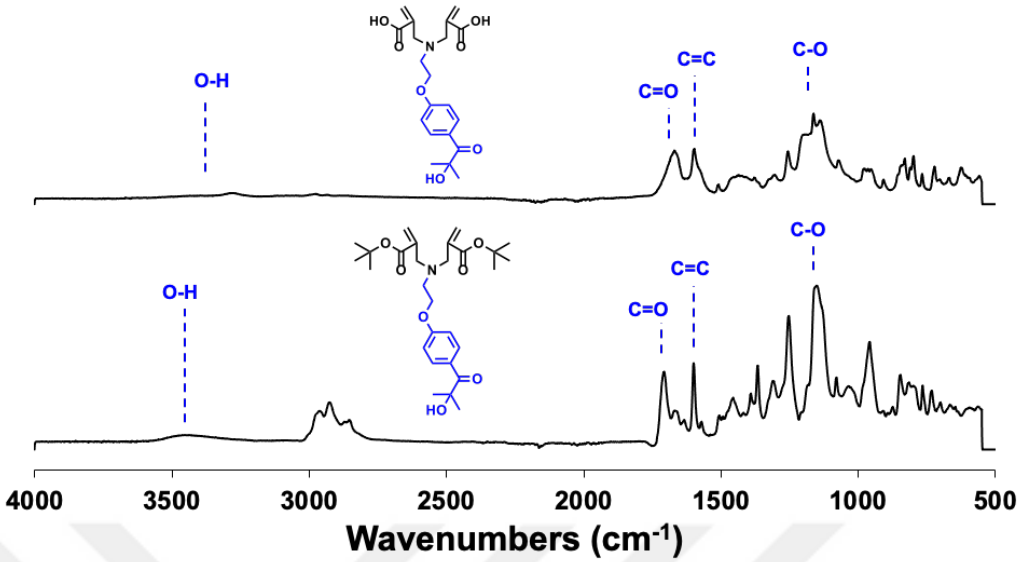


Figure 3.6. FTIR spectra of I2959-NTBDA and I2959-NDAA.

Table 3.1 summarizes the solubilities of the synthesized PIs and the commercial reference. While I2959 is soluble (<2wt%) in water, the synthesized monomers, I2959-NTBDA and I2959-NDAA are not, due to loss of hydroxyl groups of I2959 via functionalization. I2959-NTBDA is soluble in low polarity solvents such as DCM, diethyl ether and acetone due to its large *tert*-butyl groups. After replacing *tert*-butyl groups with carboxylic acid groups, I2959-NDAA has different solubility properties than I2959-NTBDA just as it has different physical features. It is soluble in methanol, but insoluble in acetone and diethyl ether. However, both of these novel monomeric PIs (I2959-NTBDA and I2959-NDAA) have good compatibility with TMPTA, PEGDA and HEMA.

3.1. Solubilities of the synthesized PIs and I2959.

PIs	H_2O	Methanol	Diethyl ether	CH_2Cl_2	THF	DMF	Acetone
I2959	+	+	+	+	+	+	+
I2959-NTBDA	-	-	+	+	+	+	+
I2959-NDAA	-	+	-	-	+	+	-
p-BA-NTBDA-*co*-I2959-NTBDA	-	-	+	+	+	+	+

3.3.2. Synthesis and Characterization Polymeric Photoinitiator

To synthesize a polymeric PI with a cyclic backbone and to control the amount of photoinitiating units, I2959-NTBDA was copolymerized with BA-NTBDA (synthesized using a procedure similar to that for I2959-NTBDA) (Figure 3.7). BA-NTBDA is expected to have high cyclization efficiency due to bulky *tert*-butyl groups and similar polymerization reactivity resulting from its dimethacrylate structure. The copolymer was synthesized in bulk at 75 °C with AIBN as thermal initiator using 90:10 mol% of BA-NTBDA and I2959-NTBDA. The copolymer is soluble in many polar solvents such as acetone, DCM, diethyl ether and THF, but insoluble in water and methanol (Table 3.1). Similarly, Esacure KIP 150, an oligomeric polyfunctional α-hydroxyketone, is insoluble in water, soluble in most common organic solvents, monomers and oligomers. Complete solubility of the copolymer indicates high cyclization efficiency of the synthesized monomeric PI, despite the fact that polymerization was carried out in bulk. This is due to bulky *tert*-butyl groups preventing intermolecular reaction and favoring intramolecular-intermolecular cyclization. Actually, no pendant unsaturation due to methacrylate groups was observed in the ^{1}H NMR spectrum (Figure 3.8). In order to assign NMR peaks coming from both monomers and calculate the copolymer composition, the homopolymerization of BA-NTBDA was also carried out under the same conditions. In the ^{1}H NMR spectrum of the copolymer, two different sets of aromatic peaks were observed, small ones at 6.91 and 8.03 ppm due to I2959-NTBDA component for p-BA- NTBDA-*co*-I2959-NTBDA, while at only 7.25 ppm for BA-NTBDA. This result demonstrated successful incorporation of I2959-NTBDA into the polymer chain. The copolymer compositions were calculated by the ratios of peak areas of aromatic protons and found to be 95:5 (BA-NTBDA: I2959-NTBDA) mol% indicating lower reactivity of I2959-NTBDA compared to BA-NTBDA. The FTIR spectrum of the copolymer exhibited an intense peak at 1711 cm^{-1} due to stretching of the ester carbonyl groups of BA-NTBDA (Figure 3.9). Because structural analysis on cyclopolymers of amine linked dimethacrylates indicated formation of cyclic units of a six-membered ring [140], the cyclopolymer is expected to have six membered ring structures at the backbone. M_n value of this polymer was around 28 000 D (PDI = 1.38). TGA study of the polymer showed two step degradation: initial cleavage of side chain *tert*- butyl groups followed by main chain cleavage (Figure 3.10).

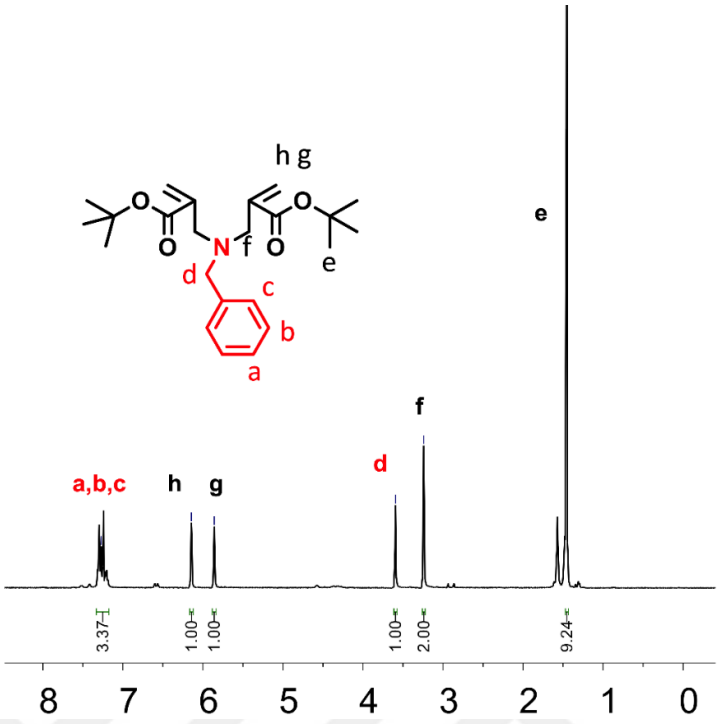


Figure 3.7. [1]H-NMR spectrum of BA-NTBDA.

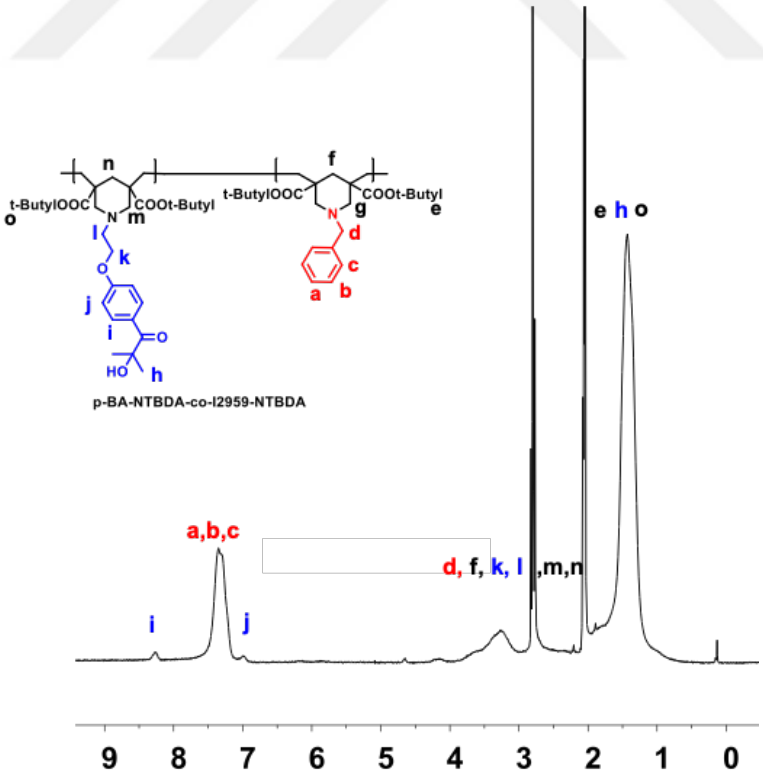


Figure 3.8. [1]H-NMR spectrum of p-BA-NTBDA-*co*-I2959-NTBDA.

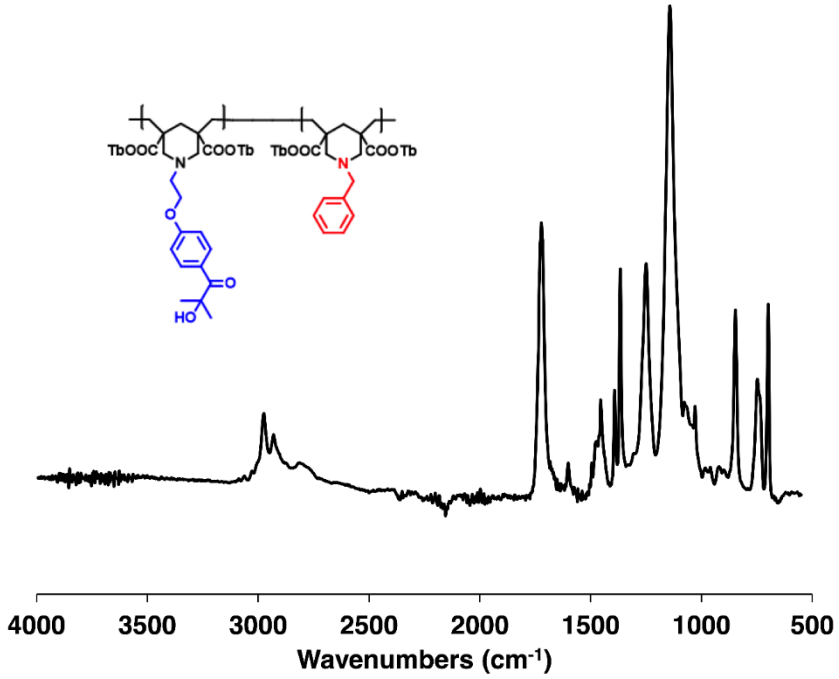


Figure 3.9. FTIR spectrum of p-BA-NTBDA-*co*-I2959-NTBDA.

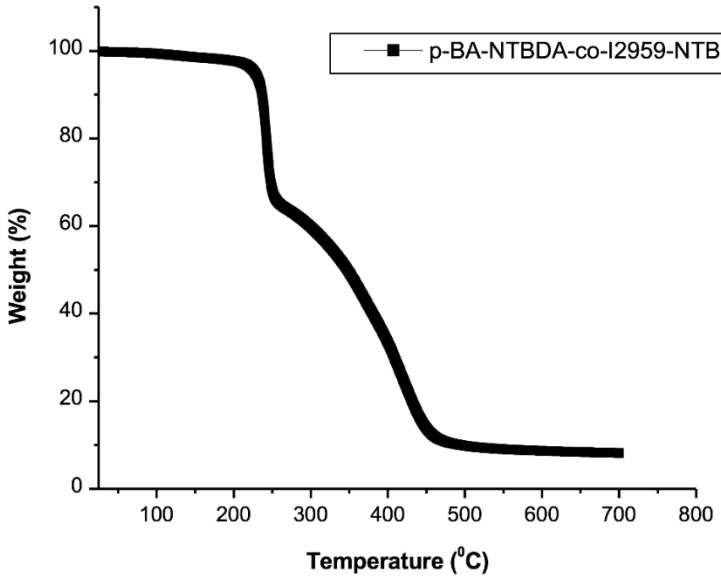


Figure 3.10. TGA plot of p-BA-NTBDA-*co*-I2959-NTBDA.

3.3.3. Light Absorption Properties

The absorption spectra of monomeric PIs are depicted in Figure 3.11A. Their absorption maxima and their molar extinction coefficients are compared with that of I2959 in Table 2. All of the monomeric PIs have absorption maxima in the range of 269-280 nm, similar to I2959 and these maxima correspond to π-π∗ transitions. No peak due to n-π∗ transition was observed around 330 nm. The molar absorption coefficients (ε = 13700-16000 M^{-1} cm^{-1}) were also similar to that of I2959 (ε = 13360-17500 M^{-1} cm^{-1}) depending on solvent (Table 3.2). These results indicated that the substitution on I2959 did not inflence its absorbtion features. The copolymeric PI also showed higher absorption (λ = 290 nm) with an extinction coefficient (ε = 78300 M^{-1} cm^{-1}), consistent with the expected value from the concentration of DAA-I2959 units (ε = 17000 M^{-1} cm^{-1}) the polymer (Figure 3.11B).

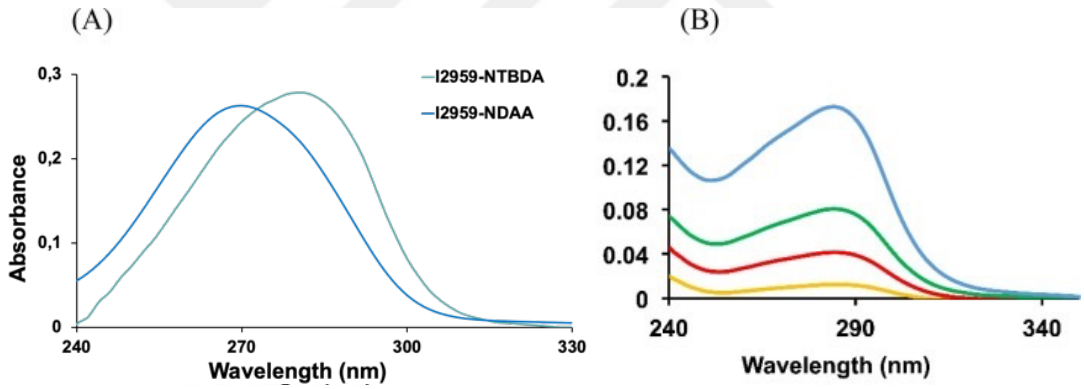


Figure 3.11. UV–vis absorption spectra of (A) I2959-NTBDA and I2959-NDAA in $CHCl_3$ and MeOH (B) p-BA-NTBDA-*co*-I2959-NTBDA ($0.2x10^{-6}$, $0.5x10^{-6}$, $1x10^{-6}$ and $2x10^{-6}$ M) in $CHCl_3$.

Table 3.2. Absorption characteristics of I2959, I2959-NTBDA and I2959-NDAA.

PIs	Solvent	λ_{max} (nm)	ε (M^{-1} cm^{-1})
I2959	$CHCl_3$	276	17510
I2959	MeOH	272	13359
I2959-NTBDA	$CHCl_3$	280	16050
I2959-NDAA	MeOH	269	13776

Photolysis experiments were carried out under 320-500 nm irradiation to investigate the efficiency of the PIs. Upon excitation the intensity of the maximum absorbtion for I2959-NTBDA, I2959-NDAA and p-BA-NTBDA-*co*-I2959-NTBDA decreased and a new peak at about 250 nm was observed (Figure 3.12, Figure 3.13). A similar peak observed during photolysis of a PEG based alpha-hydroxyalkylphenone PI was identified as acetone by Huo et al. [131]. This indicates α cleavage of PIs to benzoyl and ketyl radicals and generation of acetone due to oxidation of latter. Isobestic points are observed indicating a photochemical process (cleavage) without other side reaction.

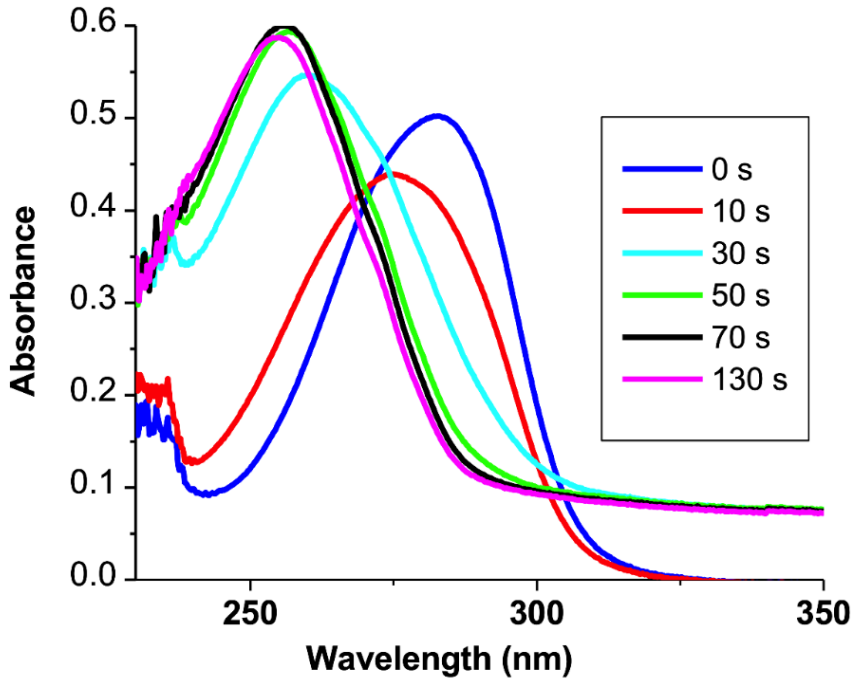


Figure 3.12. The photolysis of I2959-NTBDA ($3.2x10^{-5}$ M in $CHCl_3$) in chloroform using a 320-500 nm light source.

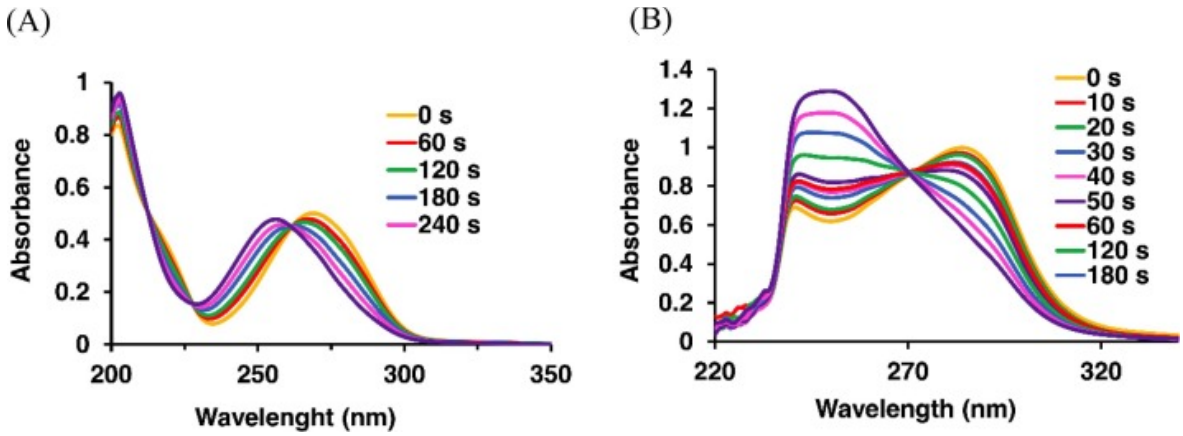


Figure 3.13. The photolysis of (A) I2959-NDAA (4 x 10^{-5} M) in methanol and (B) p-BA-NTBDA-*co*-I2959-NTBDA (1.1 x 10^{-5} M) in chloroform using a 320-500 nm light source

3.3.4. Electron Spin Resonance (ESR) Experiments

Electron spin resonance experiments of monomeric PI I2959-NTBDA and its copolymer were performed together with reference I2959. The formed radicals from toluene solution of I2959-NTBDA by a 320-500 nm light source were captured by PBN and the obtained structure constants (hfc) were found from the simulated ESR spectra. Reference I2959 was confirmed to form benzoyl and alkyl radicals with 10-50 seconds irradiation at 320-500 nm (Figure 3.14A). Markedly, for all these systems a Type I PI behavior is found i.e. free radicals are generated by irradiation of the compounds alone (Figure 3.14B). However, due to the steric effect (bulky radicals being generated), the values of hyperfine coupling constants can hardly be linked to the chemical structures (these radicals being unreported in the literature).

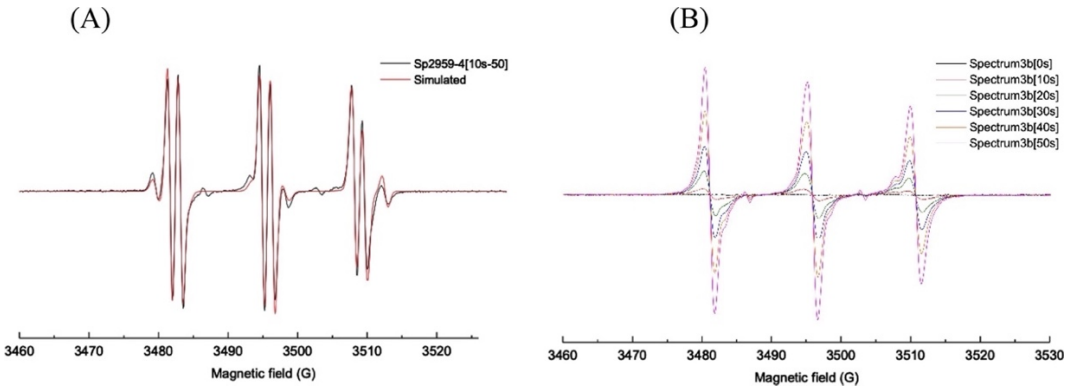


Figure 3.14. Electron spin resonance spectra of free radicals captured by PBN in a toluene solution of (A) I2959 and (B) I2959-NTBDA by a 320-500 nm light source

3.3.5. Photopolymerization

In order to investigate the relation between structure and reactivity, the photoinitiation efficiencies of the synthesized monomeric and polymeric PIs in polymerizations of HEMA, PEGDA or TMPTA were measured by photo-DSC at 25 °C under UV-visible light (320-500 nm) irradiation. Also, the homopolymerization properties of the monomeric PIs were investigated under the same conditions. The photopolymerization rates (R_{pmax}), conversions and times to reach maximum rate (t_{max}) were determined.

First, in order to determine the reactivity of I2959-NTBDA as a monomer, it was homopolymerized using UV-vis irradiation (320-500 nm) at 25 °C (Figure 3.15). It was observed that I2959-NTBDA (R_{pmax} = 0.022 s^{-1}, t_{max} = 0.18 min and conversion = 89.9%) is a highly reactive monomer. Since I2959-NDAA was a solid at room temperature, its homopolymerization could not be investigated using photo-DSC.

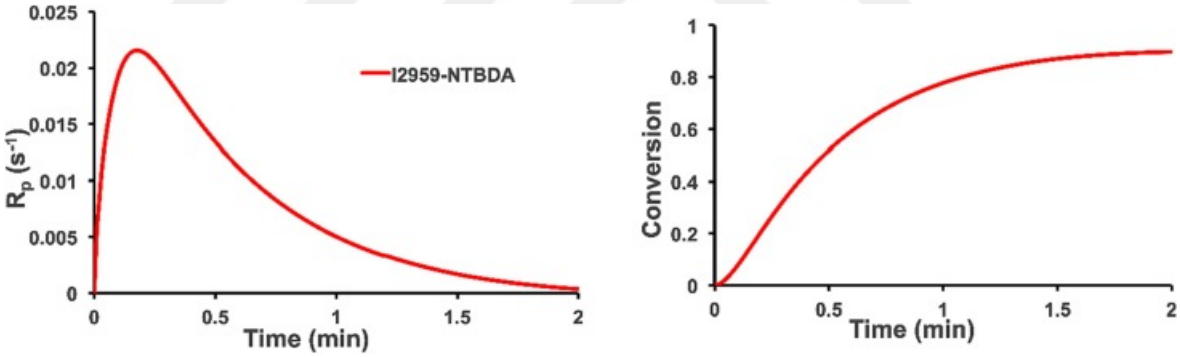


Figure 3.15. Rate-time and conversion-time graphs of I2959-NTBDA during homopolymerization at 25 ºC under nitrogen and 320-500 nm irradiation.

Then, in order to investigate the photoinitiation efficiencies of the synthesized PIs and to compare with I2959, HEMA, PEGDA or TMPTA monomers were photopolymerized using 1 wt% PI (synthesized or I2959) under UV-vis irradiation (320-500 nm) at 25 °C (Figures 3.16 and 3.17). I2959-NTBDA was observed to show similar photopolymerization kinetics to I2959 in HEMA and TMPTA. Although the polymerization rates of PEGDA/I2959-NTBDA system (R_{pmax} = 0.138 s^{-1}, t_{max} = 0.04 min) were lower than those of the PEGDA/I2959 system (R_{pmax} = 0.156 s^{-1}, t_{max} = 0.03 min), the conversions and t_{max} values were found to be similar.

I2959-NDAA showed faster photopolymerization kinetics compared to I2959-NTBDA and I2959 in HEMA. For example, I2959-NDAA has a shorter induction time (0.89 min) than I2959 (1.24 min) and I2959-NTBDA (1.55 min). In PEGDA, R_{pmax} values were found to be in the order of I2959>I2959-NDAA>I2959-NTBDA. The higher reactivity of I2959-NDAA compared to I2959-NTBDA can be ascribed to the lower steric hindrance due to cleavage of bulky *tert*-butyl groups. The hydrogen bonding of the carboxylic acid groups of this PI with the monomers can also contribute to its performance.

The rate and conversion for use of the synthesized copolymer, p-BA-NTBDA-*co*-I2959-NTBDA, were also low, but it could still successfully polymerize TMPTA.

It was observed that Type I PIs containing tertiary amine groups can be used as coinitiators in Type II sytems [44,132]. Therefore, we expect our PIs to be used as hydrogen donors for TX. The photopolymerization of HEMA was investigated in the presence of TX:I2959, TX:EDB and TX: I2959-NTBDA under visible light (Figure 3.18). The results indicated that I2959-NTBDA contribute to TX as hydrogen donor, although not as effective as EDB, whereas I2959 was not.

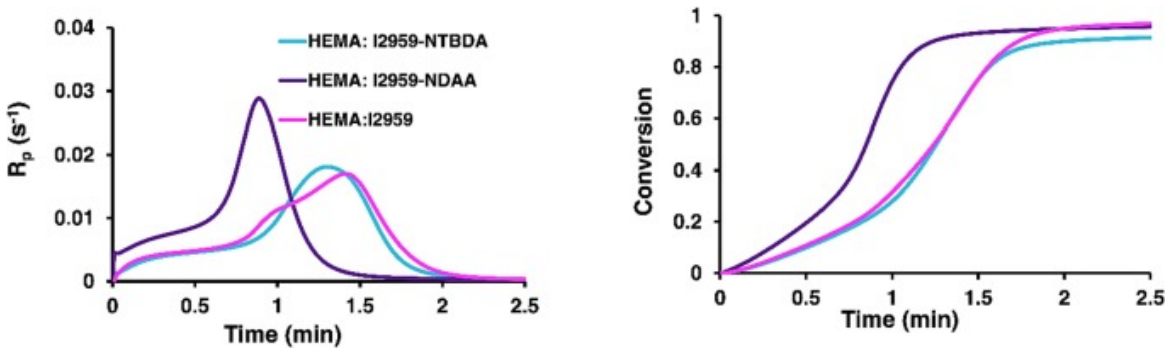


Figure 3.16. Rate-time and conversion-time plots for HEMA containing I2959-NTBDA (1 wt%, 0.41 wt % I2959-eq), I2959-NDAA (1 wt%, 0.53 wt % I2959-eq) and I2959 (1 wt%) at 25 ºC under nitrogen and 320-500 nm irradiation.

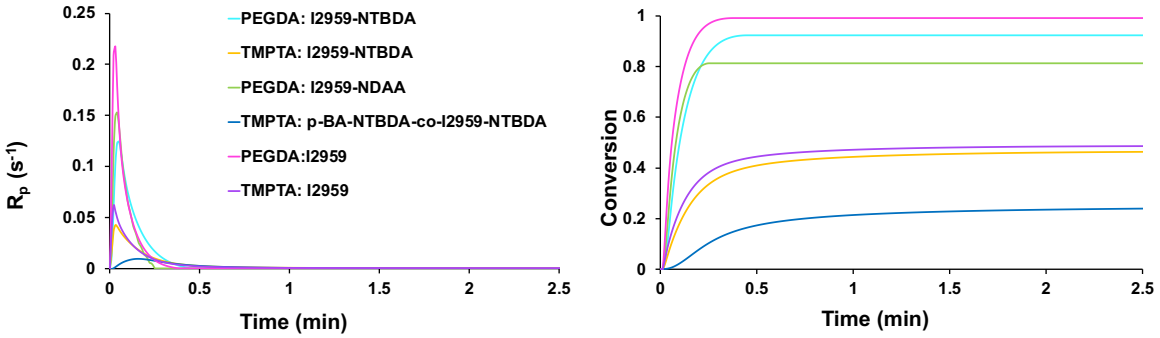


Figure 3.17. Rate-time and conversion-time plots for PEGDA and/or TMPTA containing I2959-NTBDA (1 wt%, 0.41 wt% I2959-eq), I2959-NDAA (1 wt%, 0.53 wt% I2959-eq), p-BA-NTBDA-*co*- I2959-NTBDA (1 wt%, 6.4 wt% I2959-eq) and I2959 (1 wt%) at 25 ºC under nitrogen and 320-500 nm irradiation.

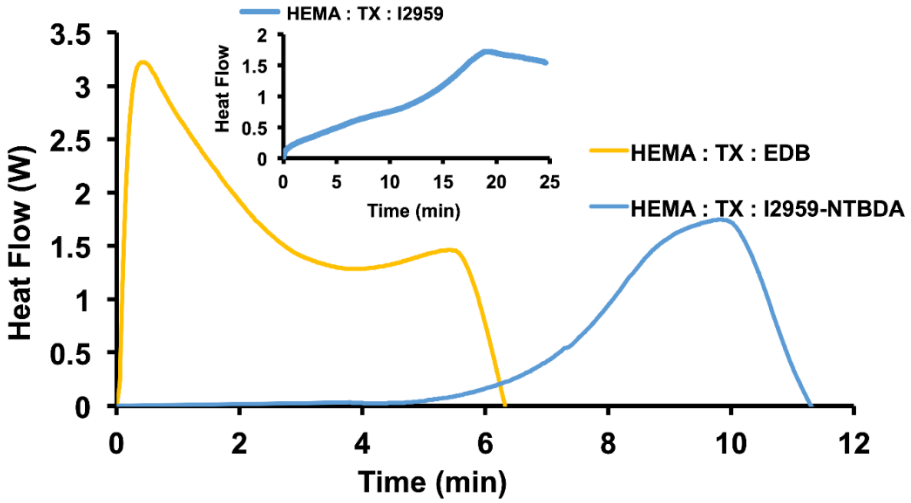


Figure 3.18. Heat Flow-time graph of HEMA formulations containing TX:EDB (0.25:0.75 wt%), TX:I2959-NTBDA (0.25:0.75 wt%) and TX:I2959 (0.25:0.75 wt%) (inset) at 25 ºC under nitrogen and 400-500 nm irradiation

3.3.6. Migration Stability

The migration stability of one of the monomeric PIs, I2959-NTBDA, was analyzed together with commercial I2959. UV-visible spectra were used to determine concentration of the PIs extracted from PEGDA gels prepared using the same concentrations of PIs and after immersion in chloroform for 3 days (Figure 3.19). It was found out that I2959-NTBDA has much higher migration stability than I2959, <1% compared to I2959 (57%). This huge

difference results from the incorporation of I2959-NTBDA into the polymer network and also from increased crosslink density of the polymer network due to its dimethacrylate functionality. The higher migration stability enables reduction of the toxicity of the PI.

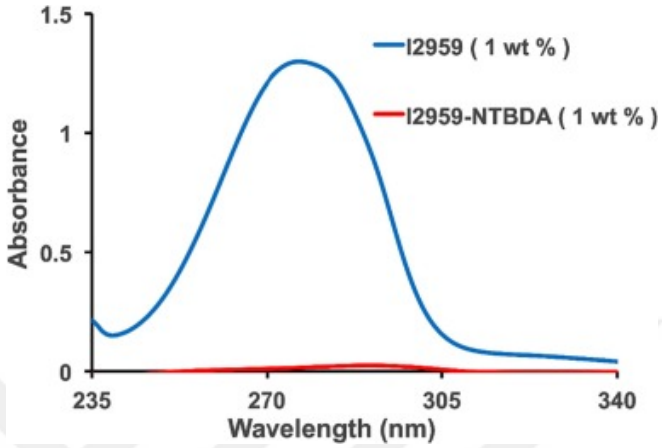


Figure 3.19. UV-VIS absorption spectra of I2959-NTBDA and I2959 extracted with chloroform from the PEGDA gels.

3.3.7. Color analysis

Synthesized PIs have tertiary amine groups in their structures which may cause yellowing of the cured films. The yellowing properties of films cured by the two of the monomeric PIs, I2959-NTBDA and I2959-NDAA, have been analysed. The colorimetric results are given in Table 3.3. The higher the b* value, the higher the yellowing properties. I2959-NTBDA showed similar value compared to I2959, while I2959-NDAA showed higher yellowing properties in the cured film.

Table 3.3. Colorimetry results of the cured films.

PIs	L*	a*	b*
I2959	91.07	-0.34	2.73
I2959-NTBDA	91.10	-0.28	2.94
I2959-NDAA	88.00	-0.23	4.36

3.4. Conclusion

In this chapter, two monomeric PIs were sucessfully synthesized and the effect of their structures on the phoinitiating efficiencies was investigated in the photopolymerizations of HEMA, PEGDA and TMPTA. These results indicated that the photoinitiation efficiency was consistent with the homopolymerization reactivity of the monomeric PIs: I2959-NDAA> I2959-NTBDA, increased with a decrease in steric effect and an increase in hydrogen bonding ability. PI with bulky *tert*-butyl groups (I2959-NTBDA) can produce soluble, linear polymers with six-membered cyclic structures efficiently, even in bulk polymerization. Copolymerization process enables not only control of PI concentration but may be used to incorporate different functionalities to tune physical properties of the final polymeric PIs. The presented PIs exhibit absorption maximum at around 270 nm similar to commercial I2959 and undergo an α-cleavage reaction after photoexcitation, leading to benzoyl and ketyl radicals. One representative PI, I2959-NTBDA, has a very good migration stability compared to I2959, enabling environmentally-friendy materials.

4. MONOMERIC PHOTOINITIATORS FROM 3-(ACRYLOYLOXY)-2-HYDROXYPROPYL METHACRYLATE

4.1. Introduction

In this study, we describe a method for synthesis of new hydroxylated methacrylate-based PIs from 3-(acryloyloxy)-2-hydroxypropyl methacrylate (AHM) which is a mixed acrylate/ methacrylate monomer. Two new functional mono- and dimethacrylate PIs were synthesized from aza-Michael addition reaction of the amine derivative of I2959 and AHM by controlling their stoichiometry. The photoinitiating ability, migration stability and photochemical mechanisms of the novel PIs were investigated.

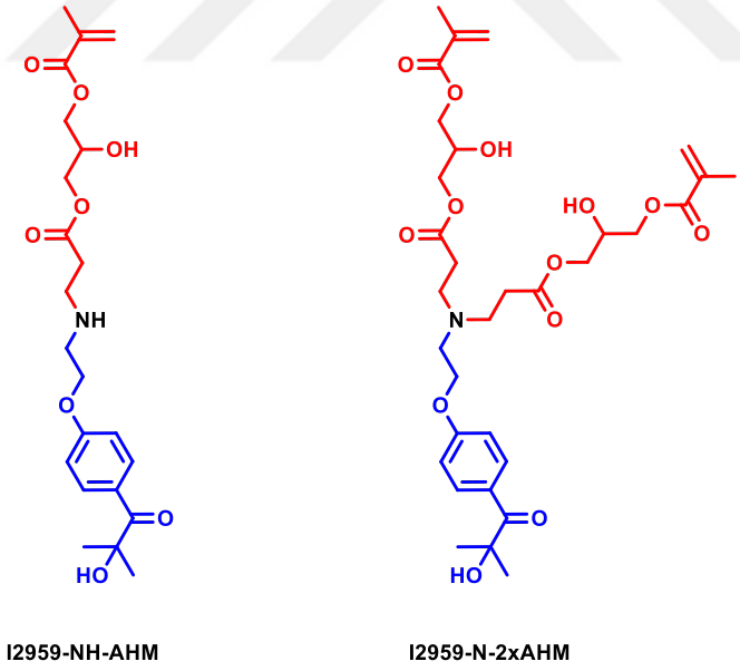


Figure 4.1. Structure of the novel photoinitiators I2959-NH-AHM and I2959-N-2xAHM.

4.2. Experimental

4.2.1. Materials and Characterization

I2959, AHM, p-toluenesulfonyl chloride (tosyl chloride, TsCl), TMPTA, HEMA, PEGDA (M_n = 575 D), EDB, benzophenone (BP) and the other reagents and solvents were purchased from Sigma-Aldrich or Alfa Aesar and used without additional purification. Bis-(4-*tert*-butylphenyl)-iodonium hexafluorophosphate (Iod or Speedcure 938) was obtained from Lambson Ltd. I2959-Ts was synthesized according to literature procedure [123].

NMR spectra were recorded in deuterated chloroform ($CDCl_3$) solvent at ambient temperature on a Varian Gemini (400 MHz) spectrometer. A Nicolet 6700 FT-IR spectrophotometer was used to obtain IR spectra. UV-vis spectra were recorded on a Varian®Cary 3 spectrometer.

4.2.2. Synthesis of Photoinitiators

4.2.2.1. Synthesis of I2959-NH-AHM. I2959-NH_2 (0.023 g, 0.1 mmol) and AHM (0.022 g, 0.1 mmol) were dissolved in methanol (0.1 mL) and the solution was stirred at room temperature for 2 days. After the reaction was completed, the solvent, methanol, was removed by rotary evaporation under vacuum to get product which was obtained as a light-yellow oil.

^{1}H-NMR ($CDCl_3$, 400 MHz, δ): 1.58 (s, 6H, CH_3), 1.91(s, 3H, CH_3), 2.54 (t, 2H, CH_2-C), 2.86 (q, 2H, CH_2-N), 3.01 (q, 2H, CH_2-N), 3.93 (t, 2H, CH_2-O), 4.10 (t, 2H, CH_2-O), 4.17 (t, 2H, CH_2-O), 4.20 (m, 1H, CH-O), 5.56 (s, 1H, CH_2=C), 6.10 (s, 1H, CH_2=C), 6.89 (m, 2H, Ar-CH), 8.03 (d, 2H, Ar-CH).

FTIR (ATR): 3391 (OH), 2930 (CH), 1667, 1716 (C=O), 1599 (C=C), 1151 (C-O) cm^{-1}.

4.2.2.2. Synthesis of I2959-N-2xAHM. I2959-NH_2 (0.012 g, 0.05 mmol) and AHM (0.022 g, 0.1 mmol) were dissolved in methanol (0.05 mL) and the solution was stirred at room temperature for 2 days. Then the solvent was removed to get product which was obtained as a light-yellow oil.

^{1}H-NMR ($CDCl_3$, 400 MHz, δ): 1.59 (s, 6H, CH_3), 1.91 (s, 6H, CH_3), 2.45 (t, 4H, CH_2-C), 2.86 (q, 2H, CH_2-N), 2.87 (q, 4H, CH_2-N), 4.06 (t, 2H, CH_2-O), 4.16 (t, 4H, CH_2-O), 4.20 (t, 4H, CH_2-O), 4.22 (m, 2H, CH-O), 5.57 (s, 2H, CH_2=C), 6.10 (s, 2H, CH_2=C), 6.91 (m, 2H, Ar-CH), 8.01 (d, 2H, Ar-CH).

FTIR (ATR): 3445 (OH), 2955 (CH), 1667-1716 (C=O), 1599 (C=C), 1151 (C-O) cm^{-1}.

4.2.3. Photopolymerization experiments

For photopolymerization experiments, a TA Instruments DSC 250 differential photocalorimeter using an Omnicure 2000 mercury lamp light source with a 320-500 nm or 400-500 nm filter was used. HEMA, PEGDA (M_n = 575 D) or TMPTA monomer (3-4 mg) containing 1 wt% of PIs or the references having the same molar concentrations in the presence and absence of 1 wt% coinitiators (Iod, BP or TX) were exposed to irradiation at 25 °C under nitrogen. The heat flow was monitored as a function of time, and the polymerization rate was calculated as

$$\text{Rate} = \frac{(Q/s)M}{n(\Delta H_p)m} \quad (4.1)$$

where *Q/s* is the heat flow per second, *M* the molar mass of the monomer, *n* the number of double bonds per monomer molecule, ΔH_p the heat of reaction evolved and *m* the mass of monomer in the sample [127]. The theoretical heat for the total conversion of a methacrylate and acrylate double bonds are 55 and 86.5 kJ mol^{-1}.

4.2.4. Migration Study

PEGDA (M_n = 575 D) was photopolymerized in the presence of I2959 (1 wt%), I2959-N-2xAHM and I2959-NA-AHM (1 wt%) via UV irradiation, using a photoreactor (Kerman UV/18) containing 12 Philips TL 8 W BLB lamps with light emission at 365 nm, for 1 h in glass vials under air. The crosslinked polymers were soaked in 25 mL chloroform for 4 days. The percentages of the extracted PIs were determined by UV–vis spectroscopy [128].

4.3. Results and Discussion

4.3.1. Synthesis and Characterization of Monomeric Photoinitiators

Two novel monomeric PIs I2959-NH-AHM and I2959-N-2xAHM were synthesized. First PI I2959-NH-AHM was prepared from the reaction of AHM and I2959-NH_2 in a mole ratio of 1:1. Since I2959-NH_2 was able to act as both nucleophile and base, AHM can undergo Michael addition in the presence of it without any catalyst. I2959-NH_2, was synthesized in three steps: i) synthesis of I2959-Ts from the reaction of I2959 with p-toluenesulfonic acid [123], ii) I2959-N_3 from the reaction of I2959-Ts with sodium azide [135] and iii) reaction of I2959-N_3 with Ph_3P [125]. Second monomeric PI I2959-N-2xAHM was synthesized from the similar reaction of AHM and I2959-NH_2 in a mole ratio of 2:1. During this reaction, Aza-Michael addition between a primary amine, I2959-NH_2, and acrylate part of AHM take place to form I2959-NH-AHM and this resulting secondary amine further undergoes aza-Michael addition at a slower reaction rate to form I2959-N-2xAHM. To obtain the pure monofuntional and difunctional PIs, it is very important to add the starting materials in the exact molar ratios. However, formation of small amounts of the other monomeric PI could not be completely prevented for both of them (Figure 4.2).

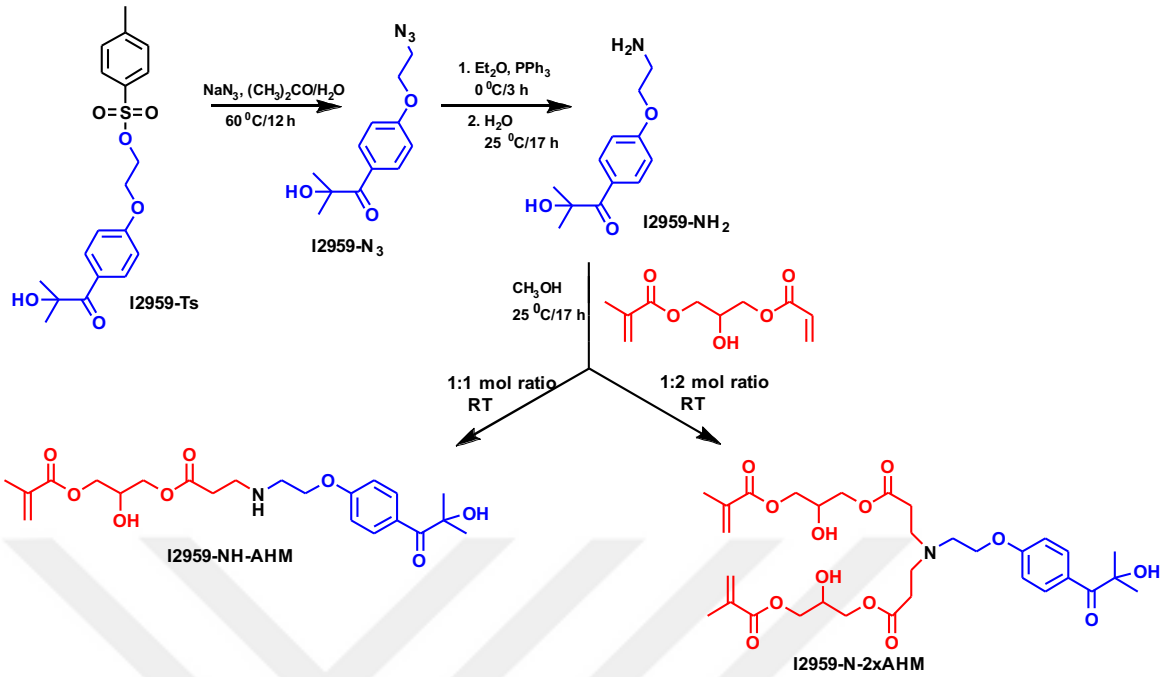


Figure 4.2. Synthesis of the PIs, I2959-NH-AHM and I2959-N-2xAHM.

^{1}H NMR and FTIR spectroscopies were used to confirm the structures of the novel monomeric PIs. ^{1}H NMR spectra of I2959-NH-AHM revealed two singlets at 5.56 and 6.10 ppm for the methacrylate double bond protons and two peaks at 6.89 and 8.03 ppm appointed to aromatic protons which are proof of successful Micheal addition reaction. Two singlets at 1.58 and 1.91 ppm correspond to the methyl groups of the I2959 and AHM. The methylene protons can be seen at 2.54, 2.86, 3.01, 3.93, 4.10 and 4.17 (Figure 4.3). ^{1}H NMR spectrum of I2959-N-2xAHM pointed out similar two distinct singlets at 5.57 and 6.10 ppm for the methacrylate double bond protons and two doublets at 6.91 and 8.01 ppm assigned to aromatic protons. Apart from that, methylene protons are observed at 2.45, 2.86, 2.87, 3.68, 4.06, 4.16 and 4.20 and 4.47 ppm and there were also two singlets at 1.59 and 1.91 ppm for the methyl groups (Figure 4.4). In their FTIR spectra ester and ketone C=O peaks were observed at 1716, 1667 (for I2959-NH-AHM) and 1715, 1667 (for I2959-N-2xAHM) cm^{-1} respectively (Figure 4.5, Figure 4.6).

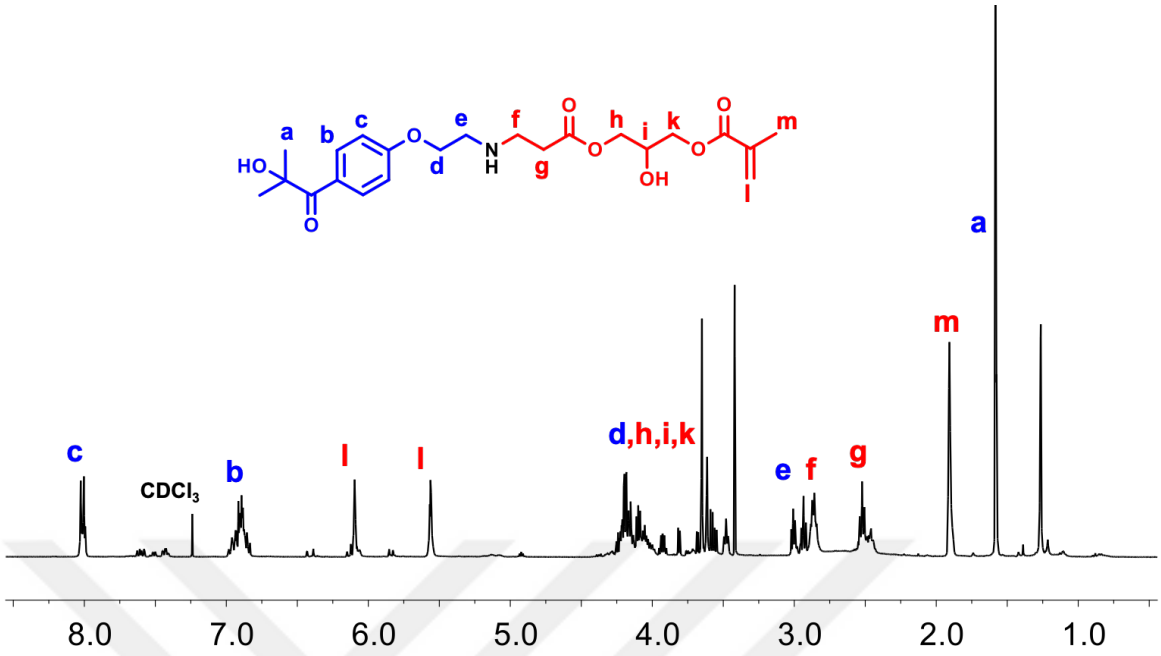


Figure 4.3. ^{1}H-NMR spectrum of I2959-NH-AHM

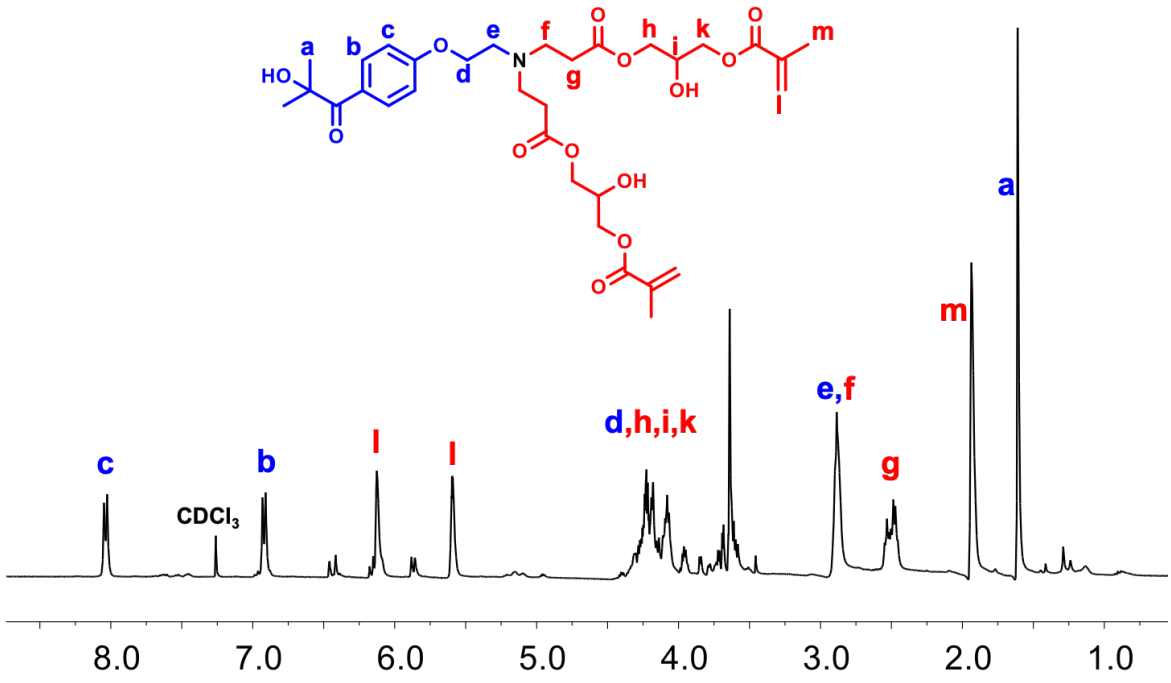


Figure 4.4. ^{1}H-NMR spectrum of I2959-N-2xAHM

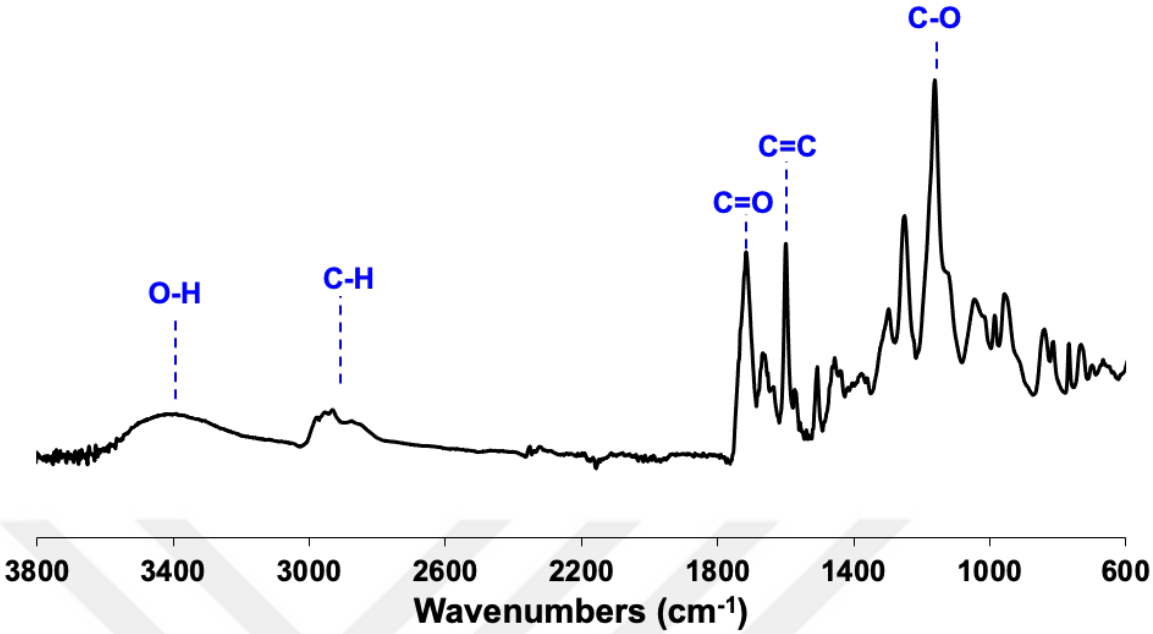


Figure 4.5. FTIR spectrum of I2959-NH-AHM

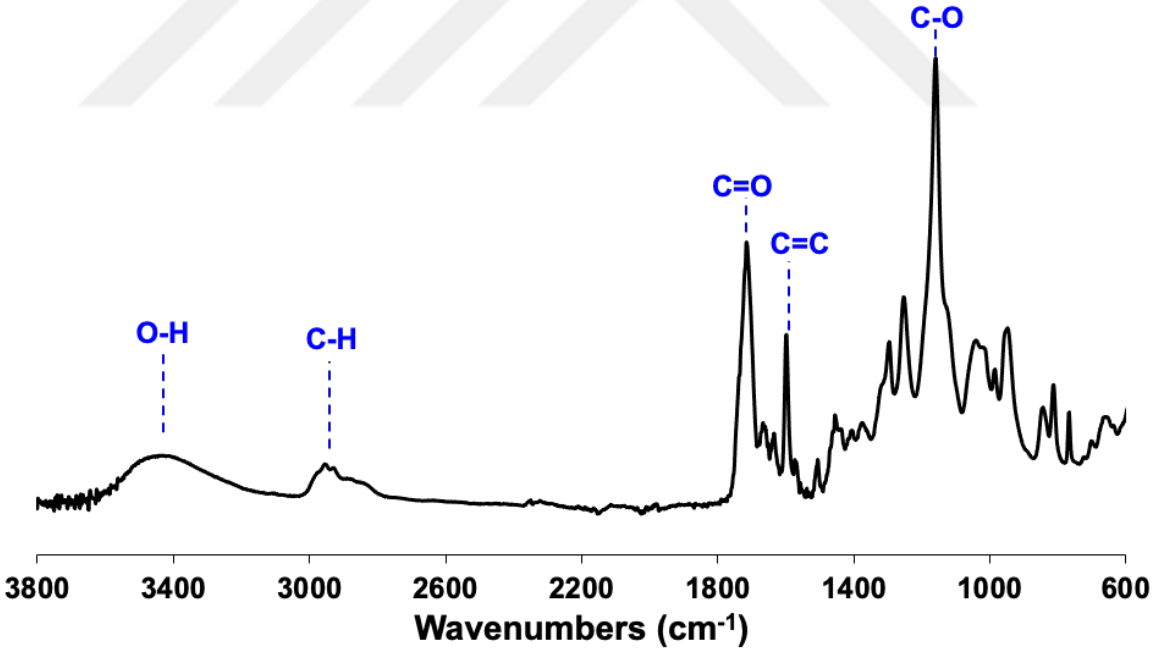


Figure 4.6. FTIR spectrum of I2959-N-2xAHM

Table 4.1 summarizes the solubility of the synthesized PIs and the commercial reference. While I2959 is soluble in water, the synthesized monomers, I2959-NH-AHM and I2959-N-2xAHM, are not soluble in water. They are soluble in methanol thanks to their -OH group. Also, they are soluble in low polarity solvents such as DCM, THF and acetone. Additionally, these novel monomeric PIs have good compatibility with TMPTA, PEGDA and HEMA.

Table 4.1. Solubilities of the synthesized and commercial PIs.

PIs	H_2O	Methanol	Diethyl ether	CH_2Cl_2	$CHCl_3$	THF	DMF	Acetone
I2959	+	+	+	+	+	+	+	+
I2959-NH-AHM	-	+	-	+	+	+	+	+
I2959-N-2xAHM	-	+	-	+	+	+	+	+

4.3.2. Light Absorption Properties

Absorption characteristic of I2959-N-2xAHM was examined by UV-vis spectroscopy. It has a maximum UV absorption wavelength at 272 nm in ethanol due to π-$\pi*$ transition. The molar absorption coefficient of I2959-N-2xAHM was found as $\varepsilon = 28265\ M^{-1}\ cm^{-1}$ in ethanol (Table 4.2).

Table 4.2. Absorption characteristics of I2959-N-2xAHM in ethanol.

PI	Solvent	l_{max} (nm)	ε ($M^{-1}\ cm^{-1}$)
I2959-N-2xAHM	EtOH	272	28265

4.3.3. Photopolymerization Results

The photoinitiation efficiencies of the synthesized monomeric PIs were measured by photo-DSC at 25 °C under UV-visible light (320-500 nm), the photopolymerization rates, conversions, and time to reach maximum rate (t_{max}) were determined and compared with the commercial PI I2959.

In order to determine the reactivity of synthesized PIs as a monomer, they were homopolymerized using UV-vis irradiation (320-500 nm) at 25 °C (Figure 4.7). It was observed that I2959-N-2xAHM (R_{pmax} = 0.102 s^{-1}, t_{max} = 0.06 min and conversion = 86%) is more reactive than I2959-NH-AHM (R_{pmax} = 0.068 s^{-1}, t_{max} = 0.1 min and conversion = 80%) as expected, due to two AHM units.

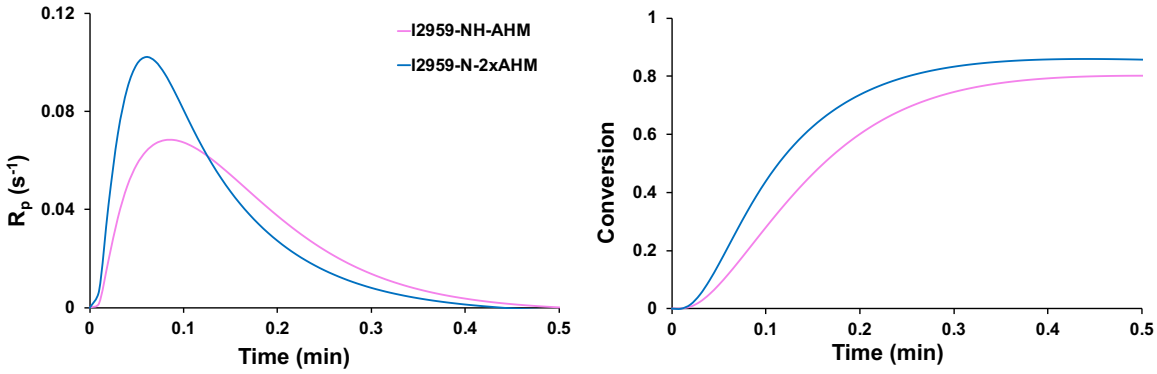


Figure 4.7. Rate-time and conversion-time graphs of I2959-NH-AHM and I2959-N-2xAHM during homopolymerization at 25°C under nitrogen and 320-500 nm irradiation.

In Figure 4.8, the rates of polymerization and the conversions of HEMA, PEGDA and TMPTA are shown by using I2959-NH-AHM as a function of time to investigate the PI efficiency of I2959-NH-AHM and the results were compared with commercial photoinitiator I2959. Formulations containing 1% by weight of PI were prepared. At the same PI concentrations of HEMA samples, I2959-NH-AHM showed similar results (R_{pmax} = 0.018 s^{-1}, t_{max} = 1.21 min and conversion = 83%) to I2959 (R_{pmax} = 0.019 s^{-1}, t_{max} = 1.24 min and conversion = 93%). Although the polymerization rate of the PEGDA monomer containing I2959-NH-AHM (R_{pmax} = 0.138 s^{-1}, t_{max} = 0.04 min and conversion = 94%) was lower than I2959 (R_{pmax} = 0.217 s^{-1}, t_{max} = 0.03 min and conversion = 99%) the conversions and t_{max}

values were found to be similar. The lowest polymerization efficiency for both I2959-NH-AHM (R_{pmax} = 0.057 s^{-1}, t_{max} = 0.03 min and conversion = 46%) and I2959 (R_{pmax} = 0.062 s^{-1}, t_{max} = 0.02 min and conversion = 49%) were obtained from the TMPTA monomer with three double bonds due to the high crosslink density.

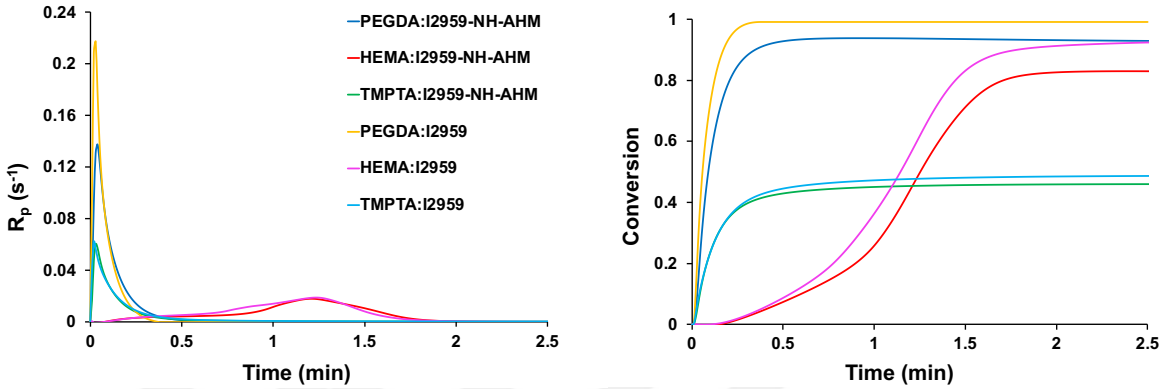


Figure 4.8. (A)Rate-time and (B) conversion-time plots for HEMA, PEGDA and TMPTA containing I2959-NH-AHM (1 wt. %) and I2959 (1 wt.%) at 25 ºC under nitrogen and 320-500 nm irradiation.

The photoinitiation efficiency of I2959-N-2xAHM was investigated in polymerizations of HEMA, PEGDA and TMPTA using UV-vis irradiation (320-500 nm) at 25 °C and compared to those of I2959-NH-AHM and commercial photoinitiator I2959 (Figure 4.9 and Figure 4.10). It was observed that I2959-N-2xAHM (R_{pmax} = 0.166 s^{-1}, t_{max} = 0.04 min and conversion = 96%) showed faster photopolymerization kinetics compared to I2959-N-AHM (R_{pmax} = 0.138 s^{-1}, t_{max} = 0.04 min and conversion = 94%) in PEGDA but it is slower than I2959 (R_{pmax} = 0.217 s^{-1}, t_{max} = 0.03 min and conversion = 99.%). The higher reactivity of I2959-N-2xAHM in PEGMA compared to I2959-NH-AHM can be ascribed to the higher number of double bond that the former one has. In HEMA, while R_{pmax} values were found to be almost similar (I2959-N-2xAHM = 0.015, I2959-NH-AHM = 0.018, I2959 = 0.019), their conversion values were found to be in the order of I2959>I2959-NH-AHM>I2959-N-2xAHM. The photopolymerization kinetics of I2959-N-2x-AHM was found to be similar to I2959 and I2959-NH-AHM in TMPTA.

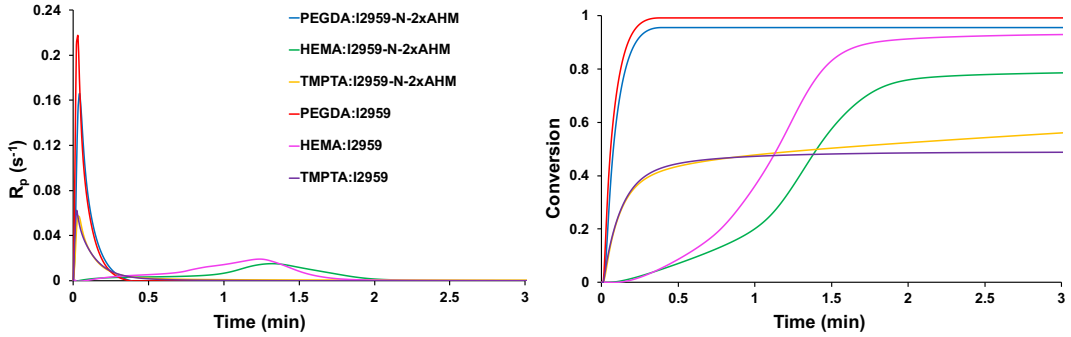


Figure 4.9. (A) Rate-time and (B) conversion-time plots for HEMA, PEGDA and TMPTA containing I2959-N-2xAHM (1 wt. %) and I2959 (1 wt.%) at 25 ºC under nitrogen and 320-500 nm irradiation.

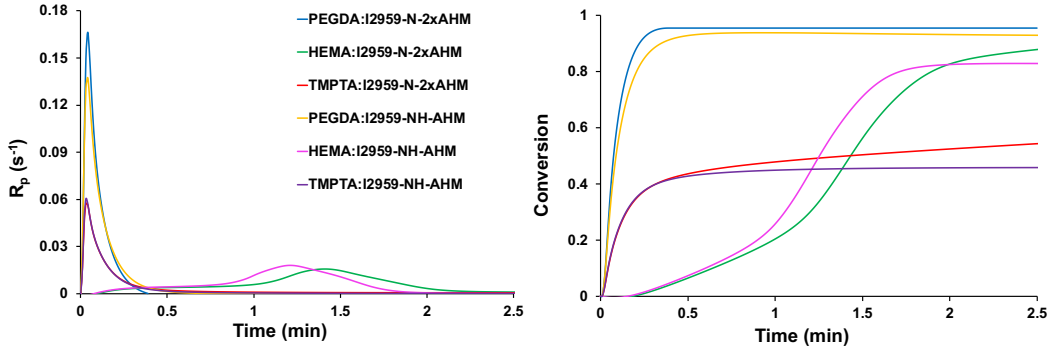


Figure 4.10. (A) Rate-time and (B) conversion-time plots for HEMA, PEGDA and TMPTA containing I2959-N-2xAHM (1 wt. %) and I2959-NH-AHM (1 wt.%) at 25 ºC under nitrogen and 320-500 nm irradiation.

4.3.4. Migration Stability

The migration stability of the monomeric PIs, I2959-N-2xAHM and I2959-NA-AHM, were analyzed together with commercial I2959. UV-visible spectra were used to determine concentration of the PIs extracted from PEGDA gels prepared using the same concentrations of PIs and after immersion in chloroform for 4 days (Figure 4.11). It was found out that I2959-N-2xAHM and I2959-NA-AHM (8% and 16% respectively) have higher migration stability than I2959 (57%). This huge difference results from the incorporation of I2959-N-2xAHM and I2959-NA-AHM into the network structure and also from higher crosslink density obtained from I2959-N-2xAHM due to its dimethacrylate functionality. The higher migration stabilities of monomeric PIs enable reduction of the toxicity.

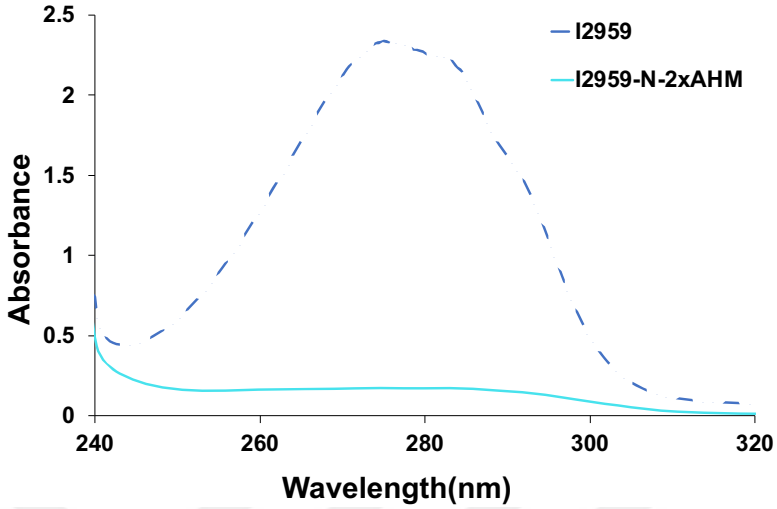


Figure 4.11. UV-Visible absorption spectra of I2959 and I2959-N-2xAHM extracted with chloroform from the PEGDA polymer samples.

4.4. Conclusion

In summary, two novel monomeric Type I PIs were successfully synthesized, and their structures were confirmed by NMR and FTIR. The phoinitiating efficiencies of these PIs were investigated via homopolymerization. It was noted that I2959-N-2xAHM shows more reactivity compared to I2959-NH-AHM, which is predicted due to the presence of two AHM units in the former. The migration stability of exemplary PI, I2959-N-2xAHM are significantly better than those of I2959, allowing for the production of ecologically benign products. Due to their high reactivity as monomeric photoinitiators, they have the ability to undergo homopolymerization or copolymerization with commercially available monomers. This results in the formation of linear or crosslinked polymers that possess various functionalities, allowing for customization of the physical properties of the resulting materials.

5. NOVEL IBUPROFEN CYSTAMINE SALTS WITH IMPROVED SOLUBILITY

5.1. Introduction

This chapter focuses on the synthesis of two novel cystamine salt derivatives of ibuprofen (IBU-CYS 1and IBU-CYS 2) to improve the solubility and bioavailability of ibuprofen (Figure 5.1). The salts are characterized by ^{1}HNMR, FT-IR and UV-Vis spectroscopy, differential scanning calorimetry (DSC) and thermogravimetry (TGA, DTA). In comparison with ibuprofen, the salts show higher solubility (around 300 and 6 times) in water and PBS. The in vitro studies indicate that the salts are effective in relieving inflammatory responses induced by lipopolysaccharide in RAW264.7 macrophage cells while indicating no cytotoxicity. Therefore, these salts may be promising candidates for the development of effective formulations of this drug.

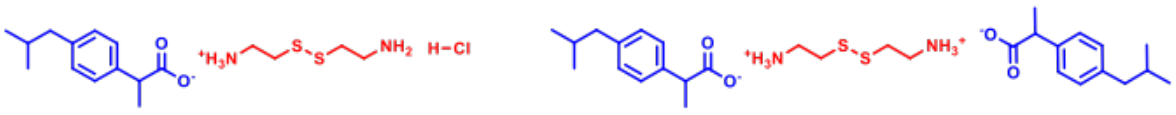


Figure 5.1. Synthesized salts IBU-CYS 1 and IBU-CYS2.

5.2. Experimental

5.2.1. Materials and Characterization

Sodium salt of ibuprofen, cystamine dihydrochloride (2,2′-diaminodiethyl disulfide dihydrochloride), HEMA, PEGDA (M_n = 575 D), I2959, indomethacin, (3-(4,5-dimethylthiazol-2-yl)-2,5-diphenyltetrazolium bromide) (MTT), lipopolysaccharide (LPS) from *Eschrechia coli* 0111: B4 and the other reagents and solvents were obtained from Sigma Aldrich (St. Louis, Missouri, USA) and used as received without purification. Sodium nitrite was purchased from Fluka Chemika-BioChemika (Buchs, Switzerland). RAW 264.7 mouse macrophages (ATCC® TIB-71 TM) were obtained from ATCC (Manassas, VA, USA). Dulbecco's Modified Eagle's Medium (DMEM) supplemented with 10% fetal bovine serum (FBS) and 1% penicillin (10.000 units/mL) and streptomycin (10.000 mg/mL) were purchased from Gibco, Thermo Fisher Scientific (Waltham, MA, USA).

NMR spectra were recorded on a Varian Gemini 400 MHz spectrometer with deuterated methanol (MeOD) as solvent. IR spectra were obtained using a Nicolet 6700 FT-IR spectrophotometer. DSC measurements were performed on a TA Instruments Q250 with a heating rate of 10 ºC/min under nitrogen atmosphere. TGA was performed by using TA Instruments Q500 under nitrogen atmosphere. The samples were heated from room temperature to 700 °C at a rate of 10 °C/min.

5.2.2. Synthesis of Ibuprofen Salts

5.2.2.1. Synthesis of IBU-CYS 1. Cystamine dihydrochloride (0.21 g, 0.97 mmol) was dissolved in 5 mL water. Ibuprofen sodium salt (0.22 g, 0.97 mmol) dissolved in 10 mL water was added slowly, and the reaction mixture was stirred for 6 h at room temperature. The resulting solution was centrifuged, and the collected precipitate was freeze-dried to obtain the product as a white solid (49 %).

^{1}H NMR (400 MHz, $CDCl_3$, δ): 0.83 (d, 6H, C*H*$_3$-CH), 1.34 (d, 3H, C*H*$_3$-CH), 1.76 (dt, 1H, $(CH_3)_2$-C*H*-CH_2), 2.35 (d, 2H, C*H*$_2$-Ar), 2.87 (t, 4H, -CH_2CH_2S-), 3.14 (q, 4H, -CH_2CH_2N-), 3.49 (q, 1H, CH-C=O) ,7.00 (d, 2H, Ar-CH), 7.18 (d, 2H, Ar-CH) ppm.
FTIR (ATR): 1615 (C=O) cm^{-1}.

5.2.2.2. Synthesis of IBU-CYS 2. Cystamine dihydrochloride (0.15 g, 0.67 mmol) was dissolved in 5 mL water. Ibuprofen sodium salt (0.3 g, 1.33 mmol) dissolved in 15 mL water was added slowly, and the reaction mixture was stirred for 6 h at room temperature. The resulting solution was centrifuged, and the collected precipitate was freeze-dried to obtain the product as a white solid (51%).

^{1}H NMR (400 MHz, $CDCl_3$, δ): 0.82 (d, 12H, C*H*$_3$-CH), 1.34 (d, 6H, C*H*$_3$-CH), 1.77 (dt, 2H, $(CH_3)_2$-C*H*-CH_2), 2.36 (d, 4H, C*H*$_2$-Ar), 2.89 (t, 4H, -CH_2CH_2S-), 3.16 (q, 4H, -CH_2CH_2N-), 3.50 (q, 2H, CH-C=O) ,7.00 (d, 4H, Ar-CH), 7.18 (d, 4H, Ar-CH) ppm.

FTIR (ATR): 1614 (C=O) cm^{-1}.

5.2.3. Synthesis of Hydrogels

IBU-CYS 2 (0.02 g, 0.035 mmol), PEGDA (0.02 g, 0.037 mmol) and HEMA (0.16 g, 1.22 mmol) were dissolved in water at 10:10:80 wt % to form precursor solutions for hydrogels. I2959 (2 wt% of total monomer weight) was added as a photoinitiator and the mixture were polymerized by exposure to UV light (365 nm) for 30 minutes in a syringe. Since the synthesized salt was encapsulated within the gel matrix, to prevent the possibility of release, no washing procedure was carried out. Water was lyophilized.

5.2.4. Solubility Study

A solubility study was carried out to determine the degree of enhancement in solubility due to the formation of the salts. First, a UV absorption spectrum of the salts were generated by scanning their aqueous solutions using a JASCO V-730 UV-vis spectrophotometer in the range of 200–300 nm. The λ_{max} of the salts was then determined. Then, the calibration curves of the IBU-CYS salts and ibuprofen were constructed by

measuring the absorbance of their solutions prepared at various concentrations at 222 nm. Finally, the saturated solutions of the salts and ibuprofen were prepared using 5 mL of water and 5 mL of PBS separately in vials. The solutions were stirred at 25 °C for 24 h. After this, the solutions were filtered, the filtrates were diluted to measure their absorbances at 222 nm. The solubilities were calculated according to the calibration curves.

5.2.5. In Vitro Drug Release Studies

The drug release studies of the parent drug ibuprofen, the synthesized salts and salts' encapsulated HEMA: PEGDA gel forms were done in phosphate buffered saline (PBS). Briefly, the pre-weighed dry samples and 3 mL PBS were transferred to dialysis membrane (3500 Da) and it was placed into a flask containing 150 mL of PBS maintained at 37 °C and stirred at 150 rpm. At predetermined time intervals 4 mL of external solution was removed and equal volume of fresh solution was added to the system. Each sample was analyzed by UV-vis spectrophotometer (JASCO V-730) and the amount of released IBU was calculated using the absorbance at 222 nm according to calibration curve. The linear correlation (R^2=0.999) between the absorption and concentration of IBU was determined using known concentration samples (0.002, 0.004, 0.008, 0.013, 0.018, 0.022, 0.045, 0.067 and 0.1 mg mL^{-1} of IBU in PBS).

5.2.6. Cell Viability Assay

To determine the effect of synthesized IBU-CYS 1 and IBU-CYS 2 on cell viability, MTT assay was used. The RAW 264.7 mouse macrophages were cultivated in complete medium, which consisted of DMEM, supplemented with 10% FBS and 1% penicillin (10.000 units/mL) and streptomycin (10.000 mg/mL). They were maintained at a temperature of 37 °C with 5% CO_2 in a humidified atmosphere [133]. The cells were subcultured once they reached a confluence of 80-90%. The RAW264.7 cells were initially seeded in 96-well culture plates at a density of 5×10^4 cells/well for 24 hours in complete medium. The cells were then treated with various concentrations of the IBU-CYS salts (ranging from 12.5-100 μM) for 24 hours. Then the MTT reagent (0.5 mg/mL in PBS) was added to the cells and incubated for 2 hours at 37 °C with 5% CO_2. After removing the culture supernatants, 100 μL of isopropanol was added to each well to dissolve the formazan

blue, and the absorbance was measured at 570 nm using a microplate reader (Thermo Fisher ScientificT9M, Inc., Waltham, MA, ABD). The cell viability assay was conducted three times, and each assay was performed in triplicate (n=9 in three separate experiments). A cell viability of cultures treated with gels of less than 70% compared to untreated control cultures (medium group) is considered as a cytotoxic [134]. The percentage of cell viability was calculated as

$$\text{Cell viability (\%)} = (As/Ac) \times 100 \quad (5.1)$$

whereas and Ac show absorbance of the samples and the control, respectively.

5.2.7. Anti-inflammatory Activity

The inhibition of NO production was assessed by measuring nitrite oxide (NO) levels in the cell culture medium using the Griess reagent (0.1% N-(1-Naphthyl)-ethylenediamine dihydrochloride in 5% phosphoric acid and 1% sulfanilamide) [135]. RAW 264.7 cells were plated in a 96-well plate at a density of 5×10^4 cells/well and incubated for 24 hours at 37°C with 5% CO_2. After pre-treating the cells with various concentrations of the IBU-CYS 1 and IBU-CYS 2 (12.5-25-50-100 µM) for 2 hours and stimulating them with 1 µg/mL of LPS for an additional 22 hours, the cell culture supernatant was collected. The cell culture supernatants were collected after 24 hours for NO analysis. Nitrite concentrations were measured using Griess' reagent. The supernatant was mixed with an equal volume of Griess reagent in a 96-well plate for 10 minutes at room temperature in the dark. The color development corresponding to NO level was assessed at 540 nm using a microplate reader (Thermo Fisher Scientific Inc., Waltham, MA USA). The nitrite concentrations were determined using a sodium nitrite standard curve. The researchers used Indomethacin (100 mM) was used as a positive control [136].

5.2.8. Statistical Analysis

Each experiment was carried out in triplicate. The GraphPad Prism 9 was used for the statistical analyses (GraphPad Software, Inc., San Diego, CA; The 8.4.3 version). Following the Tukey post hoc tests, one-way ANOVA was used to determine group differences.

5.3. Results and Discussion

5.3.1. Synthesis and Characterization of Ibuprofen Salts

Two novel ibuprofen salts (IBU-CYS 1 and IBU-CYS 2) were successfully synthesized by an electrostatic interaction mechanism between ibuprofen sodium salt and cystamine dihydrochloride in 1:1 and 2:1 mole ratios as white crystalline solids with a reasonable yield (~50%) (Figure 5.2). Their structures were investigated by IR and NMR spectroscopy. The ^{1}H NMR spectrum of IBU-CYS 1 and IBU-CYS 2 revealed the aromatic protons at 7.00 and 7.18 ppm and two methyl protons at 0.83 and 1.34 ppm as doublets of doublets and a methine proton as a multiplet due to proton/proton vicinal coupling (Figure 5.3 and Figure 5.4). The formation of cystamine salts was supported by the shift of cystamine protons, two triplets at 2.87 and 3.14 ppm, toward higher field. Also, the quartet from methine proton next to carboxylate is shifted slightly (3.56 ppm) toward lower field. In the ^{13}C NMR spectrum of IBU-CYS 2, peaks belonging to cystamine carbons were observed at 34.59 and 38.11 ppm, while aromatic carbons of ibuprofen were observed between 126 and 140 ppm (Figure 5.5). The FTIR spectra of the synthesized salts were compared to that of the precursors and confirmed the ionic structure of the synthesized compounds (Figure 5.6). The salts showed the presence of an asymmetric NH_3^+ bending at 1615 cm^{-1} and a symmetrical bend at 1514 cm^{-1}. The carboxylate anion (COO^-) absorbs strongly at around 1563 and 1359 cm^{-1} due to asymmetric and symmetric stretching vibrations.

Table 5.1 summarizes the solubility of IBU-CYS 1 and IBU-CYS 2 and IBU as reference, in various solvents. The synthesized salts exhibit enhanced solubility in polar solvents compared to non-polar solvents. They show similar solubility behavior to IBU in highly polar (methanol), slightly polar ($CHCl_3$ and THF) solvents; however, these salts diverge from Ibuprofen in terms of solubility in non-polar solvents like hexane.

The UV-vis spectra of the salts show the maximum absorbance at 223-224 nm, similar to Ibuprofen, indicating the $\pi \rightarrow \pi^*$ electronic transition (Figure 5.7).

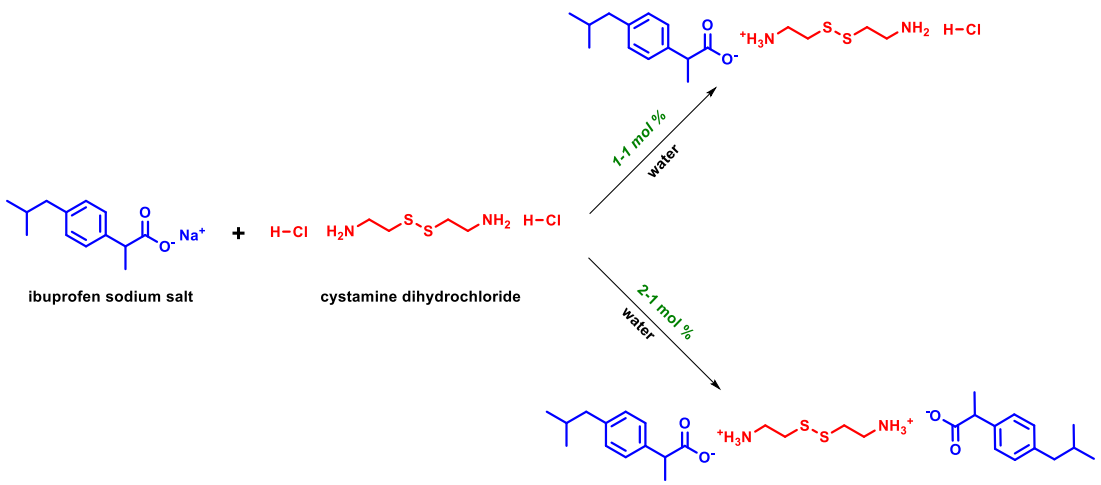


Figure 5.2. Synthesis of ibuprofen salts

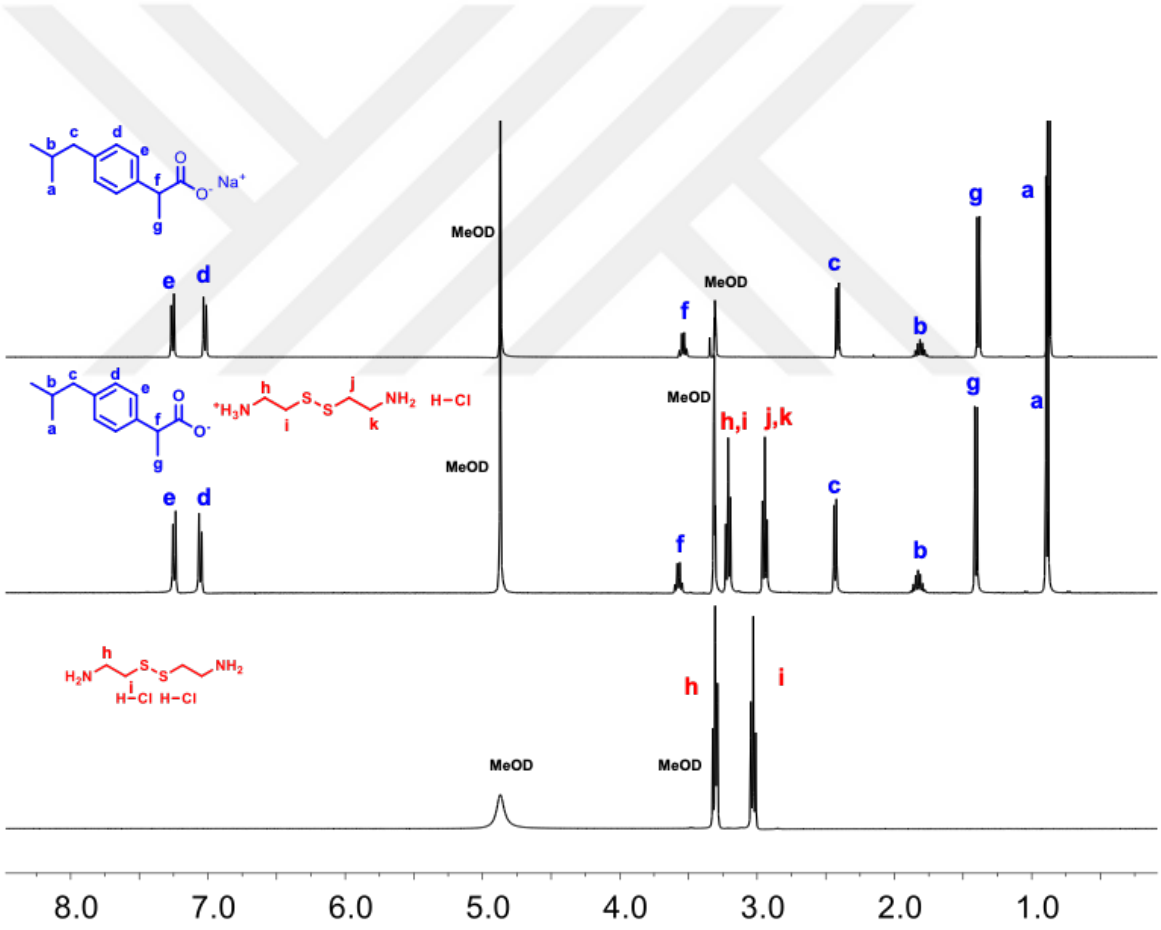


Figure 5.3. [1]H NMR spectrum of IBU-Na, cystamine dihydrochloride and IBU-CYS 1

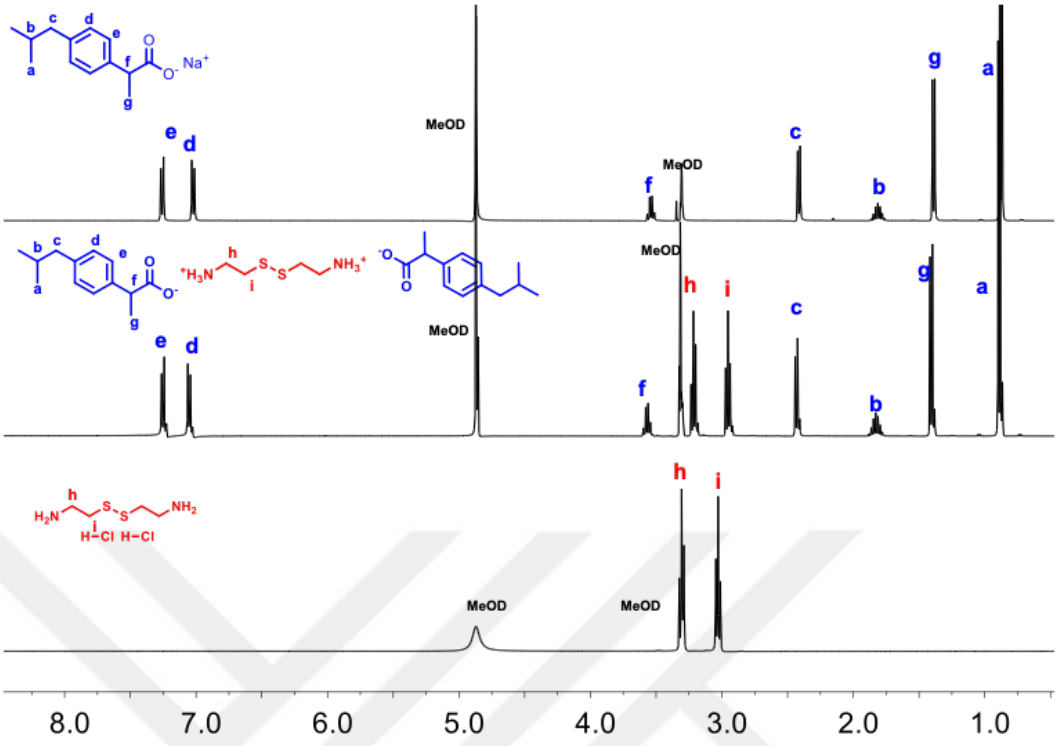


Figure 5.4. [1]H NMR spectrum of IBU-Na, cystamine dihydrochloride and IBU-CYS 2

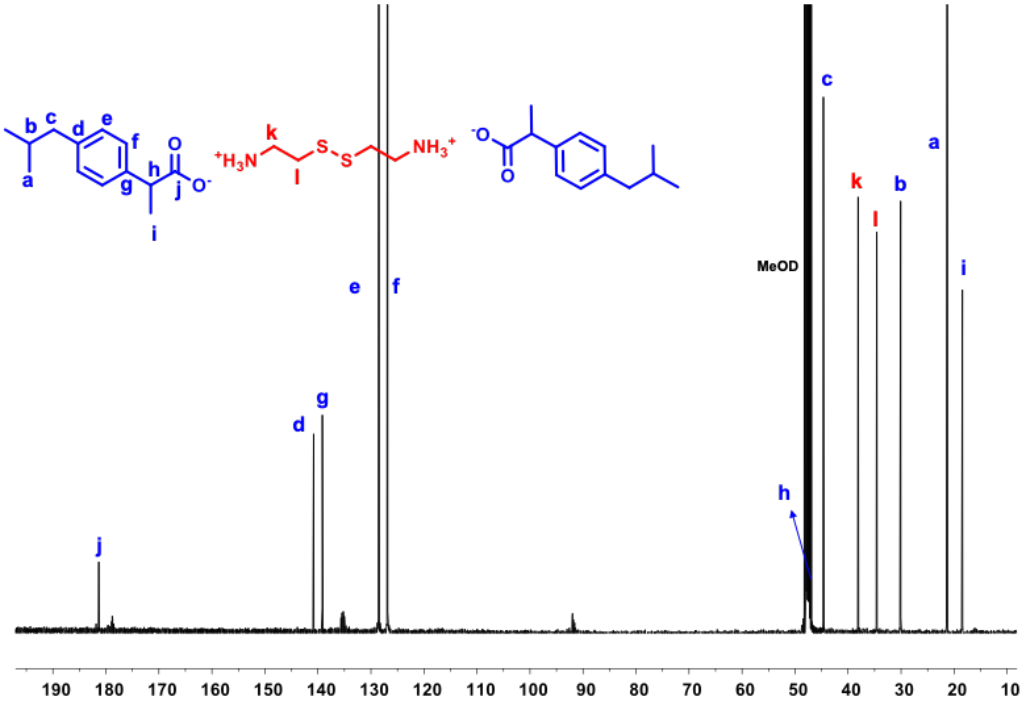


Figure 5.5. [13]C NMR spectrum of IBU-CYS

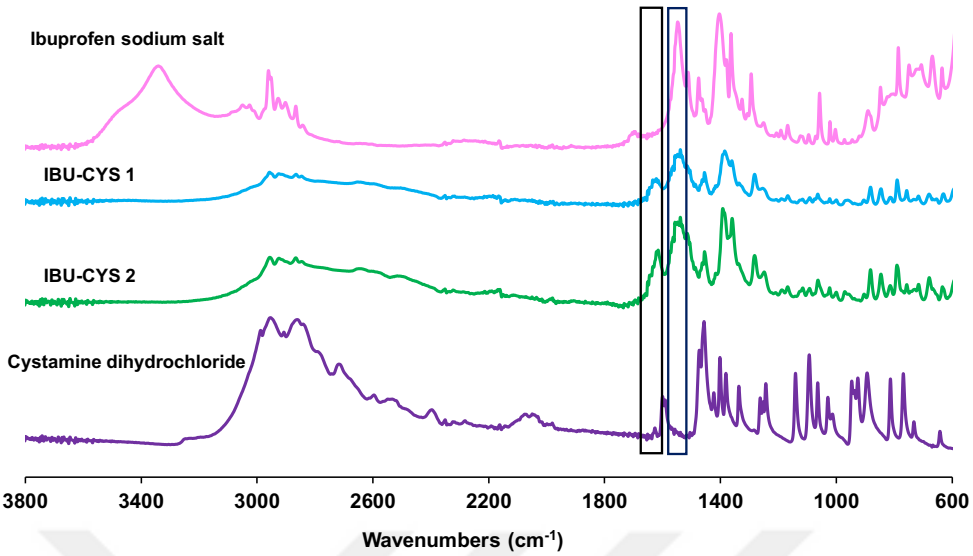


Figure 5.6. FTIR spectra of Ibuprofen sodium salt, cystamine dihydrochloride, IBU-CYS 1 and IBU-CYS 2

Table 5.1. Solubility of IBU, IBU-CYS 1 and IBU-CYS 2

Salt/IBU	H_2O	MeOH	EtOH	$(C_2H_5)_2$	$CHCl_3$	DCM	THF	Hexane	
IBU	-	+	+	+	+	+	+	+	
IBU-CYS 1	+	+	+	±	+	-	+	-	
IBU-CYS 2	+	+	+	±	+	-	+	-	

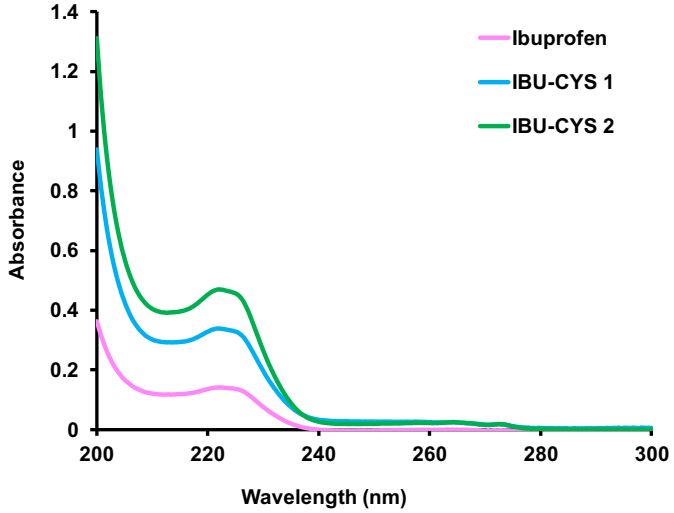


Figure 5.7. UV-Vis spectra of IBU, IBU-CYS 1 and IBU-CYS 2 (3.4×10^{-5} M) in water

5.3.2. Solubility Study

The calibration curves of the IBU-CYS salts and ibuprofen were plotted by measuring the absorbance of the solutions prepared at various concentrations at 222 nm (Figure 5.8, Figure 5.9 and Figure 5.10) and saturated solutions of the salts and ibuprofen were prepared in 5 mL water or 5 mL PBS in vials. The saturated solutions (0.5 mL) was diluted to a volume of 100 mL and their concentrations were determined by measuring their absorbances and using calibration curves. This concentration was then multiplied by the dilution factor to find the concentration of the saturated solution, representing the total amount of the salt soluble in 1 mL of water or PBS.

The solubility of IBU-CYS 1 and IBU-CYS 2 in water was found to be 6.11 and 7.81 mg/mL respectively (Table 5.2). This is a significant improvement over the solubility of pure ibuprofen which was found to be 0.04 mg/mL under the same conditions. The solubility of the salts also increased in PBS to 7.48, 9.24 compared to IBU (1.96 mg/mL).

Table 5.2. Solubility table of IBU-CYS salts and ibuprofen in both water and PBS expressed in mg/mL

Salt/IBU	Water	PBS
IBU	0.04	1.96
IBU-CYS 1	6.11	7.48
IBU-CYS 2	7.81	9.24

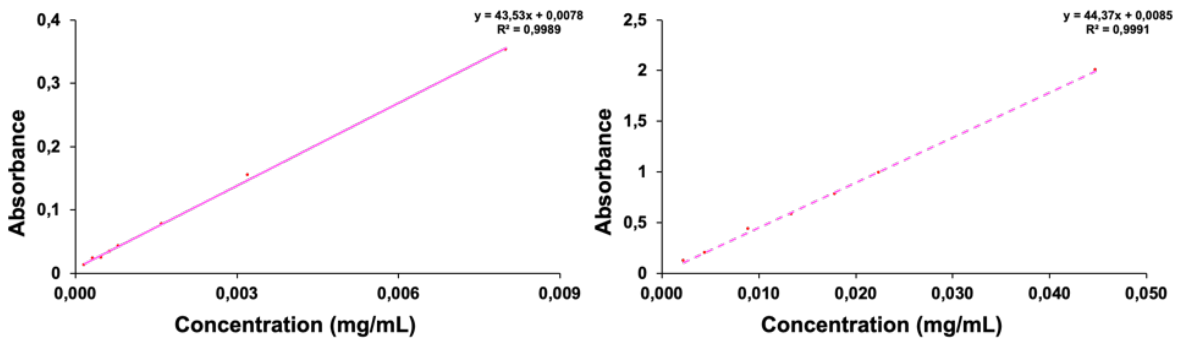


Figure 5.8. Calibration curve of ibuprofen in water and PBS

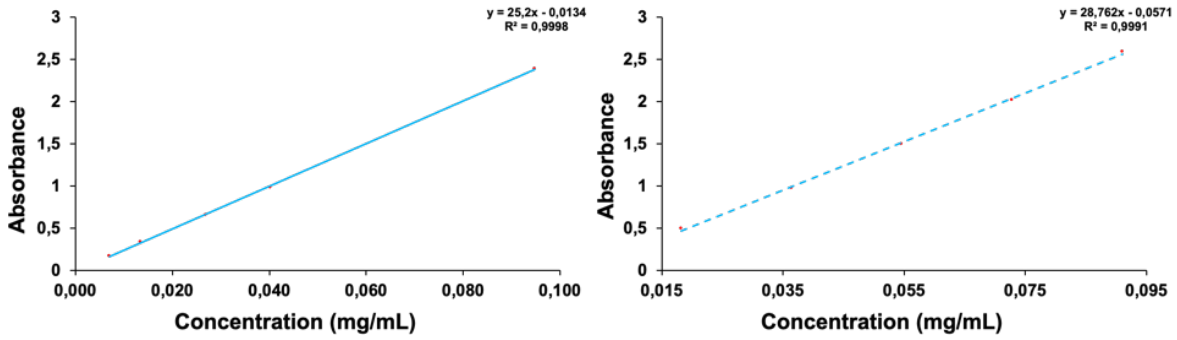


Figure 5.9. Calibration curve of IBU-CYS 1 in water and PBS

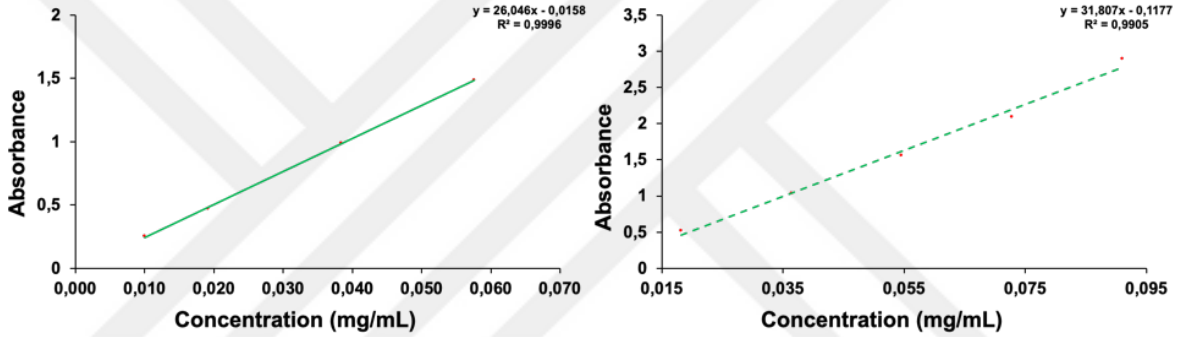


Figure 5.10. Calibration curve of IBU-CYS 2 in water and PBS

5.3.3. Thermal Studies

The thermal properties of the salts were investigated using DSC and TGA/DTA. The DSC plots of ibuprofen and the synthesized salts are given in Figure 5.11. IBU shows an endotherm at 77.36 °C, corresponding to its melting point (75-77.5 °C) [137]. On the other hand, DSC plots of IBU-CYS 1 and IBU-CYS 2 showed very sharp endotherms at 131.11 and 131.62 °C respectively, indicating their crystalline structures. The melting points was found to be independent of their structures; both are 53-54 °C higher than IBU.

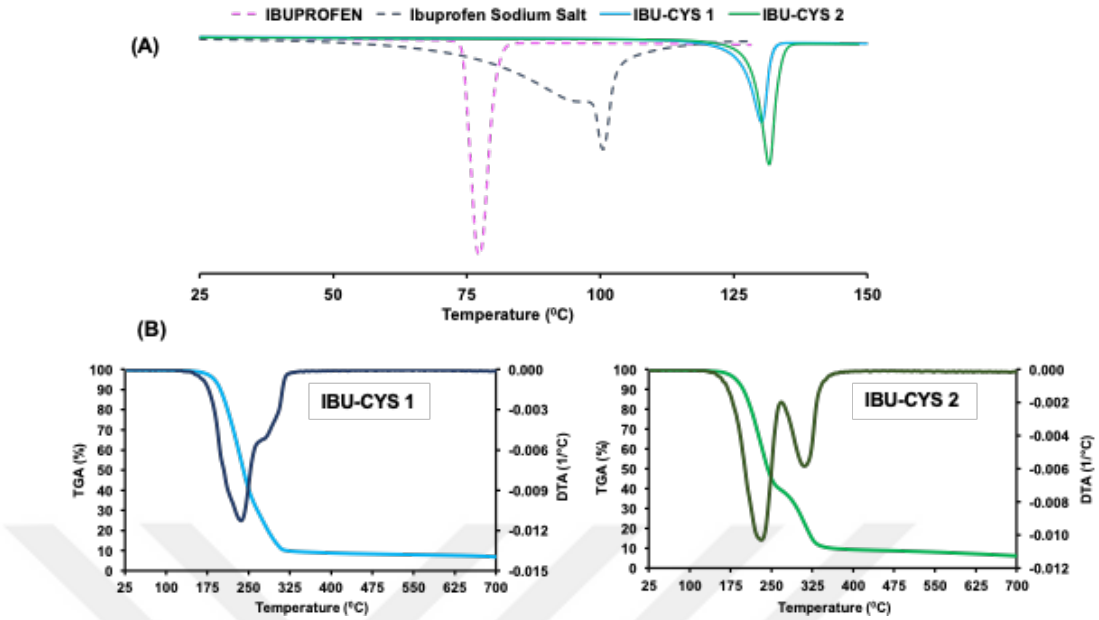


Figure 5.11. (A) DSC spectra of IBU, IBU sodium salt, IBU-CYS 1 and CYS 2, (B) TGA and DTA spectra of IBU-CYS 1 and IBU-CYS.

Thermal stability of the salts was investigated by TGA/DTA under nitrogen atmosphere (Figure 5). The thermal degradation of IBU-CYS 1 occurred at one step starting from 140 °C, a DTA peak appear with maxima at 236 °C. But then IBU-CYS 2 showed two distinct steps of thermal degradation at temperatures of approximately 140 and 220 °C. These steps showed mass loss percent of 60 and 89%, accompanied by endothermic DTA peaks at 233 and 310 °C respectively.

5.3.4. Release Studies

The release studies of the synthesized salts and IBU-CYS 2 encapsulated in HEMA:PEGDA hydrogel were investigated using the dialysis membrane. The dialysis was carried out in PBS solution at physiological pH 7.4. Figure 5.12 shows the diffusion profile of the ibuprofen and the salts through the membrane. It was clearly observed that the diffusion of the salts occurred more quickly than ibuprofen. The diffusion of hydrogel encapsulated IBU-CYS 2 through the dialysis membrane occurs slowly.

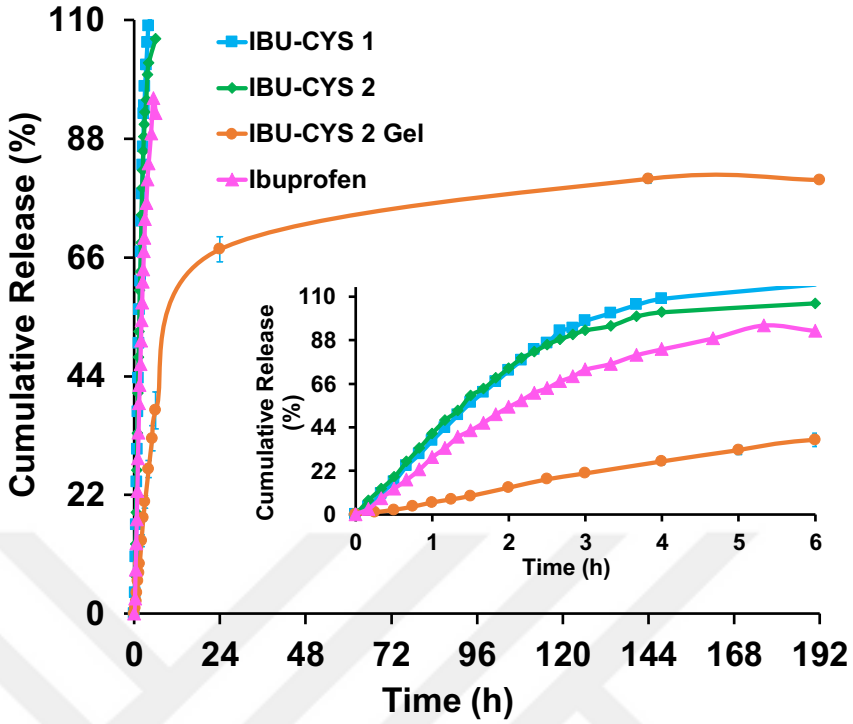


Figure 5.12. The release profiles of ibuprofen, IBU-CYS 1, IBU-CYS 2 and IBU-CYS 2 from HEMA/PEGDA gel

5.3.5. In Vitro Cytotoxicity of The Ibuprofen Salts

Prior to the evaluation of anti-inflammatory activity, non-toxic concentrations of samples were determined by cell viability of 70% and above, which both salt forms were observed to be non-cytotoxic for all concentrations. The MTT assay showed that all samples had no cytotoxic effects at concentrations up to 100 µM at 24 h as compared with control cells that received no treatment (Table 5.3).

Table 5.3. Effects of different salt forms of ibuprofen on the viability of RAW264.7 macrophage cells and the effects of the different salt forms of ibuprofen on nitrite levels and % nitrite inhibition in RAW 264.7 cells stimulated with 1 µg/mL LPS. Ctrl: Control group treated with DMEM; LPS: Control group only stimulated with LPS; LPS: Lipopolysaccharides from E. coli; IND: Indomethacin (100 µM). Statistically significant differences were indicated for each compound vs. LPS (*p<0.05, **p<0.001.)

Groups	**Dose (µM)**	**Cell Viability (%)**	**Nitrite Level (µM)**	**Nitrite Inhibition (%)**
Ctrl		112.44 ± 3.07	2.42 ± 0.20	-
LPS		100.00 ± 0.05	60.92 ± 0.79	-
L-Name	100	92.85 ± 2.05	30.93 ± 0.87**	49.23 ± 1.71
Ibuprofen	100	93.87 ± 0.35	41.73 ± 1.59**	31.50 ± 2.53
Indomethacin	100	94.12 ± 1.39	29.88 ± 0.72**	50.95 ± 0.62
IBU-CYS 1	12.5	105.86 ± 4.42	51.14 ± 1.33**	16.03 ± 2.91
	25	100.99 ± 3.50	47.34 ± 0.49**	22.28 ± 0.86
	50	93.74 ± 2.83	44.39 ± 1.33**	27.15 ± 1.53
	100	89.29 ± 3.46	40.03 ± 0.64**	34.29 ± 1.18
IBU-CYS-2	12.5	102.27 ± 0.60	54.41 ± 0.53*	10.66 ± 1.89
	25	97.91 ± 3.34	50.44 ± 0.99**	17.20 ± 1.56
	50	92.61 ± 2.46	48.13 ± 1.71**	20.99 ± 2.43
	100	87.63 ± 1.15	44.45 ± 0.26**	27.03 ± 0.84

5.3.6. In Vitro Evaluation of The Anti-Inflammatory Effect of The Ibuprofen Salts

The ability of the ibuprofen salts to inhibit LPS-induced nitrite production in RAW 264.7 cells was evaluated and compared with those of L-name (100 µM) which is a direct inhibitory agent of nitrite oxide and indomethacin (100 µM) and ibuprofen (100 µM), serving as reference compounds (Figure 5.13). Treatment with LPS (1 µg/mL) led to a significant increase in nitrite levels in the cell culture supernatant (Table 5.3). NO production after LPS stimulation increased to 60.92 ± 0.79 µM in the untreated cells. However, both salt forms exhibited a concentration-dependent reduction in LPS-induced nitrite production,

as shown in Table 5.3. The treatment of L-name (100 μM) and indomethacin (100 μM) significantly inhibited nitrite oxide production as 49% and 50% respectively ($p<0.001$). In comparison of anti-inflammatory activity of L-name and indomethacin, ibuprofen showed less anti-inflammatory effect. This is due to the information from a study that revealed the use of lower doses than 200 μM of ibuprofen produce effect out therapeutic range therefore have slight anti-inflammatory effect [138].

Moreover, nitrite inhibition of IBU-CYS 1 and IBU-CYS 2 at their highest studied concentrations was approximately 35% and 27% respectively. As a result, IBU-CYS 1 salt form at 100 μM concentration have shown greater anti-inflammatory activity in comparison to ibuprofen.

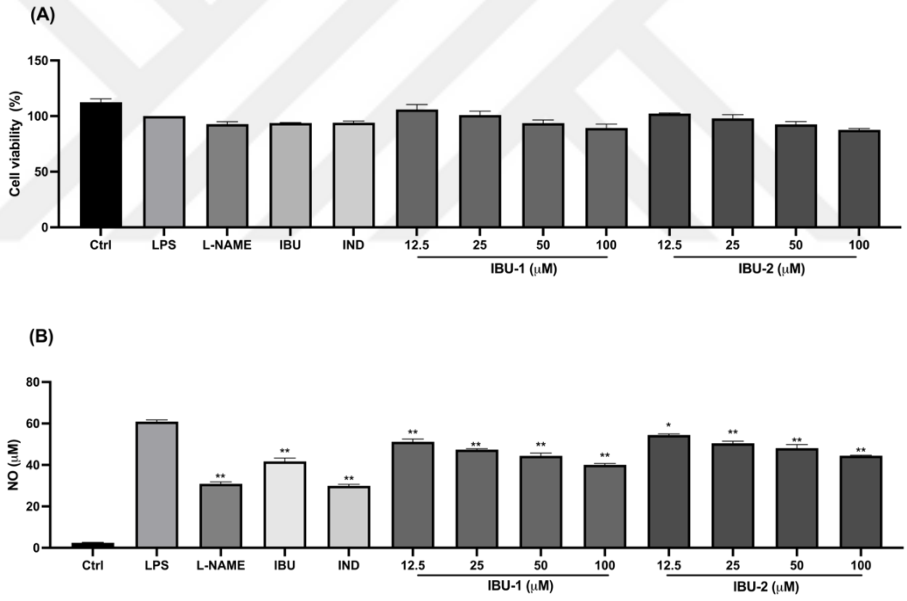


Figure 5.13 The effects of IBU-CYS 1 and IBU-CYS 2 at different doses (12.5, 25, 50 and 100 μM) on cell viability (A), on nitrite production (B) on LPS stimulated RAW 264.7 cell Ctrl: Control group treated with DMEM; LPS: Control group only stimulated with LPS; LPS: Lipopolysaccharides from E. coli; IND: Indomethacin (100 μM). Statistically significant differences were indicated for each compound vs. LPS (*$p<0.05$, **$p<0.001$.)

5.4. Conclusions

In summary, two noval ibuprofen salts with cystamine cations were successfully and quantitatively synthesized and characterized. The synthesized salts showed improved solubility in water and PBS in comparison with both the free acid and sodium salt of ibuprofen. The salts did not affect the cell viability of RAW264.7 macrophages similar to ibuprofen. The derivatives showed similar anti-inflammatory activity compared to ibuprofen.

6. SYNTHESIS OF AN IBUPROFEN FUNCTIONALIZED ALKYL α-HYDROXYMETHACRYLATE-BASED CROSSLINKER

6.1. Introduction

This chapter focuses on the synthesis of a new monomeric prodrug of ibuprofen (CYS-2xIBU) based on alkyl α-hydroxymethacrylate and cystamine to improve bioavailability, decrease toxicity and control delivery of ibuprofen (Figure 6.1). The free radical copolymerization of the synthesized crosslinker with PEGDA gave a hydrogel with ibuprofen linked through ester bonds on the side chain. The hydrogel also contains disulfide linkages, therefore may exhibit redox responsivity. It is prone to selective cleavage in the reducing environment of tumor tissue and intracellular compartments through thiol–disulfide exchange reactions. The amount of released ibuprofen from the hydrogel was found to be low, so as to increase bioavailability and decrease gastric side effects. As a result, this monomeric prodrug is a promising option for more effective delivery of the drug.

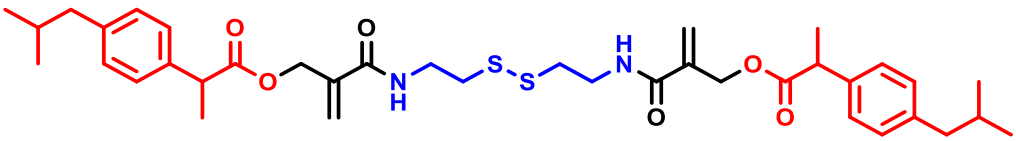


Figure 6.1. Synthesized crosslinker CYS-2xIBU.

6.2. Experimental

6.2.1. Materials and Characterization

Sodium salt of ibuprofen (α-methyl-4-(isobutyl)phenylacetic acid), I2959, cystamine hydrochloride, 1,3-dicyclohexylcarbodiimide (DCC), 4-dimethylaminopyridine (DMAP), trifluoroacetic acid (TFA), poly(ethylene glycol) diacrylate (PEGDA, M_n = 575 D), and other chemicals were purchased and available from Sigma-Aldrich. was used as directed.

NMR spectra were recorded on a Varian Gemini 400 MHz spectrometer with deuterated chloroform ($CDCl_3$) as solvent. IR spectra were obtained using a Nicolet 6700 FT-IR spectrophotometer. An orbital shaker with VWR incubator was used for ibuprofen release studies. UV-vis spectra were recorded on JASCO V-730 UV-vis spectrometer. The morphology of the hydrogel was examined using scanning electron microscopy (SEM) (JEOL Model: JCM5000).

6.2.2. Synthesis of Monomeric Prodrug

6.2.2.1. CYS-2xIBU. DCM (2mL) solution of DMAP (0.0086 g, 0.007 mmol) was added onto MA-IBU (0.041 g, 0.14 mmol) (synthesized by our group) and nitrogen was passed through the mixture for five minutes. Then, cystamine synthesized according to the method in the literature [139] was added dropwise to this mixture under ice and nitrogen. After waiting for 5 minutes, DCC (0.029 g, 0.14 mmol) was added to the reaction as a solid. The solution was stirred at room temperature for 24 hours. At the end of the reaction, the solution was diluted with 10 mL DCM and kept in the freezer for 1 hour. The precipitated solid was separated with the help of filter paper and the liquid part was extracted 3 times with 5 mL of distilled water. The organic phase was dried with Na_2SO_4 and after the solvent was evaporated, the residue was purified by column chromatography (using hexane-ethyl acetate).

^{1}H NMR (400 MHz, $CDCl_3$, δ): 0.90 (d, 12H, CH_3-CH), 1.51 (d, 6H, CH_3-CH), 1.83 (dt, 2H, $(CH_3)_2$-CH-CH_2), 2.43 (d, 4H, CH_2-Ar), 2.75 (t, 4H, -CH_2CH_2S-), 3.49 (q, 4H, -CH_2CH_2N-), 3.73 (q, 2H, CH-C=O), 4.80 (q, 4H, C-CH_2-O), 5.45 (s, 2H, CH_1H_2=C), 5.94 (s, 2H, CH_1H_2=C), 7.10 (d, 4H, Ar-CH), 7.17 (d, 4H, Ar-CH) ppm.

^{13}C NMR (100 MHz, $CDCl_3$, δ): 18.21 (*C*H_3-CH), 22.35 (*C*H_3-CH), 30.15 (*C*H-CH_2), 37.57 (CH_2-S), 38.44 (CH_2-CH_2-N), 44.98 (CH_3-*C*H), 45.07 (CH-*C*H_2), 63.34 (CH_2-CH_2-O), 62.71 (C-*C*H_2-O), 123.05 (*C*H_2=C), 127.18 (Ar-*C*H), 129.42 (Ar-*C*H), 137.30 (Ar-*C*), 138.26 (CH_2=*C*), 140.78 (Ar-*C*), 166.14 (C=O), 174.42 (C=O) ppm.

FTIR (ATR): 1660-1738 (C=O), 1615 (C=C),

6.2.3. Synthesis of Hydrogels

CYS-2xIBU (0.009 g, 0.013 mmol), PEGDA (0.082 g, 0.14 mmol) were dissolved in ethanol and water (2:1) solution at 10:90 wt % to form precursor solutions for hydrogels. I2959 (2 wt% of total monomer weight) was added as a PI and the mixture were polymerized by exposure to UV light (365 nm) for 30 minutes in a syringe. The crosslinked polymers were soaked in ethanol for 12 hours and then washed with water. Water was lyophilized.

6.2.4. In Vitro Drug Release Studies

The drug release studies of the parent drug ibuprofen and PEGDA gel prepared with the synthesized crosslinker was carried out in phosphate buffered saline (PBS) at 37 °C. Briefly, the pre-weighed dry gel samples and 3 mL PBS were transferred to dialysis membrane (3500 Da) and it was placed into a flask containing 150 mL of PBS maintained at 37 °C and stirred at 150 rpm. At predetermined time intervals 4 mL of external solution was removed and equal volume of fresh solution was added to the system. Each sample was analyzed by UV-vis spectrophotometer (JASCO V-730) and the amount of released IBU was calculated using the absorbance at 222 nm according to calibration curve. The linear correlation (R2=0.999) between the absorption and concentration of IBU was determined using known concentration samples (0.002, 0.004, 0.008, 0.013, 0.018, 0.022, 0.045, 0.067 and 0.1 mg mL^{-1} of IBU in PBS).

6.3. Results and Discussion

6.3.1. Synthesis and Characterization of Monomeric Prodrug

A novel ibuprofen functionalized α-hydroxymethacrylate based crosslinker was synthesized by the aminolysis of MA-IBU (synthesized by our group) using cystamine, which was produced following the procedure described in the literature [139] (Figure 6.2). This reaction took place in the presence of DCC and a catalytic quantity of DMAP in CH_2Cl_2 at room temperature. Subsequently, the reaction mixture was diluted with chloroform,

cooled, and filtered in order to eliminate the reaction by-product, N,N'-dicyclohexylurea. It was also extracted using water. Additionally, column chromatography was used to remove any other impurities like monoadduct and pure CYS-2xIBU was obtained as a colorless oil in 30% yield.

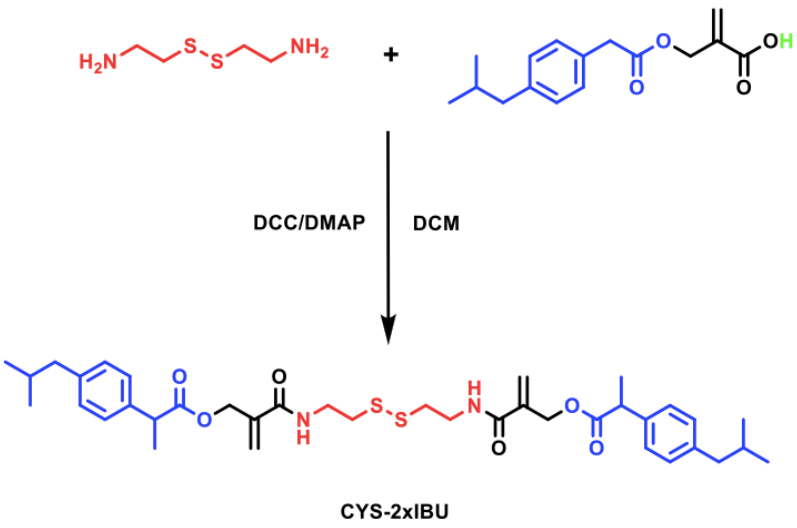


Figure 6.2. Synthesis of CYS-2xIBU.

The structural features of the monomer were confirmed by the ^{1}H NMR,^{13}C NMR and FTIR spectra (Figure 6.3, Figure 6.4 and 6.5). In the ^{1}H NMR spectrum of CYS-2xIBU, the three doublets observed at 0.90, 1.51 and 1.83 ppm belong to ibuprofen (Figure 6.3). The two singlets seen at 5.45 and 5.94 ppm belong to the methacrylate double bond. One of two different aromatic protons appears as a doublet at 7.10 ppm and the other set at 7.17 ppm. In the ^{13}C NMR spectrum, carbonyl carbons of two different esters were observed at 166.14 and 174.42 ppm (Figure 6.4). Aromatic carbons and double bond carbons were observed between 123-140 ppm. The FTIR spectrum of CYS-2xIBU displays two different carbonyl stretch at 1660 and 1738 cm^{-1} and double bond stretch at 1615 cm^{-1} (Figure 6.5)

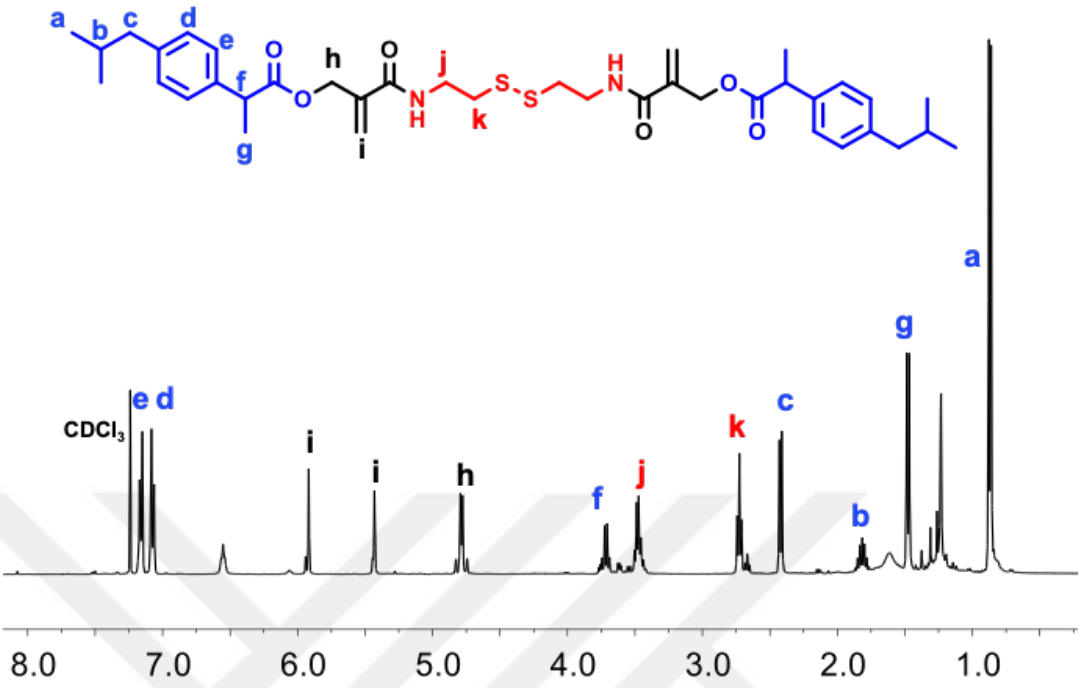


Figure 6.3. [1]H-NMR spectrum of CYS-2xIBU

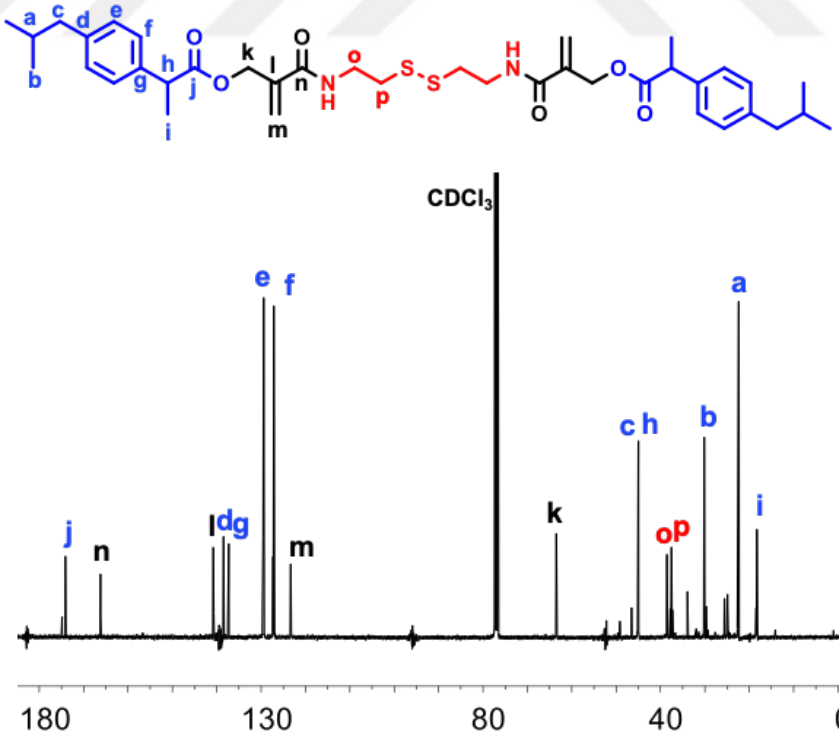


Figure 6.4. [13]C-NMR spectrum of CYS-2xIBU

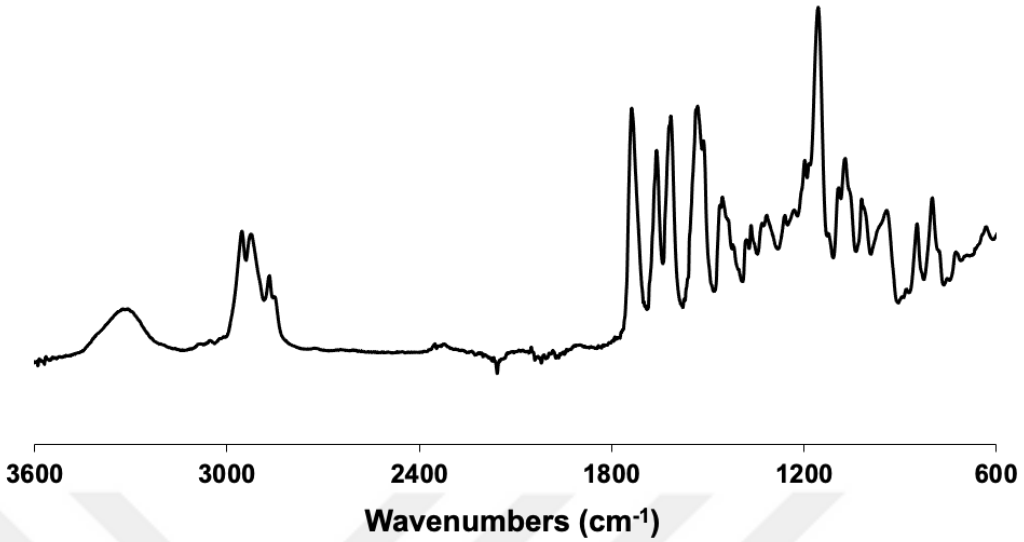


Figure 6.5. FTIR spectrum of CYS-2xIBU

Table 6.1 summarizes the solubilities of the synthesized monomer and the commercial reference. It was soluble in common organic solvents like ethanol, ether, dichloromethane and chloroform but insoluble in hexane.

Table 6.1. Solubilities of the synthesized monomer and IBU.

Monomer/IBU	H_2O	MeOH	EtOH	$(C_2H_5)_2$	$CHCl_3$	DCM	THF	Hexane	
IBU	-	+	+	+	+	+	+	+	
CYS-2xIBU	-	±	+	+	+	+	+	-	

Ibuprofen-functional hydrogel was synthesized by polymerizing PEGDA:CYS-2xIBU (90:10 wt%) with UV light (365 nm) using PI I2959 (2 wt%) in a mixture of water and ethanol (Figure 6.6). The morphologies of the hydrogel was examined by SEM (Figure 6.7).

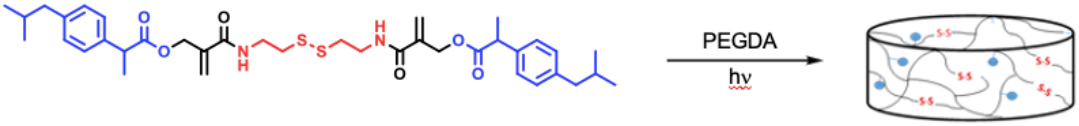


Figure 6.6. Synthesis of hydrogel

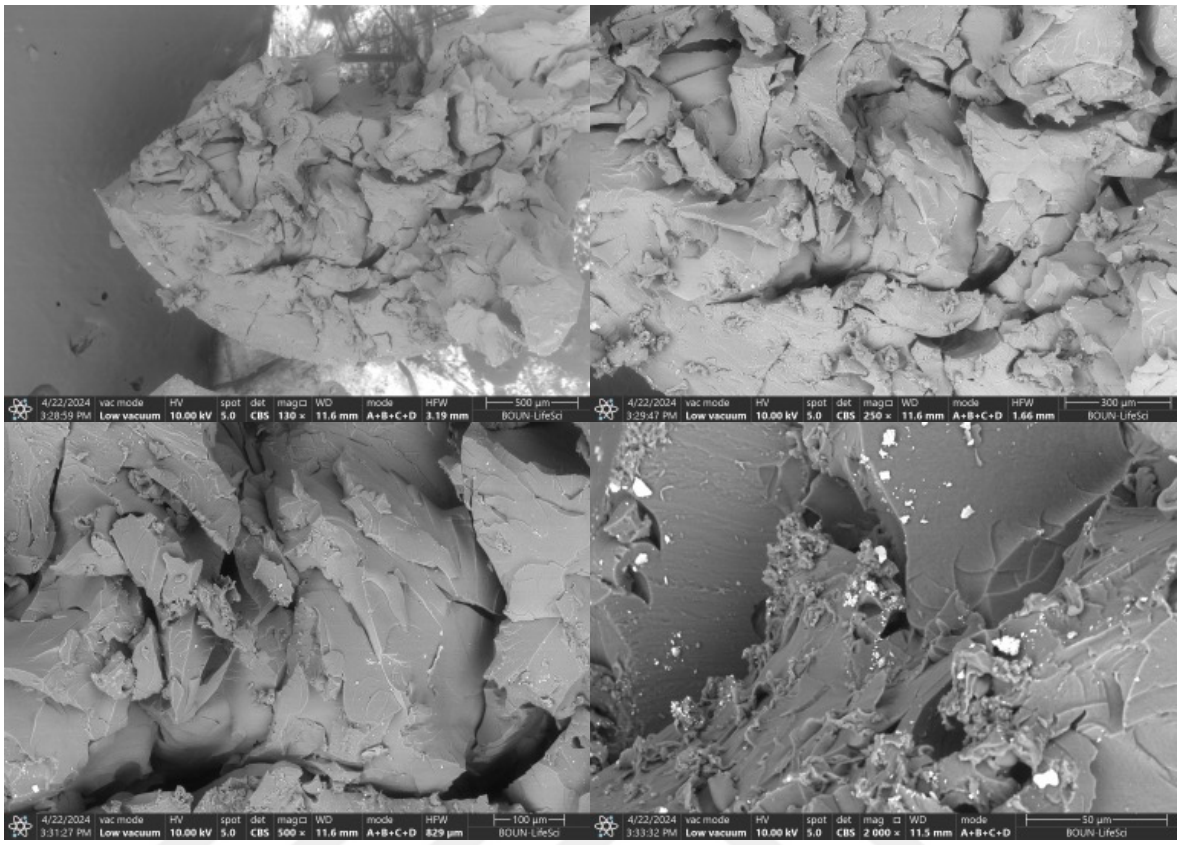


Figure 6.7. SEM images of hydrogel

6.3.2. Release Studies

The release properties of the synthesized crosslinker monomer were examined in PBS (Figure 6.8). PEGDA:CYS-2xIBU hydrogels were used. A significant decrease in the release rate was observed for PEGDA:CYS-2xIBU, as it was chemically linked to the polymer network. While it takes 6 hours for 95% of ibuprofen to be released, the observed release from PEGDA:CYS-2xIBU is only 71% after 36 days.

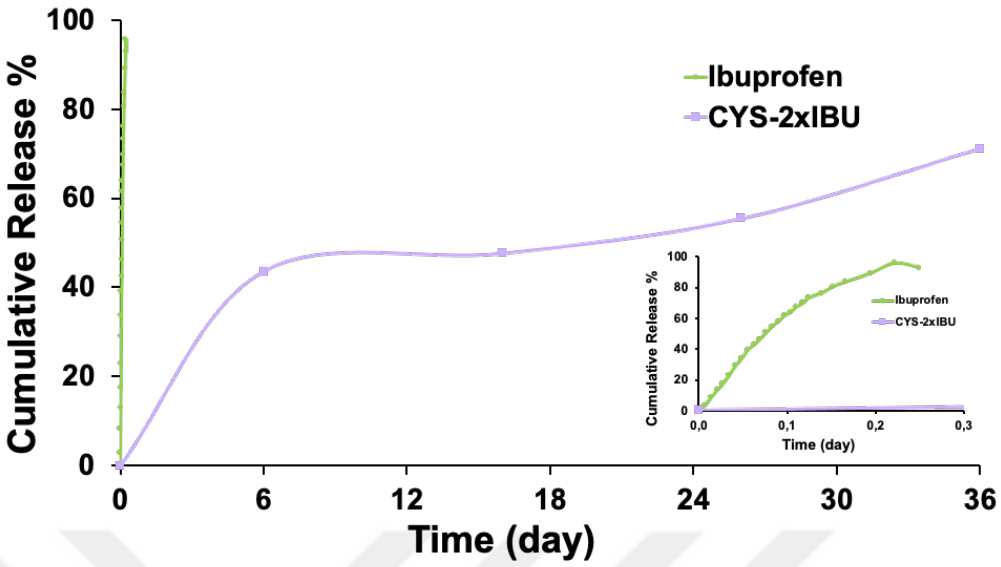


Figure 6.8. The release profiles of ibuprofen: pure drug and from CYS-2xIBU crosslinked PEGDA hydrogels in PBS

6.4. Conclusions

A novel ibuprofen functionalized crosslinker was successfully synthesized in high purity. It was used to prepare PEGDA hydrogels by photopolymerization. The synthesized hydrogel showed much slower release rate of ibuprofen by hydrolysis compared to parent drug ibuprofen. Therefore it can be said that this monomer can be the solution for the detrimental consequences of overdose of NSAIDs on different systems of the body.

7. CONCLUDING REMARKS

This thesis consists of two main parts, the first in the field of photopolymerization (Chapters 3 and 4), and the second on novel delivery methods of non-steroidal anti-inflammatory drugs (Chapters 5 and 6).

The third chapter of this thesis describes the synthesis, characterization, photochemical and photophysical properties, migration stability and photopolymerizations of two novel I2959 functionalized PIs (I2959-NTBDA and I2959-NDAA) with 1,6-heptadiene structure from *tert*-butyl α-hydroxymethacrylate and one of their cyclic polymers. The effect of differences (methacrylate ester, methacrylic acid) in the cyclopolymerizable parts of the structures on the initiating efficiencies of the PIs was investigated. The PI's structure makes it both polymerizable to give cyclopolymers or crosslinked polymers with high migration stability for environmentally friendly materials. These PIs' different functional groups have the potential e.g. for preparation of gels (from carboxylic acid functional ones) which can be crosslinked by Ca^{2+} or Fe^{3+} to form double-networks or for polymer growth from metallic surfaces they are attached to; and may also influence the properties of the final products they get incorporated into, such as thermal stability and mechanical properties.

The fourth chapter similarly describes two I2959 functionalized novel (di)methacrylate PIs (I2959-NH-AHM and I2959-N-2xAHM) from AHM. Since they are highly reactive monomeric PIs, they can homopolymerize, or copolymerize with commercial monomers to give linear or crosslinked polymers with different functionalities to tailor the physical properties of the resulting materials and will enhance migration and thermal stabilities.

The fifth chapter of this thesis focuses on the synthesis and characterization of two cystamine salt derivatives of ibuprofen. According to in vitro cell analysis, the salts had no impact on the cell survival of RAW264.7 macrophages and they exhibited comparable anti-inflammatory efficacy to ibuprofen. The higher solubility of the salts in water and PBS compared to ibuprofen which may increase their bioavalibility and their controllable release

in PEGDA hydrogels make them promising candidates for effective drug delivery formulations.

The last chapter reports synthesis and characterization of a novel ibuprofen and disulfide functionalized methacrylate crosslinker which can be utilized to obtain enzyme-responsive hydrogels by copolymerization with different monomers. The representative PEGDA hydrogel prepared using this crosslinker showed a very slow rate of hydrolytic release of ibuprofen in phosphate buffer saline. This new dosing drug system may alleviate the side effects of ibuprofen.

REFERENCES

1. Mai, S., and L. Gonzalez, "Molecular Photochemistry: Recent Developments in Theory", *Angewandte Chemie International Edition,* Vol. 59, pp. 16832-16846, 2020.

2. Belen, B., U.M. Leloğlu and M.B. Demirköz, "Exploring Relations Between Solar Activity, Cosmic Rays, Clouds and Earth Climate Using Machine Learning Techniques", *Advances in Space Research,* Vol. 74, No. 4, pp. 1883-1899, 2024.

3. Kayahan, E., M. Jacobs, L. Braeken, L. C. J. Thomassen, S. Kuhn, T. van Gerven, and M. E. Leblebici, "Dawn of A New Era in Industrial Photochemistry: The Scale-up of Micro- and Mesostructured Photoreactors", *Beilstein Journal of Organic Chemistry,* Vol. 16, pp. 2484–2504, 2020.

4. Zhu, Y., and E. Egap, "Light-Mediated Polymerization Induced by Semiconducting Nanomaterials: State-of-the-Art and Future Perspectives", *ACS Polymers. Au*, Vol. 1, No. 2, pp. 76–99, 2021.

5. Fischer, M., "Industrial Applications of Photochemical Syntheses", *Angendte Chemie,* Vol. 17, No. 1, pp. 16-26, 1978.

6. Yahia, E. M., A. Carrillo-López, G. M. Barrera, H. Suzán-Azpiri, and M. Q. Bolaños, *Postharvest Physiology and Biochemistry of Fruits and Vegetables*, Woodhead Publishing, 2019.

7. Johnson, M. P., "Photosynthesis", *Essays in Biochemistry,* Vol. 60, pp. 255–273, 2016.

8. Miller, L.W., M. I. Tejedor-Tejedor, and M. A. Anderson, "Titanium Dioxide-Coated Silica Waveguides for the Photocatalytic Oxidation of Formic Acid in Water", *Environmental Science & Technology,* Vol. 33, No. 12, pp. 2070–2075, 1999.

9. Padervand, M., G. Lammel, A. Bargahi, and H. Mohammad-Shiri, “Photochemical Degradation of The Environmental Pollutants Over The Worm-Like Nd_2CuO_4-Nd_2O_3 Nanostructures”, *Nano-Structures & Nano-Objects*, Vol. 18, pp. 100258, 2019.

10. Al-Nuaim, M. A., A. A. Alwasiti, and Z. Y. Shnain, “The Photocatalytic Process in The Treatment of Polluted Water”, *Chemical Papers*, Vol. 77, pp. 677–701, 2023.

11. Balzani, V., G. Bergamini, and P. Ceroni, “Photochemistry and Photocatalysis”, *Rendiconti Lincei*, Vol. 28, pp. 125–142, 2017.

12. Jozef, S., "Photochemistry - Development and Achievements”, *Acta Chimica Slovaca*, Vol. 10, No. 2, pp. 84-90, 2017.

13. Yılmaz, G., Y. Yagci, “Macromolecular Engineering by Photochemical Routes”, *In Macromolecular Engineering*, 2022.

14. Yağcı, Y., S. Jockusch, and N. J. Turro, “Photoinitiated Polymerization: Advances, Challenges, and Opportunities”, *Macromolecules*, Vol. 43, No. 15, pp. 6245–6260, 2010.

15. Ribas-Massonis, A., M. Cicujano, J. Duran, E. Besalú, and A. Poater, "Free-Radical Photopolymerization for Curing Products for Refinish Coatings Market”, *Polymers,* Vol. 14, No. 14, pp. 2856, 2022.

16. Bagheri, A., and J. Jin, “Photopolymerization in 3D Printing”, *ACS Applied Polymer Materials*, Vol. 1, No. 4, pp. 593–611, 2019.

17. Fors, B. P., and C. J. Hawker, “Control of a Living Radical Polymerization of Methacrylates by Light”. *Angewandte Chemie*, Vol. 51, No. 35 pp. 8850-8853, 2012.

18. Rau, D. A., M. Forgiarini, and C. B. Williams, “Hybridizing Direct Ink Write and Mask-Projection Vat Photopolymerization to Enable Additive Manufacturing of High Viscosity Photopolymer Resins”, *Additive Manufacturing*, Vol. 42, pp. 101996, 2021.

19. Jagtap, A., and A. More, “A review on Self-Initiated and Photoinitiator-Free System for Photopolymerization”. *Polymer Bulletin,* Vol. 79, pp. 8057–8091, 2022.

20. Crivello, J., and E. Reichmanis, “Photopolymer Materials and Processes for Advanced Technologies”. *Chemistry of Materials*, Vol. 26. pp. 533–548, 2013.

21. Müller, S. M., S. Schlögl, T. Wiesner, M. Haas, and T. Griesser, “Recent Advances in Type I Photoinitiators for Visible Light Induced Photopolymerization”, *ChemPhotoChem,*Vol. 6, No.11, 2022.

22. Tan, W. Z., C. H. Koo, W. J. Lau, W. C. Chong, and J. Y. Tey, *60 Years of the Loeb-Sourirajan Membrane,* Elsevier, 2022.

23. Andrzejewska, E., *Three-Dimensional Microfabrication Using Two-Photon Polymerization,* William Andrew Publishing, Oxford, 2016.

24. Tehfe, M.A., F. Louradour, J. Lalevée, and J. Fouassier,“Photopolymerization Reactions: On the Way to a Green and Sustainable Chemistry”, *Applied Science*, Vol. 3, No. 2, pp. 490-514, 2013.

25. Sangermano, M., "Advances in Cationic Photopolymerization" *Pure and Applied Chemistry*, Vol. 84, No. 10, pp. 2089-2101, 2012.

26. Decker, C., "Photoinitiated Curing of Multifunctional Monomers”. *Acta Polymerica*, Vol .45, No. 5 pp. 333-347, 1994.

27. Fouassier, J.P. and J Lalevée, *Photoinitiators: Structures, Reactivity and Applications in Polymerization*, Wiley-VCH Verlag GmbH & Co. KGaA, Weinheim, 2021.

28. Tullier, M.P., *Thiol-Acrylate Polymerization Kinetics and Applications in Microluidics,* Ph.D. Thesis, Louisiana State Universit, 2016.

29. Cai, Y., and J. L. P. Jessop, “Decreased Oxygen Inhibition in Photopolymerized Acrylate/Epoxide Hybrid Polymer Coatings as Demonstrated by Raman Spectroscopy”, *Polymer*, Vol. 47, No.19, pp. 6560-6566, 2006.

30. Myers, T.N., “Initiators, Free-Radical*”, In Encyclopedia of Polymer Science and Technology, 2022.*

31. Nakamura, Y., R. Lee, M. L. Coote and S. Yamago, “Termination Mechanism of the Radical Polymerization of Acrylates”. *Macromolecular Rapid Communications*, Vol. 37, No.6 pp. 506-513, 2016.

32. Corrigan, N., K. Jung, G. Moad, C. J. Hawker, K. Matyjaszewski, and C. Boyer, “Reversible-Deactivation Radical Polymerization (Controlled/Living Radical Polymerization): From Discovery to Materials Design and Applications”, *Progress in Polymer Science,* Vol. 111, pp. 101311, 2020.

33. Nakamura, Y., and S. Yamago, “Termination Mechanism in the Radical Polymerization of Methyl Methacrylate and Styrene Determined by the Reaction of Structurally Well-Defined Polymer End Radicals”, *Macromolecules*, Vol.48, No.18, pp. 6450–6456, 2015.

34. Turro, N. J., *Modern Molecular Photochemistry*, University Science Books, California, 1991.

35. Chatani, S., C. J. Kloxin, and C. N. Bowman, “The Power of Light in Polymer Science: Photochemical Processes to Manipulate Polymer Formation, Structure, and Properties”, *Polymer Chemistry,* Vol.5, No.7, pp. 2187-2201, 2014.

36. Fransson, T., M. G. Delcey, I. E. Brumboiu, M. Hodecker, X. Li, Z. Rinkevicius, A. Dreuw, Y. M. Rhee, and P. Norman, “eChem: A Notebook Exploration of Quantum Chemistry”, *Journal of Chemical Education,* Vol. 100, No. 4, pp. 1664–1671, 2023.

37. Tritala, K. V., J. Vaidyanathan, P. P. Lizymol, S. Ariya, and K. V. Krishnan, "Study of Visible Light Activated Polymerization in BisGMA-TEGDMA Monomers with Type 1 and Type 2 Photoinitiators Using Raman Spectroscopy", *Dental Materials*, Vol. 33, No.1, pp. 1-11, 2017.

38. Tomal, W. and J. Ortyl, "Water-Soluble Photoinitiators in Biomedical Applications", *Polymers*, Vol.12, No. 5, pp.1073, 2020.

39. Eibel. A., D. E. Fast, and G. Gescheidt, "Choosing The Ideal Photoinitiator for Free Radical Photopolymerizations: Predictions Based on Simulations Using Established Data", *Polymer Chemistry*, Vol.9, No.41, pp. 5107-5115, 2018.

40. Nguyen, K.T. and J. L. West, "Photopolymerizable Hydrogels for Tissue Engineering Applications", *Biomaterials,* Vol. 23, No. 22, pp. 4307-4314, 2002.

41. Allushi, A., C. Kutahya, C. Aydogan, J. Kreutzer, G.Yilmaz, and Y. Yağcı, "Conventional Type II Photoinitiators as Activators for Photoinduced Metal-Free Atom Transfer Radical Polymerization", *Polymer Chemistry,* Vol.8, No.12, pp. 1972-1977, 2017.

42. Lago, M. A., A R. de Quirós, R. Sendón, J. Bustos, M. T. Nieto, and P. Paseiro "Photoinitiators: a Food Safety Review", *Food Additives & Contaminants: Part A*, Vol. 32, No.5, pp. 779-798, 2015.

43. Balcerak, A., J. Kabatc-Borcz, Z. Czech, and M. Bartkowiak, "Latest Advances in Highly Efficient Dye-Based Photoinitiating Systems for Radical Polymerization", *Polymers*, Vol.15, No. 5, pp.1148, 2023.

44. Balaban, B., N. Kariksiz, T. N. Eren and D.Avci, "Cyclopolymerizable and Cyclopolymeric Photoinitiators from Diallyl Amine and α-Hydroxy Ketones, *Polymer Chemistry*, Vol. 13, No. 35, pp. 5094–5104, 2022.

45. Zheng, H., H. Lu, J. Li, J. Nie, and X. Zhu, “The Photoinitiator of Bifunctional α-Hydroxy Ketone with Long-Wavelength in Photopolymerization Under UV-LEDs”, *Progress in Organic Coatings*, Vol. 185, pp. 107936, 2023.

46. Marlton, S. J. P., B. I. McKinnon, N. S. Hill, M. L. Coote and A. J. Trevitt, “Electrostatically Tuning the Photodissociation of the Irgacure 2959 Photoinitiator in the Gas Phase by Cation Binding”, *Journal of the American Chemical Society*, Vol. 143, No. 5, pp. 2331-2339, 2021

47. Taschner, R., P. Gauss, P. Knaack, and R. Liska, “Biocompatible Photoinitiators Based on Poly-α-Ketoesters”, *Journal of Polymer Science,* Vol. 58, No. 2, pp. 242-253, 2020.

48. Kowalska, A., J. Sokolowski and K. Bociong, “The Photoinitiators Used in Resin Based Dental Composite-A Review and Future Perspectives”, *Polymers*, Vol. 13, No. 3, pp. 470, 2021.

49. Breloy, L., C. Negrell, A.-S. Mora, W. S. Jennifer Li, V. Brezová, S. Caillol and D. L. Versace, “Vanillin Derivative as Performing Type I Photoinitiator”, *European Polymer Journal*, Vol. 132, pp. 109727, 2020.

50. Fouassier, J.P. and J. Lalevée, *Photoinitiators for Polymer Synthesis: Scope, Reactivity and Efficiency,* Wiley-VCH Verlag GmbH & Co. KGaA, Weinheim, 2012.

51. Zhou, J., X. Allonas, A. Ibrahim and X. Liu, “Progress in the Development of Polymeric and Multifunctional Photoinitiators”, *Progress in Polymer Science,* Vol. 99, pp. 101165-101016, 2019

52. Eren, T.N. B. Graff, J. Lalevee and D. Avci, “Thioxanthone-functionalized 1,6-heptadiene as monomeric photoinitiator”, *Progress in Organic Coatings*, Vol. 128, pp. 148-156, 2019.

53. Corrales, T., F. Catalina, C. Peinado and N.S. Allen, “Free Radical Macrophotoinitiators: An Overview on Recent Advances”, *Journal of Photochemistry and Photobiology A: Chemistry*, Vol. 159, No. 2, pp. 103-114, 2003.

54. Muller, M., C. Bandl and W. Kern, “Surface-Immobilized Photoinitiators for Light Induced Polymerization and Coupling Reactions”, *Polymers,* Vol. 14, No. 3, pp. 608, 2022.

55. Matsushima, H., S. Hait, Q. Li, H. Zhou, M. Shirai and C.E. Hoyle, “Non-Extractable Photoinitiators Based on Thiol-Functionalized Benzophenones and Thioxanthones”, *European Polymer Journal*, Vol. 46, No. 6, pp. 1278-1287, 2010.

56. Kariksiz, N., B. Balaban, T. Gencoglu, F. Morlet-Savary, J. Lalevee and D. Avci, “A Cyclopolymerizable, Doubly Irgacure 2959 Functionalized Quaternary Ammonium Salt Photoinitiator and Its Water-Soluble Copolymer with Diallyldimethylammonium Chloride”, *Polymer Chem*istry, Vol. 14, No. 11, pp. 1195–1205, 2023.

57. Breloy, L., R. Losantos, D. Sampedro, M. Marazzi, J.P. Malval, Y. Heo, J. Akimoto, Y. Ito, V. BrezovaÃÅ, and D. L. Versace, "Allyl Amino-Thioxanthone Derivatives as Highly Efficient Visible Light H-Donors and Copolymerizable Photoinitiators", *Polymer Chemistry*, Vol. 11, No. 26, pp. 4297- 4312, 2020.

58. Wang, H., J. Wei, X. Jiang, and J. Yin, “Novel Polymerizable Sulfur-Containing Benzophenones as Free-Radical Photoinitiators for Photopolymerization”, *Macromolecular Chemistry and Physics*, Vol. 207, No. 12, pp. 1080–1086, 2006.

59. Eren, T.N., N. Kariksiz, G. Demirci, D. Tuncel, A. N. Ökte, H. Yagci Acar, and D. Avci, “Irgacure 2959-Functionalized Poly(ethyleneimine)s as Improved Photoinitiators: Enhanced Water Solubility, Migration Stability and Visible-light Operation”, *Polymer Chemistry*, Vol. 12, No. 18, pp. 2772-2785, 2021.

60. Huang, X., Y. Zhang, F. Li, J. Zhang, Y. Dai, M. Shi, and Y. Zhao, “Highly Efficient Alginate-based Macromolecular Photoinitiator for Crosslinking and Toughening

Gelatin Hydrogels", *Journal of Polymer Science*, Vol. 58, No. 10, pp. 1439–1449, 2020.

61. Akat, H., B. Gacal, D. K. Balta, N. Arsu, and Y. Yagci, "Poly (Ethylene Glycol)-Thioxanthone Prepared by Diels–Alder Click Chemistry as One-component Polymeric Photoinitiator for Aqueous Free-radical Polymerization", *Journal of Polymer Science Part A: Polymer Chemistry*, Vol. 48, No. 10, pp. 2057–2256, 2010.

62. Eren, T.N., J. Lalevee and D. Avci, "Water Soluble Polymeric Photoinitiator for Dual-Curing of Acrylates and Methacrylates", *Journal of Photochemistry & Photobiology, A: Chemistry*, Vol. 389, pp. 112288, 2020.

63. Gencoglu, T., T.N. Eren, J. Lalevee and D. Avci, "Photoinitiating Systems Based on Poly (Ethylene imine) for Michael Addition and Free Radical Photopolymerization", *Journal of Photochemistry & Photobiology, A: Chemistry*, Vol. 404, pp. 112959, 2021.

64. Peer, G., M. Kury, C. Gorsche, Y. Catel, P. Frühwirt, G. Gescheidt, N. Moszner and R. Liska, "Revival of Cyclopolymerizable Monomers as Low-Shrinkage Cross-Linkers, *Macromolecules*, Vol. 53, No. 19, pp. 8374–8381, 2020.

65. Ruppitsch, L. A., G. Peer, K. Ehrmann, T. Koch and R. Liska, "Photopolymerization of Difunctional Cyclopolymerizable Monomers with Low Shrinkage Behavior", *Journal of Polymer Science,* Vol. 59, No. 6, pp. 519–531, 2021.

66. Stansbury, J. W., "Cyclopolymerizable Monomers for Use in Dental Resin Composites", *Journal of Dental Research*, Vol. 69, No. 3, pp. 844–848, 1990.

67. Kodaira, T., M. Okumura, M. Urushisaki and K. Isa, "Cyclopolymerization. XIX. Effect of N-Substituents on Cyclopolymerizability of N-Allylmethacrylamides", *Journal of Polymer Science Part A: Polymer Chemistry,* Vol. 31, No. 1, pp. 169–176, 1993.

68. Staudinger, H. and W. Heuer, “Highly Polymerized Compounds. XCIV”. *An Insoluble Polystyrene*, Berichte Der Dtsch. Chem. Gesellschaft [Abteilung] B Abhandlungen. 67B, pp. 1164-1172,1934.

69. Butler, G.B., “Cyclopolymerization and Cyclocopolymerization”, *Accounts of Chemical Research*, Vol. 15, No. 11, pp. 370-378, 1982.

70. Butler, G.B., “Cyclopolymerization”, *Journal of Polymer Science Part A: Polymer Chemistry*, Vol. 38, No. 19, pp. 3451-3461, 2000.

71. Butler, G.B., A. Crawshaw, and W.L. Miller, “The Formation of linear polymers from diene monomers by a cyclic polymerization mechanism. I. The structure of poly-(diallylammonium halides), *Journal of the American Chemical Society*, Vol. 80, No. 14, pp. 3615-3618, 1958.

72. Butler, G. B., G. C. Corfield, and C. Aso, “Cyclopolymerization”, *Progress in Polymer Science,* Vol. 4, pp. 71-208, 1975.

73. Alison, R. B., and D. M. Knauss, “Recent Advances in The Synthesis of Diallylammonium Polymers”, *Materials Today Chemistry*, Vol. 26, pp. 101251, 2022.

74. Hall, A. W., M. J. Godber, K. M. Blackwood, P. E. Y. Milneb and J. W. Goodby, “The Photoinitiated Cyclopolymerization of Dienes in The Creation of Novel Polymeric Systems and Three-Dimensional Networks”, *Journal of Material Chemistry*, Vol. 14, No. 17, 2593-2602, 2004.

75. Kodaira, T., “Structural Control During The Cyclopolymerization of Unconjugated Dienes”, *Progress in Polymer Science*, Vol. 25, No. 5, pp. 627-676, 2000.

76. Peer, G., P. Dorfinger, T. Koch, J. Stampfl, C. Gorsche, and R. Liska, “Photopolymerization of Cyclopolymerizable Monomers and Their Application in Hot Lithography”, *Macromolecules,* Vol. 51, No. 22, pp. 9344–9353, 2018

77. Sausville, E. A., *Principles of Clinical Pharmacology,* Third Edition, Elsevier's Science & Technology, Oxford, 2012.

78. Wadud, A., P.V.V. Prasad, M.M. Rao, and A. Narayana, "Evolution of Drug: A Historical Perspective", *Journal of Indian Institute of History of Medicine*, Vol. 36, pp. 69-80, 2007.

79. Raj, G. M. and R. Raveendran, *Introduction to Basics of Pharmacology and Toxicology*: *Volume 1, General and Molecular Pharmacology: Principles of Drug Action,* Springer, Singapore, 2019.

80. Alamgir, A. N. M., *Therapeutic Use of Medicinal Plants and Their Extracts: Volume 1*, Springer International Publishing AG, Gewerbestrasse, 2017.

81. Meek, I. L., M. A. F. J. Van de Laar, and H. E. Vonkeman. "Non-Steroidal Anti-Inflammatory Drugs: An Overview of Cardiovascular Risks", *Pharmaceuticals*, Vol.3, No. 7, pp. 2146-2162, 2010.

82. Ozleyen, A., Y. B. Yilmaz and S. Donmez. "Looking at NSAIDs from a Historical Perspective and Their Current Status in Drug Repurposing for Cancer Treatment and Prevention", *Journal of Cancer Research and Clinical Oncology*, Vol. 149, pp. 2095–2113, 2023.

83. Lichterman B L., "Aspirin: The Story of a Wonder Drug", *The BMJ,* Vol. 329, pp. 1408, 2004.

84. Walker, J., P. Hutchison, J. Ge, D. Zhao, Y. Wang, P. M. Rothwell, J. M. Gaziano, A. Chan, J. Burn, J. Chia, R. Langley, V. O'Donnell, B. Rocca, and C. Hawkey, "Aspirin: 120 years of innovation. A report from the 2017 Scientific Conference of the International Aspirin Foundation, 14 September 2017, Charité, Berlin", *Ecancermedicalscience, Vol.*12, No. 813, 2018.

85. Thakur, S., B. Riyaz, A. Patil, A. Kaur, B. Kapoor, and V. Mishra, “Novel Drug Delivery Systems for NSAIDs in Management of Rheumatoid Arthritis: An Overview”, *Biomedicine and Pharmacotherapy*, Vol. 106, No. 9, pp. 1011-1023, 2018.

86. Peesa, J. P., P. R. Yalavarthi, A. Rasheed, and V. B. Rao Mandava, “A Perspective Review on Role of Novel NSAID Prodrugs in The Management of Acute Inflammation”, *Journal of Acute Disase*, Vol. 5, No. 5, pp. 364-381, 2016.

87. Bindu, S., S. Mazumder, and U. Bandyopadhyay, “Non-Steroidal Anti-Inflammatory Drugs (NSAIDs) and Organ Damage: A Current Perspective”, *Biochemical Pharmacology*, Vol. 180, pp. 114147, 2020.

88. Kowalski, ML. and J.S. Makowska. “Seven Steps to The Diagnosis of NSAIDs Hypersensitivity: How to Apply a New Classification in Real Practice?”, *Allergy Asthma and Immunol Research,* Vol.7, No. 4, pp. 312-320, 2015.

89. Conaghan, P.G., "A Turbulent Decade for NSAIDs: Update on Current Concepts of Classification, Epidemiology, Comparative Efficacy, and Toxicity”, *Rheumatology*, Vol. 32, pp. 1491–1502, 2012.

90. Howard, P.A and P. Delafontaine, “Non-Steroidal Anti-Inflammatory Drugs and Cardiovascular Risk”, *Journal of the American College of Cardiology*, Vol. 43, No. 4, pp. 519-525, 2004.

91. Knights, K. M., A. A. Mangoni, and J. O. Miners, “Non-Selective Nonsteroidal Anti-Inflammatory Drugs and Cardiovascular Events: Is Aldosterone The Silent Partner in Crime?”, *British Journal of Clinical Pharmacology,* Vol. 61, No. 6, pp. 738-40, 2006.

92. Varrassi, G., J. Pergolizzi, J. F. Peppin, and A. Paladini, *Brain and Heart Dynamics,* Springer International Publishing, Cham, 2020.

93. Adelizzi R. A., “COX-1 and COX-2 in Health and Disease”, *Journal of the American Osteopathic Association,* Vol. 99, pp. 7-12, 1999.

94. Chandrasekharan, N. and D. L. Simmons. “The Cyclooxygenases”, *Genome Biology*, Vol. 5, No. 241, 2004.

95. Grosser, T., S. Fries, and G. A. FitzGerald, “Biological Basis for The Cardiovascular Consequences of COX-2 Inhibition: Therapeutic Challenges and Opportunities”, *Journal of Clinical Investigation,* Vol. 116, No. 1, pp. 4-15, 2006.

96. Bertolini, A., A. Ottani, and M. Sandrini, “Dual Acting Anti-Inflammatory Drugs: A Reappraisal”, *Pharmacological Research*, Vol. 44, No. 6, pp. 437-450, 2001.

97. Chaiamnuay, S., J. J. Allison, and J. R. Curtis, “Risks Versus Benefits of Cyclooxygenase-2-Selective Nonsteroidal Antiinflammatory Drugs”, *American Journal of Health-System Pharmacy*, Vol. 63, No. 19, pp. 1837-1851, 2006.

98. Sohail, R., M. Mathew, K. K. Patel, S. A. Reddy, Z. Haider, M. Naria, A. Habib, Z. U. Abdin, W. R. Chaudhry and A. Akbar, “Effects of Non-steroidal Anti-inflammatory Drugs (NSAIDs) and Gastroprotective NSAIDs on The Gastrointestinal Tract: A Narrative Review”, Vol. 15, No. 4, 2023.

99. Rayburn, E. R., S. J. Ezell and R. Zhang, “Anti-Inflammatory Agents for Cancer Therapy”, *Molecular and Cellular Pharmacology*, Vol. 1, No. 1, pp. 29-43, 2009.

100. Panchal, N.K., and E. P. Sabina, “Non-Steroidal Anti-Inflammatory Drugs (NSAIDs): A Current Insight into Its Molecular Mechanism Eliciting Organ Toxicities”, *Food and Chemical Toxiology,* Vol. 172, pp. 113598, 2023.

101. Nayak, A., and A. Jain, “In Vitro and in Vivo Study of Poly(Ethylene Glycol) Conjugated Ibuprofen to Extend The Duration of Action”, *Sciantia Pharmaceutica*, , Vol. 79, No. 2, pp. 359-373, 2011.

102. Haley, R. M. and H. A von Recum, “Localized and Targeted Delivery of NSAIDs for Treatment of Inflammation: A Review”, *Experimental Biology and. Medicine*, Vol. 244, No. 6, pp. 433-444, 2019.

103. Tran, T., M. Hernandez, D. Patel, E. Burns, V. Peterman, and J. Wu, “Controllable and Switchable Drug Delivery of Ibuprofen from Temperature Responsive Composite Nanofibers”, *Nano Convergence*, Vol. 2, No. 15, 2015.

104. Natfji, A. A., H. M. I. Osborn, and F. Greco, “Feasibility of Polymer-Drug Conjugates for Non-Cancer Applications”, *Current Opinion in Colloid & Interface Science*, Vol. 31, pp. 51-66, 2017.

105. Babazadeh, M., “Synthesis and Study of Controlled Release of Ibuprofen from The New Acrylic Type Polymers”, *International Journal of Pharmaceutics*, Vol. 316, pp. 68-73, 2006.

106. Babazadeh, M., M. Sheidaei, S. Abbaspour, and L. Edjlal, “Synthesis, Characterization, and In Vitro Evaluation of New Ibuprofen Polymeric Prodrugs Based on 2-Hydroxypropyl Methacrylate”, *Scienta Pharmaceutica*., Vol. 81, No. 1, pp. 281-296, 2013.

107. Yamauchi, Y., N. Doi, Y. Sasai, S. Kondo, and M. Kuzuya, “Preparation and Characterization of Polymeric Prodrugs of Non-Steroidal Anti-Inflammatory Drugs (NSAIDs) by Cold Plasma Technique”, *Journal of Photopolymer Science and Technology,* Vol. 30, No. 3, pp. 303-306, 2017.

108. Gouda, A.M., E. A. Beshr, F. A. Almalki, H. H. Halawah, B. F. Taj, A. F. Alnafaei, R. S. Alharazi, W. M. Kazi, and M. M. AlMatrafi, “Arylpropionic Acid-Derived NSAIDs: New Insights on Derivatization, Anticancer Activity and Potential Mechanism of Action”, *Bioorganic Chemistry,* Vol. 92, pp. 103224, 2019.

109. Landoni, M. F. and A. Soraci, “Pharmacology of Chiral Compounds 2-Arylpropionic Acid Derivatives”, *Current Drug Metabolism,* Vol. 2, No. 1, pp. 37-51, 2001.

110. Costa, D., L. Moutinho, J. L.v F. C, Lima, and E. Fernandes, "Antioxidant Activity and Inhibition of Human Neutrophil Oxidative Burst Mediated by Arylpropionic Acid Non-Steroidal Anti-Inflammatory Drugs", *Biological and Pharmaceutical Bulletin*, Vol. 29, No. 8, pp. 1659-1670, 2006.

111. Reichel, C., R. Brugger, H. Bang, G. Geisslinger, and K. Brune, "Molecular Cloning and Expression of a 2-Arylpropionyl-Coenzyme A Epimerase: A Key Enzyme in the Inversion Metabolism of Ibuprofen", *Molecular Pharmacology*, Vol. 54, No. 4, pp. 576-582, 1997.

112. Guzman, J. D., D. Evangelopoulos, A. Gupta, K. Birchall, S. Mwaigwisya, B. Saxty, T. D. McHugh, S. Gibbons, J. Malkinson, and S. Bhakta, "Antitubercular Specific Activity of Ibuprofen and The Other 2-Arylpropanoic Acids Using the HT-SPOTi Whole-Cell Phenotypic Assay", *BMJ Open,* Vol. 3, No. 6, 2013.

113. Halford, G. M., M. Lordkipanidzé, and S. P. Watson, "50th Anniversary of the Discovery of Ibuprofen: An Interview with Dr Stewart Adams", *Platelets*, Vol. 23, No. 6, pp. 415–422, 2012.

114. Vardanyan, R.S. and V.J. Hruby, *Synthesis of Essential Drugs,* Elsevier Science, 2006.

115. Rahman, A. M. F. Haider1, N. Naseem and N. Rahman, "Solubility of Drugs, Their Enhancement, Factors Affecting, and Their Limitations: A Review", *International Journal of Pharmaceutical Sciences Review and Research,* Vol. 79, No. 2, pp. 78-94, 2023.

116. Ossowicz-Rupniewska, P., K. Szczepkowska, P. Bednarczyk, M. Nowak, A. Nowak, W. Duchnik, Ł. Kucharski, Ł. Struk, A. Klimowicz, and Z. Czech, "New Amino Acid Propyl Ester Ibuprofenates from Synthesis to Use in Drug Delivery Systems", *Royal Society of Chemistry Advances*, Vol. 12, No. 55, pp. 35779-35792, 2022.

117. Ossowicz, P., J. Klebeko, E. Janus, A. Nowak, W. Duchnik, Ł. Kucharski, and A. Klimowicz, "The Effect of Alcohols as Vehicles on The Percutaneous Absorption and Skin Retention of Ibuprofen Modified with L-Valine Alkyl Esters", *Royal Society of Chemistry Advances*, Vol. 10, No. 68, pp. 41727- 41740, 2020.

118. Sarveiya, V., J. F. Templeton, and H. A. Benson, "Ion-Pairs of Ibuprofen: Increased Membrane Diffusion", *Journal of Pharmacy and Pharmacology*, Vol. 56, No. 6, pp. 717–724, 2004.

119. Carvalho, R. B. and S. V. Joshi, "Ibuprofen Isobutanolammonium Salt: Synthesis, Thermal Analysis, PXRD, FTIR and Solubility Investigations", *Journal of Thermal Analysis and Calorimetry*, Vol. 139, No. 3, pp. 1971-1976, 2020.

120. Abbas, A. M., A. Aboelmagd, S. M. Kishk, H. H. Nasrallah, W. C. Boyd, H. Kalil, and A. S. Orabi, "A Novel Ibuprofen Derivative and Its Complexes: Physicochemical Characterization, DFT Modeling, Docking, In Vitro Anti-Inflammatory Studies, and DNA Interaction", *Molecules*, Vol. 27, No. 21, pp. 7540, 2022.

121. Santos, M. M., L. R. Raposo, G. V. S. M. Carrera, A. Costa, M. Dionísio, P. V. Baptista, A. R. Fernandes, and L. C. Branco, "Ionic Liquids and Salts from Ibuprofen as Promising Innovative Formulations of an Old Drug", *ChemMedChem,* Vol. 14, No. 9, pp. 907-911, 2019.

122. Shehata, S., C. J. Serpell, and S. C.G. Biagini, "Architecture-Controlled Release of Ibuprofen from Polymeric Nanoparticles", *Materials Today Communications,* Vol. 25, pp. 101562, 2020.

123. Sun, F., Y. Li, N. Zhang, and J. Nie, "Initiating Gradient Polymerization and Migration of a Novel Polymerizable Polysiloxane **α**-Hydroxy Alkylphenones Photoinitiator", *Polymer*, Vol. 55, No. 16, pp. 3656–3665, 2014.

124. Warren, S.C. and L.J. Mathias, “Synthesis and Polymerization of Ethyl α-Chloromethylacrylate and Related Derivatives”, *Journal of Polymer Science Part A: Polymer Chemistry*, Vol. 28, No. 6, pp. 1637–1648, 1990.

125. Saito, Y., K. Matsumoto, S. S. Bag, S. Ogasawara, K. Fujimoto, K. Hanawa, and I. Saito, “C8-Alkynyl- and Alkylamino Substituted 2′-Deoxyguanosines: A Universal Linker for Nucleic Acids Modification”, *Tetrahedron*, Vol. 64, No. 16, pp. 3578–3588, 2008.

126. Zhang, F., Z. Wu, P. Chen, J. Zhang, T. Wang, J. Zhou, and H. Zhang, “Discovery of A New Class of PROTAC BRD4 Degraders Based on a Dihydroquinazolinone Derivative and Lenalidomide/Pomalidomide”, *Bioorganic and Medicinal Chemistry*, Vol. 28, No. 1, pp. 115228, 2020.

127. Smith, T. J., B. S. Shemper, J. S. Nobles, A. M. Casanova, C. Ott, and L. J. Mathias, “Crosslinking Kinetics of Methyl and Ethyl (α-Hydroxymethyl)acrylates: Effect of Crosslinker Type and Functionality, *Polymer*, Vol. 44, No. 20, pp. 6211–6216, 2003.

128. Yang, J., R. Tang, S. Shi, and J. Nie, “Synthesis and Characterization of Polymerizable One-Component Photoinitiator Based on Sesamol”, *Photochemical & Photobioogical Sciences*, Vol. 12, No. 5, pp. 923–929, 2013.

129. Dogu-Baykut, E. and G. Gunes, “Effect of Ultraviolet (UV-C) Light and Gaseous Ozone on Microbial and Color Qualities of Whole Black Pepper Seeds (Piper Nigrum L.)”, *Carpathian Journal of Food Science and Technology*, Vol. 14, No. 2, pp. 122–131, 2022.

130. Avci, D., C. Haynes, and L. J. Mathias, “Cyclopolymerization of Amine-Linked Diacrylate Monomers, *Journal of Polymer Science Part A: Polymer Chemistry*, Vol. 35, No. 10, pp. 2111–2121, 1997.

131. Huo, S., H. Y. Zhou, and J. X. Wang, "Preparation and Photochemical Properties of PEG Based α-Hydroxyalkylphenone Photoinitiator", *Reactive and Functional Polymers*, Vol. 163, pp. 104892, 2021.

132. Wu, Y. P., R. Li, J. Ke, X. Cheng, R. Tang, Y. Situ, and H. Huang, "Study on Bifunctional Acyldiphenylphosphine Oxides Photoinitiator for Free Radical Polymerization", *European Polymer Journal*, Vol. 168, pp. 111093, 2022.

133. Karaoğlu, Ö., M. Serhatlı, E. Pelvan, B. Karadeniz, I. Demirtas, G. Çakırca, H. Sipahix, Y. Özhan, G. Karapınar, M. Charehsaz, A. Aydın, E. Yesilada, and C. Alasalvar, "Chewable Tablet with Herbal Extracts and Propolis Arrests Wuhan and Omicron Variants of SARS-CoV-2 Virus", *Journal of Functional Foods*, Vol. 105, pp. 105544, 2023.

134. Okur, M. E., A. E. Karadağ, N. Üstündağ Okur, Y. Özhan, H. Sipahi, Ş. Ayla, B. Demirci, and F. Demirci, "In Vivo Wound Healing and in Vitro Anti-Inflammatory Activity Evaluation of Phlomis Russeliana Extract Gel Formulations", *Molecules*, Vol. 25, No. 11, pp. 2695, 2020.

135. Okur, M. E., A. E. Karadağ, Y. Özhan, H. Sipahi, Ş. Ayla, B. Daylan, Ş. Kültür, B. Demirci, and F. Demirci, "Anti-Inflammatory, Analgesic and in Vivo-in Vitro Wound Healing Potential of The Phlomis Rigida Labill. Extract", *Journal of Ethnopharmacology*, Vol. 266, pp. 113408, 2021.

136. Erdoğan, M., R. Konya, Y. Özhan, H. Sipahi, I. Çinbilgel, M. Masullo, M., S. Piacente, and H. Kırmızıbekmez, "Secondary Metabolites from Scutellaria Brevibracteata Subsp. Subvelutina and Their in Vitro Anti-Inflammatory Activities", *South African Journal of Botany*, Vol. 139, pp.12-18, 2021.

137. Stuart, N.J.,and A.S. Sanders, "Phenyl Propionic Acids", U. S. Patent 3385886A, accessed on May 28, 1968. https://patents.google.com/patent/US3385886A/en.

138. Shackelford, R. E., P. B. Alford, Y. Xue, S. F. Thai, D. O. Adams, and S. Pizzo, “Aspirin Inhibits Tumor Necrosis Factoralpha Gene Expression in Murine Tissue Macrophages”, *Molecular Pharmacology*, Vol. 52 No. 3, pp. 421–429, 1997.

139. Dispinar, T., W. V. Camp, L. J. De Cock, B. G. De Geest, and F. E. Du Prez, “Redox-Responsive Degradable PEG Cryogels as Potential Cell Scaffolds in Tissue Engineering”, *Macromolecular Bioscience,* Vol. 12, No. 3, pp. 383-394, 2012.